

*Thermo-dynamical study of steady  
state and transient process in a  
dilution refrigerator*

*By*

**JEDIDIAH PRADHAN**

**(Enrollment No. PHYS04200904007)**

**VARIABLE ENERGY CYCLOTRON CENTRE**

**Kolkata-700064, India**

*A thesis submitted to the*

*Board of Studies in Physical Sciences*

*in partial fulfillment of requirements*

*For the Degree of*

**DOCTOR OF PHILOSOPHY**

*of*

**HOMI BHABHA NATIONAL INSTITUTE**

**Mumbai-400 094, India**



February 2016

# Homi Bhabha National Institute

## Recommendations of the Viva Voce Committee

As members of the Viva Voce Committee, we certify that we have read the dissertation prepared by Jedidiah Pradhan entitled "Thermo-dynamical study of steady state and transient process in a dilution refrigerator" and recommend that it may be accepted as fulfilling the thesis requirement for the award of Degree of Doctor of Philosophy.

Chairman: Prof. Saila Bhattacharyya  Date: 26/2/16

Guide / Convener: Prof. Alok Chakrabarti  Date: 26/2/16

Co-guide: Dr. Nisith Kumar Das  Date: 26.02.16

Examiner: Dr. Upendra Behera  Date: 26/2/2016

Member: Prof. Parthasarathi Barat  Date: 26/02/2016

Member: Prof. Rajarao Ranganathan Date:

Technical Advisor: Shri Subimal Saha  Date: 26/2/2016

Final approval and acceptance of this thesis is contingent upon the candidate's submission of the final copies of the thesis to HBNI.

We hereby certify that I/we have read this thesis prepared under my/our direction and recommend that it may be accepted as fulfilling the thesis requirement.

Date: 26/2/2016

Place: Kolkata



Co-guide



Guide

## STATEMENT BY AUTHOR

This dissertation has been submitted in partial fulfillment of requirements for an advanced degree at Homi Bhabha National Institute (HBNI) and is deposited in the Library to be made available to borrowers under rules of the HBNI.

Brief quotations from this dissertation are allowable without special permission, provided that accurate acknowledgement of source is made. Requests for permission for extended quotation from or reproduction of this manuscript in whole or in part may be granted by the Competent Authority of HBNI when in his or her judgment the proposed use of the material is in the interests of scholarship. In all other instances, however, permission must be obtained from the author.

JEDIDIAH PRADHAN

## DECLARATION

I, hereby declare that the investigation presented in the thesis has been carried out by me. The work is original and has not been submitted earlier as a whole or in part for a degree / diploma at this or any other Institution / University.

JEDIDIAH PRADHAN

**Dedicated**

**to**

**my father Victor Pradhan**

# Contents

<b>Acknowledgements</b> .....	<b>i</b>
<b>Preamble</b> .....	<b>ii</b>
<b>List of Figures</b> .....	<b>v</b>
<b>List of Tables</b> .....	<b>ix</b>
<b>List of Symbols</b> .....	<b>x</b>
<b>Synopsis</b> .....	<b>xv</b>
<b>1. Introduction</b>	
1.1 Historical survey .....	1
1.2 Properties of $^3\text{He}/^4\text{He}$ mixtures.....	5
1.3 Working principle of Dilution refrigerator .....	14
1.4 Reviews of Previous Work .....	17
<b>2. Mechanical Components of Dilution Refrigerator</b>	
2.1 Introduction .....	23
2.1.1 Bath Cryostat .....	24
2.1.2 $^4\text{He}$ Evaporator (1K-pot).....	28
2.1.3 Flow Impedance .....	34
2.1.4 $^3\text{He}$ Distillation Chamber (Still).....	36
2.1.5 Heat Exchanger (HeX) .....	40
2.1.6 Mixing Chamber(MC).....	43
2.1.7 Gas Handling System (GHS).....	44
2.1.8 Electrical System and Data Acquisition (DAQ).....	46

2.2 Operation of Dilution Refrigerator -----	47
2.2.1 Preparation for Run -----	47
2.2.2 Charging of Isotopic Helium gas Mixture -----	50
2.2.3 Condensation of Isotopic Helium gas Mixture -----	51
2.2.4 Normal Circulation -----	52
2.2.5 Shutdown & Gas Recovery -----	53

### **3. Thermodynamics and Model Simulation under Steady State**

3.1 Factors Degrading Refrigerator Performance -----	55
3.1.1 Convective Instability in Dilute side -----	55
3.1.2 Improper Pressure Distribution in Concentrate side -----	56
3.1.3 Effect of $^4\text{He}$ in Concentrate side -----	57
3.1.4 Composition of Isotopic Helium gas Mixture -----	58
3.1.5 Flow Impedance Across Heat Exchanger -----	59
3.1.6 Residual Heat Load -----	60
3.2 Numerical Modeling -----	62
3.2.1 Still and Molar Flow Rate -----	65
3.2.2 Cooling Power and Continuous Counter-flow HeX -----	69
3.3 Results and Discussion -----	79

### **4. Thermodynamics and Model Simulation of Transient Phenomena**

4.1 Introduction -----	93
4.2 Process Simulation -----	94
4.2.1 Process Description -----	95
4.2.2 Numerical Model -----	97
4.2.3 Solution Method -----	101

4.3 Results and Discussion-----	104
<b>5. Conclusions and Future Outlook</b>	
5.1 Summary-----	112
5.2 Scope of Future Works-----	114
<b>Bibliography -----</b>	<b>116</b>
<b>Appendix A:</b> Flow Impedance Analysis -----	<b>119</b>
<b>Appendix B:</b> Flow Chart for Steady State Simulation -----	<b>121</b>

# Acknowledgements

I would like to express my gratitude to Prof. Alok Chakrabarti and Dr. Nisith Kr. Das, my supervisors for their continuous support and guidance. I am indebted to all members of the team involved in building the dilution refrigerator. In particular, measurements presented in the thesis would not have been possible without the contribution from Mr. Anindya Roy who dedicated a lot of time for instrumentation and data acquisitions of the system. I am grateful to all the members of the Helium Technology & Low Temperature Physics section, VECC for their co-operation. Special thanks are also due to VECC workshop for helping me to build the experimental apparatus. Finally, I thank my wife Jaya for her constant support and encouragement that helped me in completing my thesis.

# Preamble

This thesis deals with thermo-dynamical studies of dilution refrigerator leading to the design and developments of a dilution refrigerator. A thermal model of dilution refrigerator has been established using numerical simulation which allowed us to carry out a comprehensive study of time dependent analysis of transitory phase. The simulation was used for design and optimization of the dilution refrigerator, which was built and tested in laboratory as a part of this thesis work.

The introductory **Chapter 1** describes briefly the historical development of thermodynamic process for producing low temperature, more specifically the process involved in development of dilution refrigerator. A property of helium isotopic mixture relevant to dilution refrigerator has been discussed. Also working principles of dilution process and its practical implementation for producing sub-Kelvin temperatures is presented in this chapter. Different thermo-dynamical models of dilution refrigerator and their limitations are also briefly discussed in this chapter.

In **Chapter 2** different components of dilution refrigerator which were designed and fabricated are described. The chapter also highlights the design features and performance of each component in the perspective of the present work. The operational procedures necessary to identify the transient simulation carried out in the present work are also described in this chapter.

In **Chapter 3**, complete thermal model of dilution refrigerator and analysis under steady state have been described. The possible factors responsible for performance degradation of dilution refrigerator are identified. Finally our simulation results as well as results based on other existing models are compared with available experimental data.

In **Chapter 4** the transient process during cool down and phase separation leading to steady state configuration is discussed. For this, steady state simulation is extended by introducing additional time variable. The results are compared with measured values of cool down time during experimental run.

Finally **Chapter 5** contains a summary of the work done in this thesis and identifies possible areas for future studies.

The work presented in the thesis has led to a number of publications. The list is given below:

1. *Transient phenomena initiating phase transition in dilution refrigerator*,  
**Jedidiah Pradhan**, Nisith K. Das and Alok Chakrabarti  
Cryogenics 63(2014), 69-76.
2. *Thermodynamic process simulation of dilution refrigerator*,  
**Jedidiah Pradhan**, Nisith K. Das and Alok Chakrabarti  
Cryogenics 57(2013), 158-165.
3. *Design and performance of a  $^4\text{He}$ -evaporator at  $< 1.0\text{K}$* ,  
N.K. Das, **J. Pradhan**, Md. Z.A. Naser, A. Roy, B.Ch. Mandal, C. Mallik and  
R.K. Bhandari  
Cryogenics 52(2012), 679-684.
4. *Three stage vacuum system for ultralow temperature installation*,  
N.K.Das, **J. Pradhan**, Md. Z.A. Naser, B.C. Mandal, A. Roy, P. Kumar, C. Mallik  
and R.K. Bhandari  
Jour. Of Phys.: 390 (2012) 012055
5. *Design Optimization of 1K-Helium Evaporator*  
N. K. Das, **J. Pradhan**, Md. Z.A. Naser, C. Mallik and R.K. Bhandari,  
Indian. Jour. of Cryogenics, 36(2011), 55-57.

6. *Design of still for dilution fridge*

Bidhan Chandra Mandal, Md Zamal Abdul Naser, Nisith Kumar Das, **Jedidiah**

**Pradhan**, Aninday Roy, Chaturanan Mallik and Rakesh Kumar Bhandari

Indian Jour. of Cryogenics, 38(2013), 160-165.

# List of Figures

1.1	Phase diagram of liquid $^3\text{He}/^4\text{He}$ mixtures at saturated vapour pressure with three different regions. Fermi temperature $T_F$ of $^3\text{He}$ is also shown -----	7
1.2	Specific heat $C/RT$ of $^3\text{He}$ and of two dilute solutions of $^3\text{He}$ in $^4\text{He}$ at saturated vapour pressure [13, 27]. In this figure $C$ is specific heat per total number of helium moles -----	9
1.3	$T^2 - x$ diagram giving the lines of constant osmotic pressure $\Pi$ ( solid lines and value in Pa) and lines of constant osmotic enthalpy ( dotted lines and value in J/mole) -----	10
1.4	Vapour pressure of liquid $^3\text{He}$ and liquid $^4\text{He}$ -----	11
1.5	Comparison of cooling power between $^3\text{He}/^4\text{He}$ dilution refrigerator and $^3\text{He}$ evaporative cooling-----	16
2.1.1	Dilution Insert showing different components along with schematic diagram -----	23
2.2	Dilution refrigerator set-up developed in the laboratory -----	24
2.3	General layout of housing cryostat -----	25
2.4	Cryostat top plate is mounted on three air springs and all the pumping lines are connected through bellows to reduce vibrations -----	27
2.5	Details of 1K pot suspended from IVC flange -----	28
2.6	Flow chart for pumping line optimization -----	29
2.7	Contours of temperature depicting different sections of pumping line -----	30
2.8	Cooling power at different temperatures measured by varying heater power attached to 1K pot ( $^4\text{He}$ evaporator)-----	31

2.9	Temperature of 1K pot ( <sup>4</sup> He evaporator) over a period of time -----	32
2.10	Evaporative <sup>4</sup> He mass flow rate Vs pressure drop across pumping line measured by varying heater power attached to 1K- pot-----	33
2.11	Characteristics behavior of 1K pot for three different impedance values -----	34
2.12	Impedance value and corresponding leak rate-----	35
2.13	Schematic of still and its photograph-----	37
2.14	Minimum heater power required to vaporise superfluid <sup>4</sup> He film creep under different liquid levels inside the still -----	38
2.15	Molar flow rates under different pressure across still pumping lines -----	39
2.16	3D- Model of HeX and its photograph showing with mixing chamber -----	42
2.17	Scheme as well as measurement of flow impedance in both dilute and concentrate channels of HeX -----	42
2.18	Gas circulation and handling system along with schematic flow diagram -----	45
2.19	Instrumentation rack and Labview based Graphical User Interface for monitoring different parameters of DR -----	46
2.20	MSLD connected for leak testing of different joints and interfaces -----	50
3.1	Schematic flow diagram of dilution refrigerator used in simulation-----	64
3.2	Schematic diagram of still and its control volume showing flow lines into and out of it-----	66
3.3	Normalized cooling power verses normalized temperature based on Frossati, Takano and the present model-----	80
3.4	Comparison of the maximum cooling power for $T_i=T_m$ -----	81

3.5	Degradation of cooling power with $^4\text{He}$ percentage in the circulating flow -----	81
3.6	Decrease of incoming $^3\text{He}$ temperature $T_i$ with MC temperature for a given flow rate $\dot{m}$ - -----	82
3.7	(a)Variation of molar flow rate on still heater power showing the film suppression effect and (b) comparison with measurement for total flow ( $^3\text{He}+^4\text{He}$ )-----	83
3.8	Comparison of simulation and measurement of mixing chamber temperature under different still heater powers -----	84
3.9	Comparison between simulation and measurement for applied power $Q_m$ to the mixing chamber under different MC temperature for still power of 0.4mW -----	85
3.10	Relation between the total molar flow rate, the $^4\text{He}$ concentration in the circulating gas and the still temperature $T_s$ -----	86
3.11	Variation of osmotic pressure across mixing chamber and still with molar flow rate for various mixing chamber temperatures -----	87
3.12	Required pressure margins with respect to $^3\text{He}$ vapour pressure before still under three different heater settings -----	88
3.13	Variation of total pressure head with still heater power under three different pot temperatures -----	89
3.14	Typical temperature profile along the HeX for $T_{mc}=50\text{mK}$ -----	90
3.15	Parameters responsible for the convection instability to grow as a function of temperature along the dilute channel -----	91

4.1	Algorithm used in transient simulation for extended SIDFO. It involves sub-routines for each components making up the complete dilution refrigerator ---	103
4.2	Cool-down of MC under four different still temperatures along with experimental cool-down curve -----	105
4.3	Variation of still heater powers with time to maintain a given still temperature -----	106
4.4	Time evolution of phase separation interface along the length of the concentrate channel of HeX -----	107
4.5	Time evolution of accumulated fraction of dilute solution $h_m$ , and within the MC under two different rr values -----	108
4.6	Time evolution of $^3\text{He}$ concentration within the MC and still -----	109
4.7	Fraction of accumulated dilute solution inside MC, $h_m$ under different MC temperatures for a given rr, considering an initial $^3\text{He}$ concentration of 0.25 and 0.3 respectively -----	109
4.8	Comparisons between simulation results and experimental data for transient response of MC temperature by reducing heater power attached to MC -----	110
A.	Temperature and pressure variation along the length of impedance ( $Z_p = 2 \times 10^{12} \text{ cm}^{-3}$ ) -----	119
B.	Algorithm for simulating steady state -----	121

# List of Tables

2.1.	Heat load to helium bath -----	26
2.2.	Heat load to 1K pot-----	30
2.3.	Parameters of tubular helical HeX -----	43
3.1.	Maximum build up pressure for non-accelerating superfluid column -----	92
4.1.	Phase separation temperatures under different $^3\text{He}$ concentration in the $^3\text{He}/^4\text{He}$ mixture-----	107

# List of symbols

## Nomenclature

### Subscripts

Symbol	Name
3	$^3\text{He}$
4	$^4\text{He}$
c	Concentrate solution of $^3\text{He}/^4\text{He}$
d	Dilute solution of $^3\text{He}/^4\text{He}$
s	Still
l	Lower dilute solution
u	Upper concentrated solution
i	Initial homogenous mixture
visc	Viscous
cond	Conduction
opt	Optimum
MC/m	Mixing Chamber
HeX	Heat Exchanger
GHS	Gas Handling System
SIDFO	Simulation of Integrated Dilution Refrigerator for Optimization
DR	Dilution Refrigerator

## Symbols used in equations

He	Helium
He-I	Normal fluid He
He-II	Superfluid He
LHe	Liquid helium

LIN/LN <sub>2</sub>	Liquid nitrogen
P	Pressure
P <sub>sat</sub>	Saturated vapour pressure
P <sub>v</sub>	Vapor pressure in the still
P <sub>i</sub>	Pump inlet pressure
ΔP	Pressure drop
P <sub>c</sub>	Total pressure at an elevation h <sub>c</sub> above phase boundary in the MC
Π	Osmotic pressure of <sup>3</sup> He in the dilute solution of <sup>3</sup> He/ <sup>4</sup> He
Δ Π	Osmotic pressure drives across MC and still
T	Temperature
T <sub>m</sub>	MC temperature
T <sub>i</sub>	Temperature of concentrated mixture before entering MC
T <sub>F</sub>	Fermi temperature
T <sub>λ</sub>	Normal to superfluid temperature
T <sub>pot</sub>	1K pot temperature
T <sub>s</sub>	Still temperature
ΔT	Temperature step/change
S	Entropy
m <sup>*</sup>	Effective mass of <sup>3</sup> He in the <sup>3</sup> He/ <sup>4</sup> He solution
C	Specific heat
C <sub>d</sub> , C <sub>c</sub>	Specific heat of dilute and concentrate solution
μ	Chemical potential
ρ	Mass density
η	Viscosity
β	Coefficient of thermal expansion

$k$	Thermal conductivity
$g$	Acceleration due to gravity
$\mu_4$	Chemical potential of $^4\text{He}$ in dilute solution
$\mu_4^0$	Chemical potential of pure $^4\text{He}$
$R$	Gas constant and also radius
$H$	Enthalpy
$\Delta H$	Change of enthalpy
$H_d$	Enthalpy of dilute solution
$H_c$	Enthalpy of concentrate solution
$H_l$	Saturated enthalpy (dilute solution)
$H_{30}$	Enthalpy of pure $^3\text{He}$ component
$H_{40}$	Enthalpy of pure $^4\text{He}$ component
$h_d$	Elevation of the vapour interface in the still above the phase boundary
$h_c$	Elevation on the concentrate side above phase boundary in the MC
$x$	$^3\text{He}$ molar concentration and also length unit
$x_i$	Concentration of dilute phase at temperature $T_i$
$x_s$	$^3\text{He}$ molar concentration in the still liquid phase
$x_v$	$^3\text{He}$ concentration in vapor phase
$x_m$	$^3\text{He}$ concentration in MC
$x_{l,u}$	Moles of $^3\text{He}$ in lower dilute or upper concentrated solution
$y_{l,u}$	Moles of $^4\text{He}$ in lower dilute or upper concentrated solution
$M_4$	Molecular weight of $^4\text{He}$
$R_k$	Kapitza resistance
$R_{kt}$	Kapitza resistivity coefficient
$\dot{Q}$	Heat flow/cooling power and also throughput of pump

$Q_c$	Critical cooling power (1K pot)
$Q_{hc}$	Critical heater power of still
$Q_{ht}$	Still heater power
$\Delta Q$	Change of heat flow/cooling
$Q_{mr}$	Residual heat leak
$Q_s$	Available cooling in still
$Q_m$	Cooling power at MC
$dH_c$	Increase of enthalpy of the dilute solution inside still due to circulating mixture
$A$	Contact surface area
$z$	Position along the HeX / vertical distance
$Z_p$	Flow impedance
$d$	HeX tube diameter
$t$	Thickness of superfluid film and also time
$v_s$	Superfluid velocity
$v_{crit}$	Critical velocity of $^4\text{He}$ superfluid film
$h$	$^4\text{He}$ superfluid film height from liquid surface
$dx$	Small length/section of the heat exchanger along axial direction
$S_{eff}$	Effective surface area of the HeX
$S_{geom}$	Geometric surface area of the HeX
$S_d, S_c$	Cross section normal to flow direction in the dilute and concentrated side
$L$	HeX length
$L_{sep}$	Position of interface from the warm ends of HeX
$p$	Surface area per unit length

$\varepsilon$	Heat exchange effectiveness
$N$	No of section of heat exchanger
$\dot{V}$	Volume flow rate
$V_m$	Molar volume
$V_3$	Molar volume of $^3\text{He}$
$V_4$	Molar volume of $^4\text{He}$
$V_{mc}$	Liquid volume in the MC
$V_s$	Liquid volume inside the still
$V^i$	Molar volume of initial mixture
$V_{hx}$	Liquid volume inside HeX
$V_c$	Condenser volume
$rr$	Ratio of volumes, $\frac{V_s}{V_{mc}}$
$h_s$	Ratio of liquid volumes, $\frac{V_s}{V_s^i}$
$h_m$	Fraction of mixer volume occupied by dilute solution
$\dot{m}$	Molar flow rate
$\Delta t$	Time step
$n$	Number of moles
$S_p$	Effective pumping speed
IVC	Inner Vacuum Chamber
OVC	Outer Vacuum Chamber
DAQ	Data Acquisition
MSLD	Mass Spectrometer Leak Detector

# Synopsis

Dilution refrigerator is a device that can achieve and maintain continuous refrigeration in the millikelvin temperature range with substantial cooling power. It is uniquely qualified for continuous cooling required for advanced research and emerging technologies. This is the only refrigerating method for temperature below 0.3 K and can run uninterruptedly over months. In addition, magnetic fields often needed in low temperature experiments have negligible effects on its performance. Today dilution refrigerators are the essential part of virtually all apparatus for achieving and maintaining temperature of less than 0.3 K. Low temperature quest in terms of strange physical phenomena in experimental physics and technology are really not possible without sufficient knowledge on the properties of matters at low temperature. A good many properties of matter are revealed only at sub-Kelvin temperature. For example super fluidity in  $^3\text{He}$  occurs only at sub-Kelvin temperature range. Behavior of materials that are obscured by thermal motion at relatively higher temperature can be studied in great details down to sub-Kelvin temperature. The active research area includes quantization of lattice vibrations (phonons), electronic excitations, superconductivity, super fluidity, dilute magnetic alloys and many aspects of magnetism. Radiation and particle detectors are cooled to a temperature of several hundredth of Kelvin that finds various applications due to high sensitivity and energy resolutions at this temperature range. Several frontier experiments in Physics, such as nuclear orientation experiments, gravitational wave antennas, cryogenic dark matter detectors and precision observation of rare events like the suspected neutrino less double beta decay are in need of dilution refrigerators to maintain sub-Kelvin temperatures.

Following the liquefaction of  $^4\text{He}$  in 1908 by Kamerlingh Onnes[1], it was successfully used further to achieve low temperature by reducing its vapour pressure. By

conventional evaporative method, temperature as low as 0.9 K are readily obtainable. There are difficulties in achieving temperature further down with liquid  $^4\text{He}$  by evaporative cooling since the vapour pressure of liquid helium decreases rapidly below 1K. The other difficulty is the presence of the super fluid  $^4\text{He}$  that creeps up along the wall at these temperature regimes until it reaches to some higher temperature. This results in an extra loading to the pumping system without enhancing to the cooling capacity. The other rare isotope of helium i.e.  $^3\text{He}$  having boiling point at 3.2 K was first liquefied in 1948 by Sydoriak, Grilly, and Hammel[2]. The vapour pressure of liquid  $^3\text{He}$  is much higher than that of liquid  $^4\text{He}$  over the operating temperature zone. For example, the vapour pressure of  $^3\text{He}$  at 0.71 K is about 1.5 mbar, which is around  $10^3$  times more than that of liquid  $^4\text{He}$ . The conventional evaporative cooling with liquid  $^3\text{He}$  provides temperature as low as 0.2K. The problem associated with superfluid film creeping does not occur with liquid  $^3\text{He}$  in this temperature range. A third common method of obtaining low temperatures is using adiabatic demagnetization of paramagnetic salts which can produce temperature as low as 2 mK. However the primary drawback of this demagnetization method is requirement of its intermittent operation unlike dilution refrigerator which operates in continuous mode. Further, application of external magnetic field as may be required for low temperature experiments affects its performance. The poor thermal conductivity of the paramagnetic salt limits to achieve the thermal equilibrium leading to temperature gradients and long thermal relaxation time in the sub-Kelvin temperature range.

In 1951, H. London [3] proposed a new cooling process which makes use of the entropy of mixing of  $^3\text{He}$  and  $^4\text{He}$  at low temperatures. London pointed out that the dilution of either  $^3\text{He}$  in  $^4\text{He}$  or vice versa is analogous to the adiabatic expansion of gas. Following the concept of London, a group at Leiden University built the first refrigerator in 1965 and reached a temperature as low as 0.22 K, the lowest temperature obtained with

$^3\text{He} / ^4\text{He}$  isotopic mixture. Following the developments of dilution refrigerator at Leiden, many such units are developed and are under operation in various laboratories all over the world.

Dilution refrigerator uses an isotopic mixture of  $^3\text{He}$  and  $^4\text{He}$  which undergoes phase separation below about 0.85 K into  $^3\text{He}$  -rich (concentrated) and a  $^3\text{He}$  -poor phase (dilute). Owing to a large zero point motion of  $^3\text{He}$  compared to  $^4\text{He}$  because of its smaller mass, it has a higher vapor pressure than  $^4\text{He}$  at all temperatures. Moreover at sub-Kelvin temperature, almost all of the  $^4\text{He}$  atoms occupy the ground state orbital of the system and act as inert superfluid  $^4\text{He}$  background through which the  $^3\text{He}$  particle moves in dilution refrigerator. Concentrated,  $^3\text{He}$  -rich phase is less dense than dilute phase and floats over the dilute phase. The amount of  $^3\text{He}$  in dilute phase under equilibrium is about 6%, whereas the concentration of  $^4\text{He}$  in the concentrated phase is negligibly small. By pumping the  $^3\text{He}$  atoms from the dilute phase, the equilibrium is disturbed and  $^3\text{He}$  atoms have to cross the phase boundary to restore equilibrium. The energy required to evaporate  $^3\text{He}$  from concentrated phase to dilute phase is extracted from the fluids resulting in cooling of the system.

The dilution refrigerator system has mainly four distinct components, 1) 1K-pot, where  $^4\text{He}$  condenses, 2) Still, a container filled with  $^3\text{He} / ^4\text{He}$  solution in dynamic equilibrium with its vapour phase, 3) Heat exchanger, where the incoming concentrate phase cools by transferring heat to the returning dilute phase and 4) Mixing chamber, the coldest part where interface between the concentrated and dilute phases is situated. However gas circulation and handling system at room temperature also happens to be an important component of the system. The functioning of a dilution refrigerator primarily concerns with the condensation of circulating gas mixture and occurrence of phase separation within the mixing chamber. Dilution refrigerator starts with condensation of

isotopic gas mixture, which takes an hour or so to reach equilibrium at temperature of about 1.2-1.5 K. At this temperature,  $^4\text{He}$  becomes superfluid and  $^3\text{He}$  begins to condense. Based on the desired base temperature and cooling power of the refrigerator, an isotopic mixture of  $^3\text{He}$  and  $^4\text{He}$  is prepared. As the  $^3\text{He}$  molecules are pumped out from the still, temperature of the mixture gradually reduces leading to phase separation at high temperature end of concentrated channel of the heat exchanger. This eventually leads to the propagation of interface toward the mixing chamber. The performance of the system primarily depends on the effectiveness of the condenser, heat exchanger, initial isotopic gas composition, still heater power and the circulating system.

The available cooling power at the required sub-Kelvin temperature is the most important parameter of a dilution refrigerator. Various models have been developed to predict the cooling power of a dilution refrigerator as a function of the mixing chamber temperature. The available cooling power in continuous process of operation depends on the effective cooling of incoming  $^3\text{He}$  to the temperature of mixing chamber. Smaller flow rate of circulating  $^3\text{He}$  provides insufficient number of atoms that crosses the phase boundary resulting low cooling power. However, for higher flow rate, the concentrated stream ( $^3\text{He}$ ) is not cooled sufficiently in the heat exchanger and gives additional heat load into the mixing chamber. As a consequence, there is a optimum  $^3\text{He}$  flow rate for which maximum cooling power is achieved. Niinikoski[4] was the first to derive the theoretical model of dilution refrigerator which takes into account the finite efficiency of heat exchanger. The thermodynamic model proposed by Niinikoski allows one to calculate the mixing chamber temperature as a function of heat load and heat exchanger surface area at the optimum flow rate. Frossati[5] and co-workers derived the analytical solution which expresses the base temperature of the refrigerator in terms of the Kapitza resistance in the heat exchanger,  $^3\text{He}$  circulation rate and the heat leak to the mixing chamber. The model

developed by Frossati, however, does not correctly take into account the characteristics of the heat exchanger. Frossati's model may thus yield reasonable results for very high and very low flow rates, but not for moderate flow conditions. The difficulty arises from a somewhat unrealistic assumption on the temperature profiles in the concentrated and dilute side of heat exchangers. This drawback is further improved by Takano [6] considering suitable boundary conditions that describe properly the temperature profile along the heat exchanger. Another method based on nodal modeling technique has been developed at CERN in the framework of project which aims at developing powerful dilution refrigerators for future generations of cryogenic dark matter detector arrays [7]. In this model, the dilution refrigerator is considered as a number of discrete nodes which are linked by conductors. A solution is then obtained by solving for thermal equilibrium.

The present work describes the dovetail of all components of the dilution refrigerator making up a complete closed cycle simulation where the boundary conditions are fixed by the performance of other ancillary components. The calculation takes care of any flow condition which might occur in practice. Hence, in the thesis a numerical model has been developed for dilution refrigerator based on the thermodynamics of the  $^3\text{He}/^4\text{He}$  isotopic mixture. The required cooling power is determined in combination with heat dissipation obtained from the experiment and the residual heat load due to mechanical vibration, etc.

While some scattered results of discrete analyses of the thermo-dynamical processes related to dilution refrigeration have been published, a comprehensive and closed thermodynamic process simulation of dilution refrigeration from room temperature down to the base temperature of less than 50mK has not been done so far. Further, no detailed study to investigate the time dependent manifestation of transitory phases has been made earlier. All these practical considerations have been addressed by developing a

comprehensive numerical simulation model SIDFO (Simulation of Integrated Dilution Refrigerator for Optimization) [8]. It yields several unique results of the underlying phenomena occurring at various stages of the very low temperature process. The presence of  $^4\text{He}$  in the circulating gas and its consequences for the generalized cooling power is thoroughly examined and revisited. In addition, the simulation also takes into account the effect of arbitrary flow rates in the circulating  $^3\text{He}$  gas on the resulting performance. The interplay between the still power and flow rate on the cooling power and the mixing chamber temperature is also investigated in details. The simulation code has been benchmarked by verifying the results from SIDFO with the measurements obtained from dilution refrigerator systems which have been designed, built and tested at different laboratories. The results of SIDFO is also compared with models developed by others like Frossati and Takano and is found to yield better results while estimating cooling power with traces of  $^4\text{He}$  in the circulating gas under different flow conditions. The thermodynamic property of helium isotopic mixture has been compiled for temperature range down to sub-Kelvin from several literatures for the purpose of simulation. The fact that these properties vary with both temperature and concentration make them difficult to study using analytical approach due to its inherent limitations.

The transient process during cool down has also been extensively studied that involves phase separation of  $^3\text{He}/^4\text{He}$  mixture into concentrated and dilute solutions [9]. The base temperature is obtained following the phase separation in an iterative way from a homogenous mixture of liquid  $^3\text{He}$  and super fluid  $^4\text{He}$ . The transient behaviour provides various thermodynamic process parameters responsible for the optimal cool-down and operation of the machine. The simulation also takes care of the intricate relationships among the subsystems and provides a better understanding for trouble shooting during operation of the refrigerator. The importance of the  $^3\text{He} / ^4\text{He}$  composition in the mixer,

the flow rate and the still power on the phase separation has been thoroughly investigated and details are presented. The consequences of several relevant thermodynamic parameters and the composition of isotopic mixture for successful operation of the dilution refrigerator are set forth here.

The design, analysis and optimization of a dilution refrigerator system which is developed at VECC, Kolkata are carried out using SIDFO. The refrigerator is designed to achieve minimum temperature of less than 50mK. The designed flow rate at steady state is about 20 micro-moles/secs with maximum flow of about 200 micro-moles/sec. The tube-in-tube helical heat exchanger is used for transferring heat between incoming concentrate and returning dilute solution from mixing chamber. As a way of maintaining the desired circulation, condensing pressure, impedance and flow rate in the 1K-pot were designed using SIDFO. The 1K-pot with flow impedance has been fabricated and successfully tested and cooling power of 18mW at 1.2K is obtained [10]. The heater power in the still for a given flow rate yielding maximum cooling power is derived through simulation. Selection of suitable still heater power and still temperature during cool-down is optimized so as to attain the steady state temperature in minimum time. To ensure the maximum possible heat exchange between the concentrated and dilute phase, the effective surface area, the flow rate and tube sizing, etc. have been optimized using SIDFO.

The thermo dynamical analysis of steady state and transient processes through SIDFO has helped us to conceptualize and design a complete dilution refrigeration system. The results of simulation were compared with experimental data derived from measurements carried out with our dilution refrigerator.

## **Bibliography**

1. H. Kamerlingh Onnes, KNAW, Proceedings 11, 1908-1909, Amsterdam (1909), p 168-185.

2. S. G. Sydoriak, E. R. Grilly and E. F. Hammel, *Phys. Rev.* 75(1949), 303.
3. H. London, G.R. Clarke, E. Mendoza, *Phys. Rev.* 128(1962), 1992.
4. Niinikoski T.O. *Nucl. Instr. and Methods* 97(1971), 95.
5. G. Frossati, *J. Low Temp. Phys.* 87(1992), 595.
6. Y. Takano, *Rev. Sci. Instrum.* 65(5), 1667 (1994).
7. Patrick Wikus, T.O. Niinikoski, *J. Low Temp. Phys.* 158(2010), 901-921.
8. Jedidiah Pradhan, Nisith K. Das and Alok Chakrabarti, *Cryogenics* 57(2013), 158-165.
9. Jedidiah Pradhan, Nisith K. Das and Alok Chakrabarti, *Cryogenics* 63(2014), 69-76.
10. N.K. Das, J. Pradhan, Md. Z.A. Naser, A. Roy, B.Ch. Mandal, C. Mallik and R.K. Bhandari, *Cryogenics* 52(2012), 679-684.

# Chapter 1

## Introduction

### 1.1 Historical Survey

The properties of materials are controlled to a large extent by thermal lattice vibrations. Thermal vibrations greatly influence the elastic, magnetic and transport properties of solids and therefore to study materials the temperature often needs to be lowered to a point where the thermal lattice vibrations are drastically reduced. In particular, electron-phonon interactions, which are extremely important in the transport properties of solids, will normally be observable only at very low temperatures. The lower the temperature, the larger are the chances to detect these interactions. Many subtle behaviors of materials can be comprehensible only after matter is cooled to the sub-Kelvin range or even lower temperatures. For example, unusual phase transition in matter such as super fluidity in  $^3\text{He}$  manifest only at millikelvin temperature.

Helium evaporation is an important cooling technique. The lowest temperature it can reach is limited by the vapour pressure. Since the vapour pressure decreases exponentially with falling temperature, cooling by evaporation of  $^4\text{He}$  liquid only allows us to reach a temperature of about 1K. Below this temperature, the vapour pressure is very small, so very little would evaporate. Because of the lower mass of the  $^3\text{He}$  atom, it has higher vapour pressure and therefore higher vaporisation rate. Hence, we can reach further down to 0.3K, if we use  $^3\text{He}$  instead of  $^4\text{He}$ . Cooling below 0.3K is not possible by conventional refrigeration technique. Another method of obtaining low temperatures uses adiabatic demagnetization of paramagnetic materials which is capable of reaching

extremely low temperatures. However, low temperature is attained only for short time-intervals and thus it is a one-shot process. Furthermore, application of external magnetic field as may be required for low temperature experiments affects its performance. All these methods provide different low temperature, cooling power, and the time dependent stability and control of temperature. Each of these techniques has its advantages in some cases and disadvantages for others.

Dilution refrigerator is uniquely qualified to provide continuous cooling in the millikelvin temperatures with substantial cooling power. It can produce a stable base temperature of few millikelvin to serve as a starting point for very low temperature experiments. The concept of a  $^3\text{He}/^4\text{He}$  mixture being used for the cooling process in dilution refrigerator was first proposed by Heinz London in 1951[2]. It was thought as a dramatic macroscopic quantum effect, predicting a cooling process resulting from the mixing of particles following two different statistical thermodynamic laws. London suggested that perhaps the demagnetization of paramagnetic salts was not the only method to reach lower temperatures. However with the discovery of phase separation in liquid  $^3\text{He}/^4\text{He}$  mixtures below  $0.8^\circ\text{K}$  by Waiters and Fairbank [3] in 1956 meant that a more powerful cooling process analogous to liquid evaporation was available where two layers of liquid were formed below  $0.8^\circ\text{K}$  temperature,  $^3\text{He}$  rich floating on top of the  $^4\text{He}$  rich phase. The upper  $^3\text{He}$  rich phase plays the part of the liquid and the lower dilute phase plays the part of the vapour, whereas the osmotic pressure of the solution plays the part of the vapour pressure. This phase separation was a year later visualised in a glass apparatus by Zinove'va and Peashkov [4]. However already in 1948 Daunt, Probst and Johnston had observed some kind of osmotic pressure in solution of  $^3\text{He}$  in superfluid  $^4\text{He}$  [5]. A complete analysis of thermodynamics of the helium isotopic mixtures ( $^3\text{He}/^4\text{He}$ ) was given in 1960 by de Bruyn, Oubutor, Taconis, Le pair and Beenakker [6]. With the discovery of

a  $^3\text{He}/^4\text{He}$  phase separation at low temperatures, London suggested the clear feasibility of a continuous dilution cooling process. In 1962, London and co-workers suggested some experimental techniques for building such a refrigerator with possible methods of re-circulating  $^3\text{He}$  in order to provide continuous cooling [7]. This involves dilution across the phase boundary at a low temperature and re-concentration of  $^3\text{He}$  by distillation at a higher temperature and re-circulating  $^3\text{He}$  for continuous refrigeration. The atoms of  $^3\text{He}$  dissolves into the lower superfluid phase at the phase separation surface and "evaporates" as an ideal gas resulting in the cooling effect. Londons designs use separate  $^3\text{He}$  refrigerators to re-condense the gas from the distillation chamber called still. Hall [8] suggested that the separate  $^3\text{He}$  refrigerator may be eliminated and the  $^3\text{He}$  from the still be recompressed at room temperature and condensed at 1K in  $^4\text{He}$  bath. By the late 1960's, several groups had reported construction of dilution type refrigerators. At the LT9 conference Das and co-workers [9] reported the first dilution refrigerator built at Leiden which obtained a temperature of 0.22K but was not very impressive. A year later, in 1965, Edwards, Brewer, Sel- igman, Scertic and Yagub [10] made the very important discovery that even at absolute zero 6.4% of  $^3\text{He}$  remained dissolved in the superfluid  $^4\text{He}$ . It meant that even at absolute zero temperature there is still an osmotic pressure and hence  $^3\text{He}$  could evaporate into the superfluid phase.

The first truly successful dilution refrigerators were built in 1966 by two independent groups. One of these was Neganov et.al. [11] who obtained a low temperature of 25m K with a large set up and later reached to temperature of 8mK The other group was Hall et. al. [8] who obtained a low temperature of 50mK. It is the Kapitza heat resistance between the liquid helium and the wall of the heat exchanger that finally limits the attainable temperature. Subsequently, research effort was focussed on the construction of very effective heat exchangers with large surface to volume ratio. And considerable

effort was spent in optimizing the performance of the various parts of the dilution refrigerator. In 1968 Wheatley, Vilches and Abel [12] introduced sintered copper, a porous sponge, to increase effective surface between liquid and metal wall. The dilution refrigerator built by Vilches and Wheatley achieved a continuous operating temperature of 20mK. After optimizing their heat exchangers and experimenting with a wide variety of geometries and construction materials, Vilches and Wheatley constructed a dilution refrigerator with a cooling capacity of 100  $\mu$ W which could be operated continuously at 10mK [13, 14]. It could also be operate in a single cycle mode by removing  $^3\text{He}$  from a mixture without recycling the  $^3\text{He}$ . This obtained the temperature of 4.5 mK for at least 30 minutes [15]. This design represents the current state of the art in  $^3\text{He}/^4\text{He}$  dilution refrigerators. Wheatley formed a company called the S.H.E. Corporation and markets a line of commercially manufactured dilution refrigerator systems and support components. Niinikoski was quite successful in obtaining very high cooling power by introducing copper sponge heat exchangers provided with a hole to decrease the impedance to the flow [16]. In terms of  $^3\text{He}$  circulating machine the most successful improvements are due to the Grenoble group who worked with the idea of continuous, perfect heat exchangers. Here large specific areas (surface to volume ratio) were obtained with silver powder by evaporating it in a partial pressure of an inert gas. More than  $10 \text{ m}^2 / \text{cm}^3$  for a 400  $\text{\AA}$  diameter particle size are obtained after this sintering process. Currently the lowest temperature they achieved is 2mK. An improvement of the  $^3\text{He}$  circulation circuit in the refrigerator has been explored since 1976 and is still studied. In 1972 Richardson and Lee [17] discovered the superfluidity of  $^3\text{He}$  below 2.6mK. Soon many low temperature laboratories concentrated their attention on the behaviour of superfluid  $^3\text{He}$  with its complicated new and unexpected phase diagram and other related extraordinary features.

However there are many dilution refrigerator under construction or operating but they are based on the general design of the earlier refrigerator.

## 1.2 Properties of $^3\text{He}/^4\text{He}$ Mixtures

Helium is the second lightest element and it has two stable isotopes,  $^4\text{He}$  and  $^3\text{He}$ , of which  $^4\text{He}$  is the more abundant on earth. Because of the small mass and the complete electron shell structure of the atom, the inter-atomic bonds are weak compared to the zero point energy, which makes helium unique in several ways. At low temperature, quantum mechanical effects are strong and govern the helium physics. Both the isotopes remain liquid even at absolute zero under its own vapour pressure. Although solid state too can be achieved but at considerably high pressure (2.5 MPa for  $^4\text{He}$  and 3.4 MPa for  $^3\text{He}$ ). Also their boiling points are the lowest known (4.2 K for  $^4\text{He}$  and 3.19 for  $^3\text{He}$  at saturated vapour pressure). The difference of mass of two helium isotopes results in different zero-point motions and follows different statistics which helps to understand their properties at low temperature. The  $^4\text{He}$  atom has integer spin and is governed by Bose-Einstein statistics.  $^3\text{He}$  on the other hand, has a half integer spin and is governed by Fermi-Dirac statistics. At temperature of about 2 K (2.17K at saturated pressure),  $^4\text{He}$  goes through what is known as a  $\lambda$ -transition. This transition is analogous to Bose-Einstein condensation. Above the  $\lambda$ -transition temperature,  $^4\text{He}$  behaves like a normal fluid, which is designated as He-I. Its behaviour, however, is quite different below  $\lambda$ -transition temperature, where it is designated as He-II. He-II exhibits a viscosity several orders of magnitude less than that of normal liquid and an apparent thermal conductivity several orders of magnitude greater than normal liquid. It is frequently modelled as being made of two fluids – a superfluid and a normal fluid. The superfluid carries no entropy and exhibits no viscosity. The normal fluid has a viscosity and entropy equal to the actual liquid

entropy. The number densities of the superfluid and the normal fluid sum up to the density of fluid. The superfluid density is zero at 2.17K, whereas normal fluid density is zero at 0 K, when all the  $^4\text{He}$  atoms are in the ground state. Although superfluidity is also observed in  $^3\text{He}$ , it occurs at very low temperature, i.e. below 3mK. Since this is beyond the reach of dilution refrigerator using  $^3\text{He}/^4\text{He}$  mixture, the present work  $^3\text{He}$  is assumed to be normal fluid.

Helium mixtures have even more diverse systems than pure isotopes. Experiments have shown that  $^3\text{He}$  is not miscible in  $^4\text{He}$  for all concentrations and temperatures. However, phase separation of  $^3\text{He}/^4\text{He}$  isotopic mixture below 0.87K produces two layers of liquid: a lighter  $^3\text{He}$  rich one floating on top of the  $^4\text{He}$  rich phase. The phase separation opens a great possibility for cooling as specifically indicated by London et al., in their paper of 1962 [2]. Three independent thermodynamic variables are required for the binary mixture of  $^3\text{He}$  and  $^4\text{He}$  to describe the thermodynamic state and its behaviour. It is conveniently chosen to be the temperature (T), pressure (P) and molar  $^3\text{He}$  concentration (x). Figure 1.1 showing the phase diagram of  $^3\text{He}/^4\text{He}$  mixture at saturated vapour pressure, in T-x plane. The left vertical axis describe pure  $^4\text{He}$ . Below the  $\lambda$ -point, at 2.17 K, pure  $^4\text{He}$  is superfluid. In region II (see figure 1.1), on the left side of the  $\lambda$ -curve, the  $^4\text{He}$  component in the mixture is superfluid. On the right side of this curve, in region I, the  $^4\text{He}$  in the solution is a normal fluid. It is seen that the super fluid phase transition of liquid  $^4\text{He}$  is depressed, if we dilute the Bose liquid  $^4\text{He}$  with the Fermi liquid  $^3\text{He}$ . Eventually the  $^4\text{He}$  super fluidity ceases to exist for  $^3\text{He}$  concentrations above 67%. At this concentration and at temperature of 0.87K the  $\lambda$ -line meets the phase separation line. Below 0.87K the phenomena of phase separation occur where the two isotopes are only miscible for certain limiting concentrations, which depend on the temperature. The shaded phase separation region III in the figure 1.1 is a non-accessible range of temperatures and

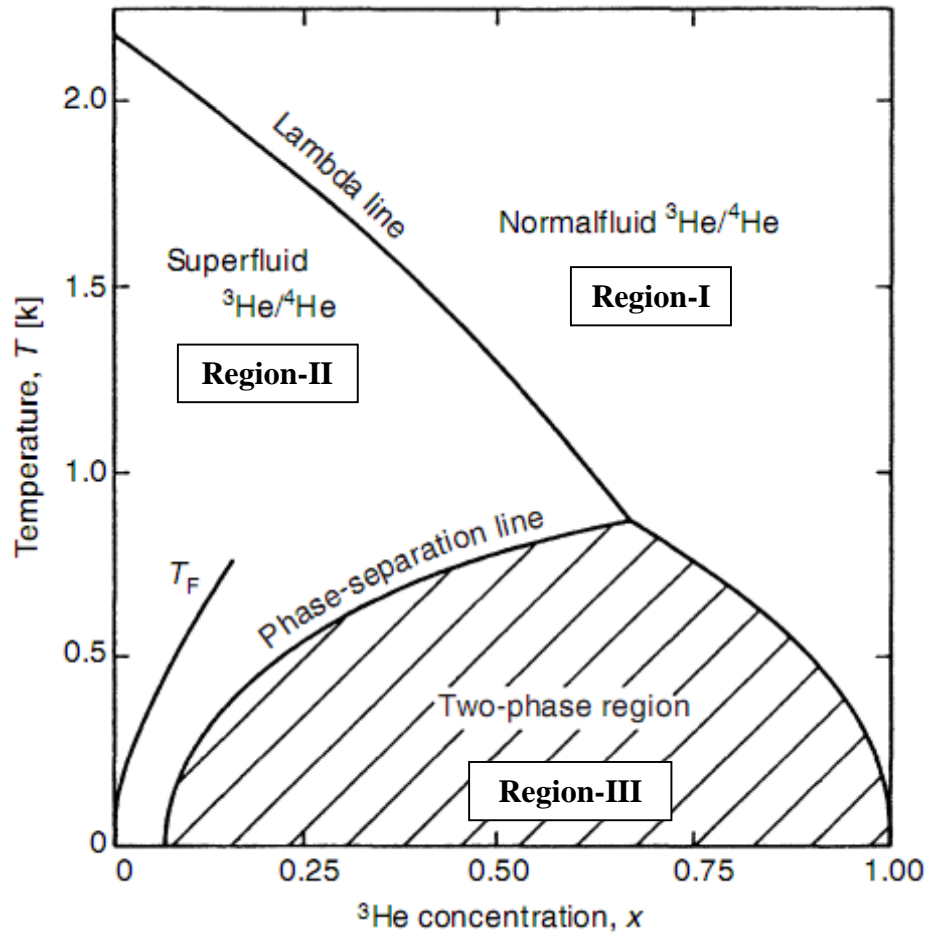


Figure 1.1 Phase diagram of liquid  $^3\text{He}/^4\text{He}$  mixtures at saturated vapour pressure with three different regions. Fermi temperature  $T_F$  of  $^3\text{He}$  is also shown.

concentrations for helium mixtures. Even though the two helium isotopes are chemically identical, the lighter  $^3\text{He}$  occupies larger volume due to larger zero point motion and thus the binding energy for any  $^3\text{He}$  atom is stronger in surroundings of  $^4\text{He}$  atoms. Because of Fermi statistics and Pauli exclusion principal the effective binding energy of  $^3\text{He}$  atom amongst the  $^4\text{He}$  atoms decreases with concentration, until a value close to that of a pure  $^3\text{He}$  system is reached and  $^3\text{He}$  rich phase is formed. The available states for Bosonic  $^4\text{He}$  atoms are not limited by quantum statistics. So the separated mixture has two phases: one rich with  $^3\text{He}$  and the other rich with  $^4\text{He}$ . The  $^3\text{He}$  rich phase is called simply concentrate phase and it becomes pure  $^3\text{He}$  as the temperature approaches zero. The phase with more

$^4\text{He}$  is called dilute phase and its  $^3\text{He}$  concentration remains finite even at absolute zero temperature. This finite solubility of  $^3\text{He}$  even at absolute zero temperature enables the dilution process to be carried out at any low temperature.

The heat capacity of both isotopes and their solution is an important property. At low temperatures the properties of materials are strongly influenced by statistical or quantum effects. This is particularly important for the specific heat of helium isotopes. The isotope of  $^4\text{He}$  has nuclear spin  $I=0$ , such a Bose liquid will undergoes a so called Bose condensation in momentum space which corresponds to its transition to the superfluid state. As a result its entropy and heat capacity decreases rapidly with reducing temperature, due to relative absence of excitations in particular the lack of rotons below 0.6K. Also this results in  $^4\text{He}$  component being in its ground state and acts only as an inert environment for the Fermi gas of  $^3\text{He}$  quasiparticles in dilute solution. In the  $^3\text{He}/^4\text{He}$  mixture,  $^4\text{He}$  contributes to the volume of the liquid and to the effective mass of dissolved isotope of  $^3\text{He}$  but has a negligible heat capacity. In the dilute phase  $^3\text{He}$  behaves as a classical ideal gas and the  $^4\text{He}$  entropy is negligible.

The rare and lighter isotope  $^3\text{He}$  with its nuclear spin  $I=1/2$  obeys Fermi statistics and the Pauli principle similar to conduction electrons in metal and the Fermi temperature is of the order 1K (see figure 1.1). The  $^3\text{He}$  atoms cannot undergo Bose condensation into super fluid state as the Bosons  $^4\text{He}$  does. However, there exists a weak attractive interaction between  $^3\text{He}$  atoms at very low temperatures  $T < 3\text{mK}$  which gives rise to pairing of two  $^3\text{He}$  atoms. The paired  $^3\text{He}$  atoms then behave like bosons and can undergo a transition into a super fluid state. The properties of liquid  $^3\text{He}$  at low temperatures are fundamentally different from those of  $^4\text{He}$ . At low temperatures the  $^3\text{He}$  component behaves as a degenerate Fermi gas, this leads to a specific heat of dilute solution which is high compared to pure  $^3\text{He}$  and pure  $^4\text{He}$  as shown in figure 1.2. This property together with the

solubility of  $^3\text{He}$  in  $^4\text{He}$  at zero temperature, leads to a relatively high osmotic pressure in the  $^3\text{He}/^4\text{He}$  mixture. Below the Fermi temperature, entropy of the dilute phase is directly proportional to temperature and the osmotic pressures has quadratic temperature dependence (figure 1.3) and are measurable quantities.

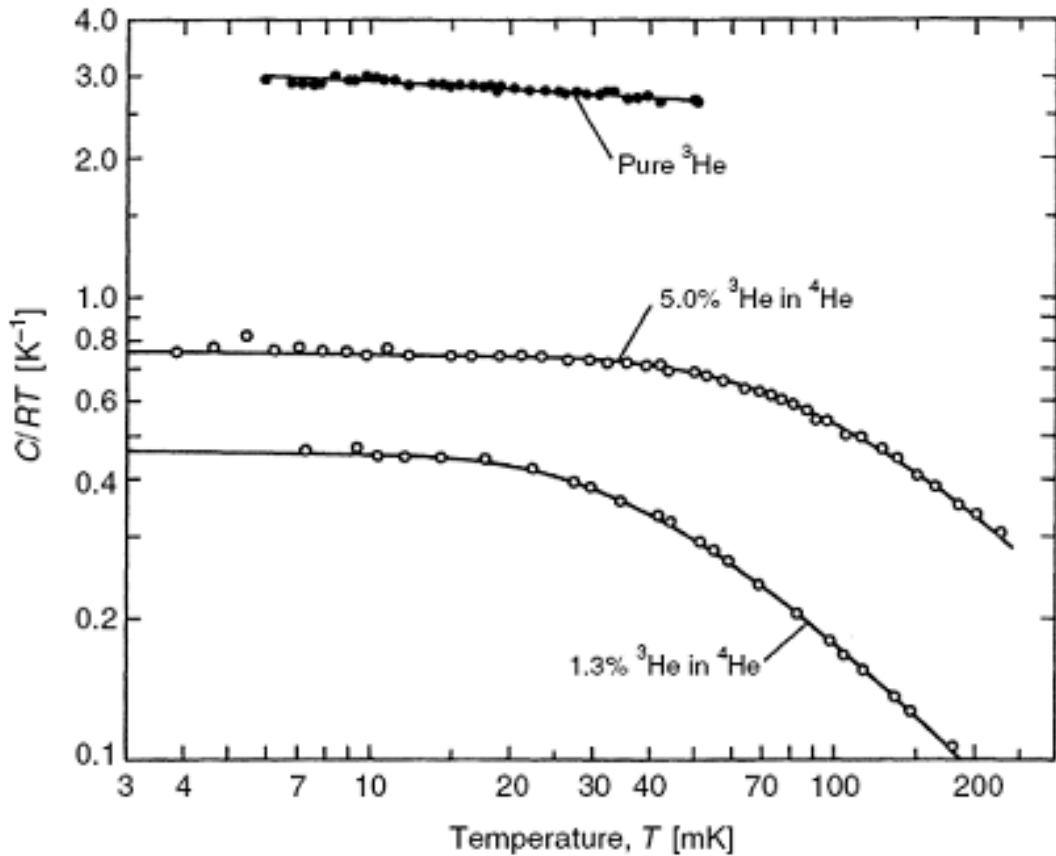


Figure 1.2 Specific heat  $C/RT$  of  $^3\text{He}$  and of two dilute solutions of  $^3\text{He}$  in  $^4\text{He}$  at saturated vapour pressure [13, 27]. In this figure  $C$  is specific heat per total number of helium moles.

The suggestion that  $^3\text{He}$  would behave as a Fermi gas in the super fluid  $^4\text{He}$  was first made by Landau and Pomeranchuk [18]. The thermodynamic properties of weakly interacting Fermi-Dirac gas are in very good agreement with all existing experimental data on  $^3\text{He}/^4\text{He}$  solutions for temperature below 1.5K. Edwards et al., [10] showed that the specific heat data fitted very well at all temperatures by treating the  $^3\text{He}$  as Fermions with

an effective mass  $m^*$  which is 2.5 times the mass of  $^3\text{He}$  atom, and is a measure of its interaction with the surrounding. The Fermi-Dirac gas model shows excellent promise for predicating the thermodynamic properties of  $^3\text{He}$  in liquid  $^3\text{He}/^4\text{He}$  solution at all temperatures. In this description  $^3\text{He}$  is treated as an interacting quasi-particle Fermi gas with a pressure equal to the osmotic pressure of  $^3\text{He}$  in  $^4\text{He}$ . The general property of interest is that the enthalpy of pure  $^3\text{He}$  is less than that of mixtures of  $^3\text{He}$  in  $^4\text{He}$  so that an adiabatic dilution of  $^3\text{He}$  in  $^3\text{He}/^4\text{He}$  solution results in a cooling process.

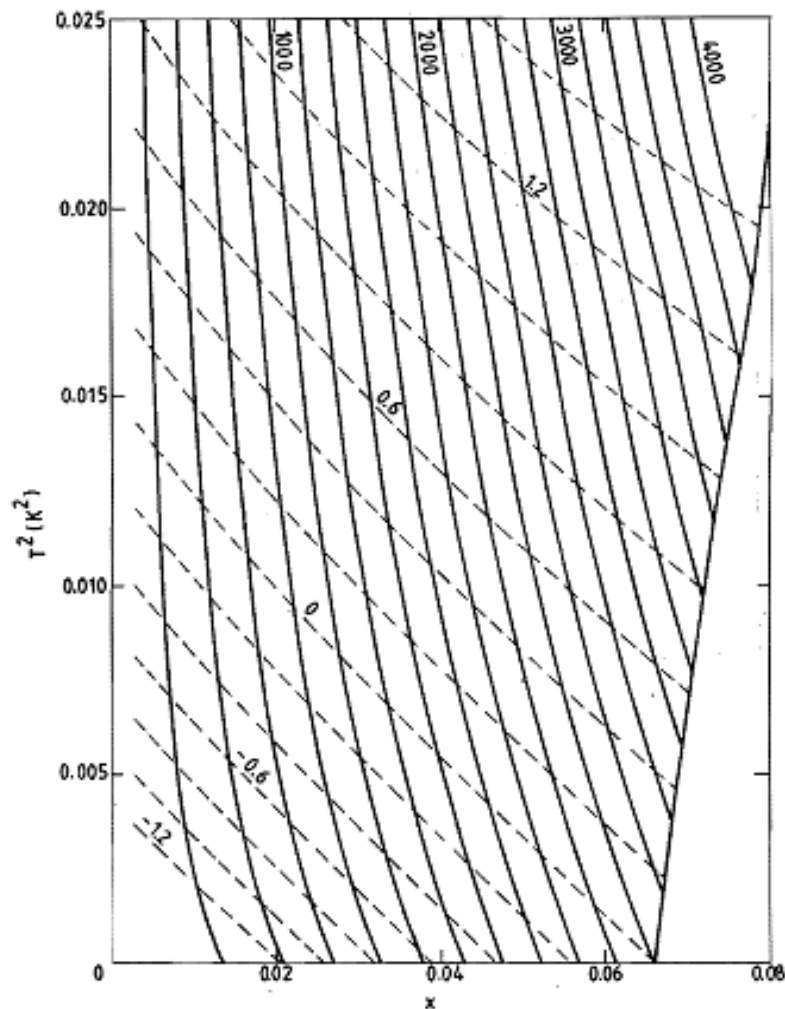


Figure 1.3  $T^2 - x$  diagram giving the lines of constant osmotic pressure  $\Pi$  (solid lines and value in Pa) and lines of constant osmotic enthalpy (dotted lines and value in J/mole).

Radebaugh published a comprehensive text on the thermodynamics underlying  $^3\text{He}/^4\text{He}$  dilution refrigeration with a compilation of the properties of the working fluid in 1967 [28]. Some of the Radebaughs property values were later found to be inconsistent with subsequent experimental measurements of the osmotic pressure and osmotic enthalpy [22]. In 1985 Kuerten et al [22] developed calculation scheme quite similar to Radebaugh's in that they treated the  $^3\text{He}$  component as an ideal Fermi gas too. However, they used experimentally determined values of osmotic pressure instead of Radebaugh's theoretical model. They determined thermodynamic properties only for temperatures below 0.25K and  $^3\text{He}$  mole fraction below 8%, because it was clear by that time (from experiments) that the theory for dilute solution of  $^3\text{He}$  in  $^4\text{He}$  did not extend up to the temperatures and concentrations covered by Radebaugh.

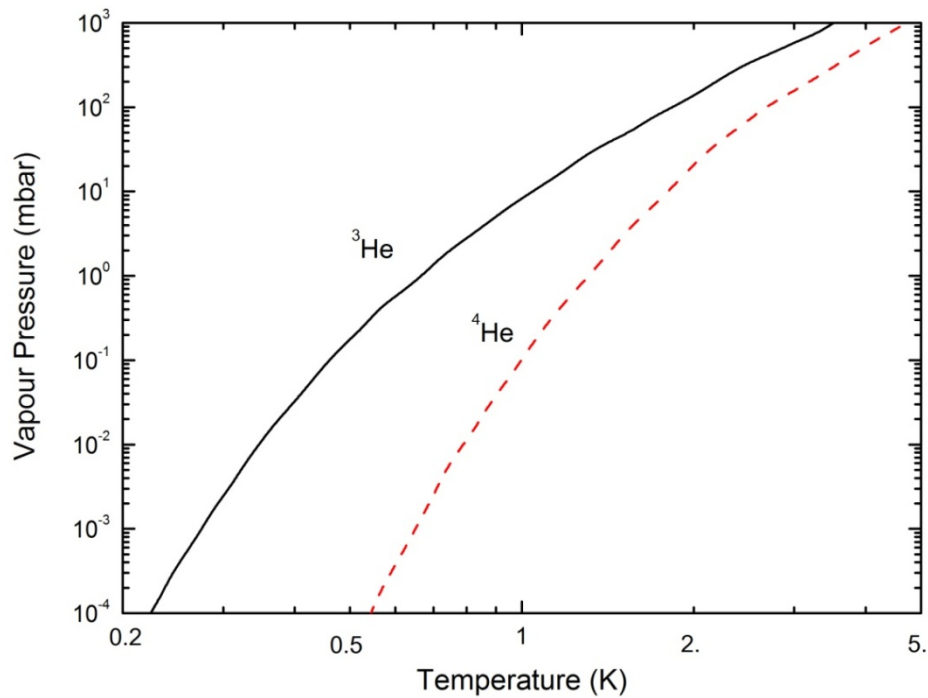


Figure 1.4 Vapour pressures of liquid  $^3\text{He}$  and liquid  $^4\text{He}$

Owing to the smaller mass of  $^3\text{He}$ , the influence of the zero-point energy is more pronounced for  $^3\text{He}$ , giving rise to its lower boiling point, smaller density, smaller latent

heat of evaporation and larger vapour pressure. The relative vapour pressure of  $^3\text{He}$  and  $^4\text{He}$  is given in figure 1.4. For typical still temperature of 0.7K or less, the vapour pressure of  $^3\text{He}$  is about  $10^3$  times that of  $^4\text{He}$ . The enrichment factor for distilling  $^3\text{He}$  from  $^3\text{He}/^4\text{He}$  mixture depends directly on the ratio of  $^3\text{He}$  and  $^4\text{He}$  vapour pressure. Thus the fractional distillation is a powerful means of separating  $^3\text{He}$  and is a convenient method for separation  $^3\text{He}$  in dilute refrigerators for close cycle circulation.

In a  $^3\text{He}$  circulating dilution refrigerator  $^3\text{He}$  flows through the super fluid  $^4\text{He}$  background of  $^4\text{He}$ . As such there is no generally accepted model for the hydrodynamics of  $^3\text{He}/^4\text{He}$  mixtures. Though, there is a mechanical vacuum model by Wheatley [13], in which it is assumed that there is no dissipative interaction between  $^3\text{He}$  and  $^4\text{He}$ . The validity of this model was confirmed at low  $^3\text{He}$  velocity [19], however it was not valid at higher  $^3\text{He}$  velocity [20, 21]. As at higher  $^3\text{He}$  velocity mutual friction arises from the interaction between the  $^3\text{He}$  particles and quantised vortices in  $^4\text{He}$ . There is a continuous transition from the mechanical vacuum model to a mutual friction model [22]. However in the intermediate regime of  $^3\text{He}$  velocity, the combined- dissipation of mutual friction and viscous force are both important, whereas in both extreme cases of  $^3\text{He}$  velocity one force dominates the other. Some measurements show that for  $^3\text{He}/^4\text{He}$  mixtures no mutual friction occurred below a certain critical  $^3\text{He}$  velocity [23]. This depends on the diameter of the flow channel. This mutual friction between  $^3\text{He}$  and  $^4\text{He}$  components plays an important role in dilution refrigerator.

The transport properties of liquid  $^3\text{He}$  in the Fermi-liquid temperature range, too, show a distinct T-dependence. Thermal conductivity increases as  $\frac{1}{T}$  at  $T \ll T_F$  and viscosity increases as  $\frac{1}{T^2}$  in the low milikelvin temperature range above its super fluid transition, making  $^3\text{He}$  a very viscous but well-conducting fluid at low temperatures.

However, viscous heating of  $^3\text{He}$  diffusing through the dilute phase is a limiting factor in determining the minimum temperature of the mixing chamber [14]. Though, the effect of viscous heating is negligible unless under very low temperature of less than 10mK.

Heat flow between two materials at low temperatures is impeded by a thermal boundary resistance which is known as the Kapitza boundary resistance when one of the materials is liquid helium. [24, 25, 26]. The thermal boundary resistance establishes a temperature discontinuity at the boundary whenever there is a heat flow. This temperature steps is given by

$$\Delta T = R_k \dot{Q}$$

where  $R_k$  is the thermal boundary resistance or Kapitza resistance, named after the Russian physicist P. Kapitza who discovered this thermal boundary resistance in 1941 for the case of liquid helium in contact with solid. In the different materials acoustic like mismatch of the thermal phonons suggest that there should be a thermal boundary resistance however predictions of this theory differ by several orders of magnitude from experimental results. For helium/solid interfaces, the acoustic impedances are  $\rho_g v_g = 10^6$  g/(cm<sup>2</sup>.s) for solid materials and  $\rho_h v_h = 10^3$  g/(cm<sup>2</sup>.s) for liquid helium. However critical angle of incidence at which phonons from helium may enter the solid is very small. The combination of acoustic mis-match and small critical angle severely limits the energy exchange between helium and other solid materials. This thermal Kapitza resistance, increases drastically at lower temperatures and sets a practical limit for cooling helium by external means. A rigorous treatment of the boundary resistance due to acoustic mismatch has to take into account the structure and properties of solid and of helium near to the interface and also the excitations there. However surface excitations as well as deviation from crystalline structure and compression of helium resulting from the Van der Waals attraction of the solid may influence the transmission coefficient for phonons. The thermal

boundary resistance varies as  $R_k \propto 1/(AT^3)$  and is the most severe obstacle for establishing thermal contact between helium and other substances at  $T < 1\text{K}$ , where  $A$  is the contact surface area. The only way to compensate for the decreased conductance is to increase the interface area  $A$ , across where the heat is transferred. This is mostly done by using heat exchangers made from sintered metal powders.

### 1.3 Working principle of Dilution refrigerator

To carry out research at very low temperature it is necessary to have a refrigerator that cools down to the required temperature and operates continuously for days or weeks as long as the experiment continues and should preferably be automated. All these requirements are almost reliably fulfilled by dilution refrigerator. It is a device that can achieve and maintain temperature as low as a few millikelvin continuously with sufficient cooling power. It is the workhorse of the millikelvin temperature range and relies on the unique properties of  $^3\text{He}/^4\text{He}$  mixtures (see section 1.2). It takes advantage of the low temperature behaviour of the  $^3\text{He}/^4\text{He}$  isotopic mixture below  $0.87\text{K}$ , producing phase separation between the two isotopes. The lighter liquid rich in  $^3\text{He}$  is called concentrate phase which floats on top of  $^4\text{He}$  rich phase called the dilute phase. The dilute phase is so called because, as the temperature approaches absolute zero, there is a limiting solubility of 6.5%  $^3\text{He}$  in  $^4\text{He}$ . Continuous cooling by this method is possible because dilute phase concentration of  $^3\text{He}$  remains at about 6.5% unlike cooling by evaporation, where the vapour pressure reduces rapidly with temperature, making it increasingly difficult to maintain a reasonable cooling power. The cooling resulting from the dilution process is somewhat analogous to the cooling process that occurs when the vapour is pumped from a liquid. The upper concentrated phase corresponds to the liquid phase and the lower dilute phase corresponds to the less dense gas phase. In an ordinary  $^3\text{He}$  refrigerator, cooling

occurs by evaporation of liquid  $^3\text{He}$  into less dense  $^3\text{He}$  gas across the phase boundary, where the gas is pumped away. Whereas in dilution refrigerator,  $^3\text{He}$  atoms moves across the phase boundary into the non-interacting  $^4\text{He}$  background containing the dilute  $^3\text{He}$ , where it is removed by osmotic pressure to the still and eventually pumped away. In a pumped liquid  $^3\text{He}$  refrigerator, the latent heat of evaporation per atom or the energy required to remove one atom from the liquid to the gas is weakly temperature dependent while the vapour pressure decreases exponentially as the temperature is reduced so that it becomes physically difficult to remove sufficient numbers of atoms to achieve cooling. In a dilution refrigerator at low temperatures, the concentration of  $^3\text{He}$  atoms in the dilute phase is weakly temperature dependent while the heat of mixing per atom or the energy required removing a  $^3\text{He}$  atom from the  $^3\text{He}$  phase to dilute  $^3\text{He}$  phase is proportional to the square of the temperature. Since most mechanical pump has a fixed pumping speed for a given design pressure range, so the amount of gas pumped or throughput will be proportional to the pressure. Hence the cooling available is the product of heat of mixing and the amount of gas pumped. Thus for  $^3\text{He}$  refrigerator, the cooling capacity decreases exponentially with decreasing temperature while for a dilution refrigerator the cooling capacity decreases approximately to the square of the temperature. The cooling capacity below 0.4K is generally larger for dilution refrigerator than  $^3\text{He}$  evaporator refrigerator. The comparison of cooling power of dilution refrigerator and  $^3\text{He}$  evaporative cooling with the assumption that the same helium gas circulation rate of 5l/sec is taken is shown in figure 1.5 for illustration [1].

Dilution refrigerator can be divided into four main sections: helium evaporator (1K- pot),  $^3\text{He}$  distillation chamber (still), Heat exchanger (HeX) and mixing chamber (MC) though the gas circulation and handling system at room temperature is also an important part of the dilution refrigerator. The room temperature gas mixture after being

successively cooled to 77K and 4.2K condenses inside the 1K pot, a small container which is continuously filled with  $^4\text{He}$  through flow impedance. This is maintained below 1.5 K temperature by evaporative cooling of  $^4\text{He}$ . The condensed liquid after 1K-pot is passed down flow-limiting capillary called primary impedance, designed to produce adequate pressure drop for condensation to occur. This ensures local pressure above its vapour pressure for all designed flow rates.

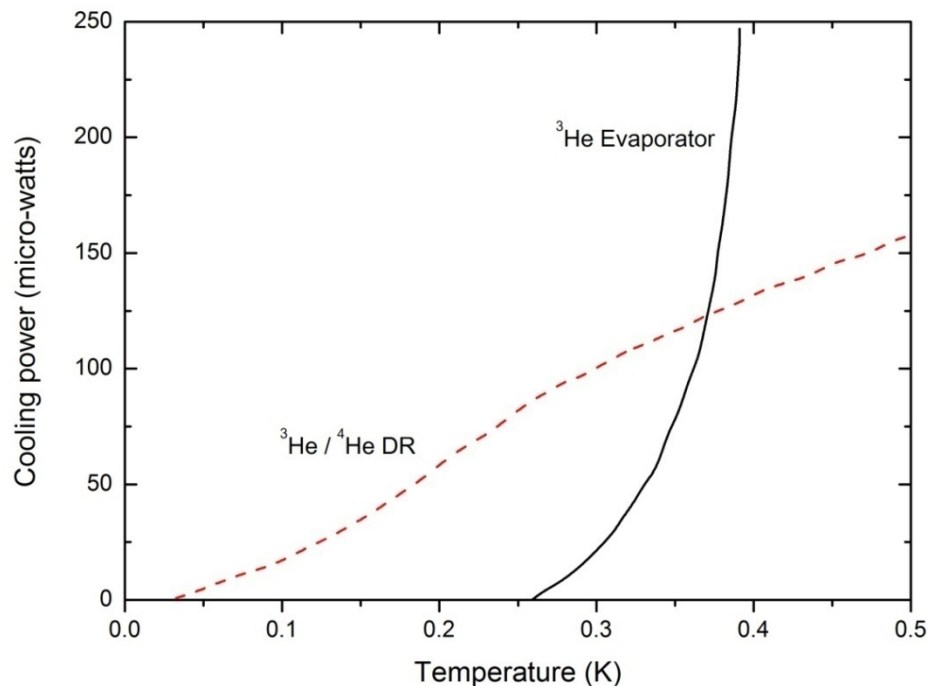


Figure 1.5 Comparison of cooling power between  $^3\text{He}/^4\text{He}$  dilution refrigerator (DR) and  $^3\text{He}$  evaporative cooling

The still is a container filled with  $^3\text{He}/^4\text{He}$  solution which is in dynamic equilibrium in its vapour phase. It acts as  $^3\text{He}$  distillation chamber and is continuously pumped through a separate circulating pump. As the still is pumped, difference of vapour pressure between the two isotopes leads to  $^3\text{He}$  being primarily removed from the dilute solution of  $^3\text{He}$  in superfluid  $^4\text{He}$ . The still is maintained at about 0.6K under steady state using a heater. The condensed  $^3\text{He}$  after 1K-pot further cools down to still temperature. Then it enters to the HeX, and is further cooled by exchanging its heat with the returning

cold fluid from the mixing chamber. Below 0.8K the mixture of  $^4\text{He}$  and  $^3\text{He}$ , phase separates into two phases: one is pure  $^3\text{He}$  and the other is  $^4\text{He}$  with a small quantity of  $^3\text{He}$  which is called dilute phase. The boundary between these two phases sits in the MC, the coldest part of the dilution refrigerator. The osmotic pressure of the solution drives the  $^3\text{He}$  from the dilute phase of the mixer inside MC through the stationary superfluid  $^4\text{He}$  to the still, where it evaporates and is sucked to the pump inlet. It is energetically favourable for  $^3\text{He}$  in the pure side to move across the phase boundary to replenish  $^3\text{He}$  in dilute solution to maintain equilibrium concentration of  $\sim 6.5\%$ . This movement of  $^3\text{He}$  from the concentrate phase into the dilute phase results cooling. The performance of HeX plays very crucial role for obtaining lower temperature. At low temperature the heat transfer is limited by the Kapitza resistance between liquid helium and solid metal surface. It is necessary to have maximum surface area for a given volume of the heat exchanger. The sintered metal heat exchanger is used to achieve this condition with varying designs. The  $^3\text{He}$  that is pumped off at the still is returned back to the concentrate pure side of the mixing chamber by liquefaction at the 1 K-pot and pre-cooled through a series of heat exchangers in order to continue the cooling process.

Gas Handling System (GHS) at room temperature comprises of  $^3\text{He}/^4\text{He}$  storage system,  $^3\text{He}$  circulation system, and pumping system for 1K pot. It includes large collection of pumps, pipes, gauges and valves and operates under sub-atmospheric pressure of about 100-300 mbars.

## **1.4 Review of Previous Work**

Several thermodynamic models of dilution refrigeration have been published in the past and is readily available in literature [16, 28-32]. Different models are reviewed, compared and the limitations are discussed. Niinikoski presented the first

thermodynamic model of dilution refrigerators which permitted to calculate the mixing chamber temperature as a function of the heat load and heat exchanger surface area at the optimum flow rate [16]. Frossati and co-workers subsequently developed a different model for arbitrary  $^3\text{He}$  flow rate [29, 30] and subsequently modified that model [31]. In 1994, Takano published an improvement of Frossati's model [32]. A numerical method using nodal modelling technique has been developed at CERN at arbitrary flow rate [33].

The cooling power  $\dot{Q}_c$  of dilution refrigerator as function of the mixing chamber temperature,  $T_m$ , and the temperature of liquid  $^3\text{He}$  that enters the mixing chamber,  $T_i$ , is discussed in several contemporary textbooks [1, 35, and 36]. It comes from the energy balance inside the mixing chamber for a  $^3\text{He}$  molar flow rate  $\dot{m}_3$

$$\dot{Q}_m = \dot{m}_3 * (H_d(T_m) - H_c(T_i)) \quad (1.1)$$

where  $H_d(T_m)$  the enthalpy of the  $^3\text{He}$  in the saturated dilute solution at the mixing chamber temperature  $T_m$  and  $H_c(T_i)$  is the enthalpy of the concentrated  $^3\text{He}$  at the temperature  $T_i$  of the liquid entering to mixing chamber. It is assumed that the temperature of liquid inside the mixing chamber is uniform and equal to  $T_m$ .

At temperature below roughly 50mK the pure liquid  $^3\text{He}$  and the dilute  $^3\text{He}$  in super fluid  $^4\text{He}$  are both normal Fermi liquids and so its heat capacity and entropy are same and is proportional to temperature. Greywall measured the specific heat of pure  $^3\text{He}$  [37] which can be approximated by the expression

$$C_c(T) = 23 * T \frac{J}{mol K} \quad (1.2)$$

And so the enthalpy  $H_c(T)$  of pure  $^3\text{He}$  can be calculated by integrating Eq. (1.2) with respect to temperature  $T$  and amounts to

$$H_c(T) = H_c(0) + \int_0^T C_c(T') dT' = H_c(0) + 11.5 T^2 \quad (1.3)$$

The specific heat of dilute solution of  $^3\text{He}$  has been measured by Anderson et al. [27] and can be expressed for each mole of  $^3\text{He}$  as

$$C_d(T) = 107 * T \frac{J}{mol K} \quad (1.4)$$

The chemical potential of the two separated phases inside mixing chamber must be same. Since chemical potential  $\mu(T) = H(T) - T S(T)$ , it is thus possible to write

$$H_d(T) = H_c(T) - T * \int_0^T \frac{C_c(T')}{T'} dT' + T * \int_0^T \frac{C_d(T')}{T'} dT' \quad (1.5)$$

which is used to calculate the enthalpy  $H_d(T)$  of  $^3\text{He}$  in dilute solution along the solubility line:

$$H_d(T) = H_c(0) + 95.5 * T^2 \frac{J}{mol K^2} \quad (1.6)$$

The coefficient may vary slightly, though the discrepancies do not amount to more than few percent. This is the saturated enthalpy of  $^3\text{He}$  in dilute solution present in the mixing chamber of the dilution refrigerator. However along the heat exchanger dilute solution is not saturated and osmotic enthalpy must be used for calculation as described later in section 3.2.1

Eq. (1.1), Eq (1.3) and Eq. (1.6) yield the cooling power of dilution refrigerator put forward by Radebaugh [28]:

$$\dot{Q}_m = \dot{m}_3 * (H_d(T_m) - H_c(T_i)) = \dot{Q}_m = \dot{m}_3 * (95.5 * T_m^2 - 11.5 * T_i^2) \quad (1.7)$$

If the incoming pure  $^3\text{He}$  which enters the mixing chamber is at the same temperature as the mixing chamber temperature i.e.  $T_i = T_m$ , then cooling power is given by

$$\dot{Q}_m = \dot{m}_3 * 84 * T_m^2 \frac{J}{\text{mol K}^2} \quad (1.8)$$

This gives the maximum cooling power at any temperature  $T_m$  of the MC. This cooling power can only be reached in single-shot operation, when the incoming flow of  $^3\text{He}$  is stopped. Whereas under continuous operation, it can be achieved in a hypothetical dilution refrigerator with an infinite heat exchanger surface area. It describes the cooling power of the actual process of  $^3\text{He}$  atoms crossing an isothermal phase boundary into dilute solution and does not take into account the heat transported to the mixing chamber by the concentrated stream at its temperature  $T_i > T_m$ . The actual temperature  $T_i$  of the incoming  $^3\text{He}$  depends on how well the liquid is pre-cooled in the heat exchanger by the outgoing flow of the dilute  $^3\text{He}$  in super fluid  $^4\text{He}$ . Since the Kapitza resistances between the pure  $^3\text{He}$  and the heat exchanger wall and between the wall and the dilute  $^3\text{He}$  are strong functions of temperature, the refrigerator eventually reaches a temperature, below which, the incoming  $^3\text{He}$  cannot be cooled to  $T_m$  by the heat exchangers. In the extreme case of no cooling power being available, i.e.  $\dot{Q}_m=0$ , Eq. 1.7 yields the maximum temperature at which the  $^3\text{He}$  may enter the mixing chamber

$$T_i = 3 * \sqrt{\frac{95.5}{11.5}} T_m \sim 3 * T_m \quad (1.9)$$

It is clear that if  $^3\text{He}$  is circulated at a higher rate, the positive effect of more atoms crossing the phase boundary in the mixing chamber can outweigh the negative

effect of a higher heat load to the mixing chamber due to increased temperature of the concentrated stream. This makes us to maintain an optimum  $^3\text{He}$  flow rate in the circuit. Niinikoski[16] was the first to derive a theoretical model of dilution refrigeration which takes into account the finite efficiency of heat exchangers. Niinikoski used the energy balance at an arbitrary position  $z$  of the heat exchanger to obtain a relation between temperatures of concentrated stream  $T_c$ , dilute stream  $T_d$  and  $^3\text{He}$  molar flow rate  $\dot{m}_3$  as

$$H_c[T_c(z)] + \frac{Q_m}{\dot{m}_3} = H_d[T_d(z), x] \quad (1.10)$$

This equation is obtained by balancing the flow of energy through an imaginary cut through the heat exchanger.  $Q_m$  which stands for the heat input to the mixing chamber. Frossati and Takano obtained a relation between concentrated stream temperature  $T_c$  and dilute stream temperature  $T_d$  at any position  $z$  of the heat exchanger by requiring that the heat absorbed by the dilute stream is equal to the heat given off by the concentrated stream,

$$\dot{m}_3 * dH_c[T_c(z)] = \dot{m}_3 * dH_d[T_d(z), \mu_4(x_m, T_m)] \quad (1.11)$$

Since the dilute stream is not saturated along the heat exchanger, osmotic enthalpy  $H_d$  is used rather than saturated enthalpy on the solubility line of dilute solution. The osmotic enthalpy depends on the temperature and the chemical potential  $\mu_4$  of the  $^4\text{He}$  component of the dilute solution. It is determined by the  $^3\text{He}$  concentration  $x_m$  and mixing chamber temperature  $T_m$ . Frossati model [29-31] has yielded analytical solutions which expresses the mixing chamber temperature  $T_m$  of the refrigerator in terms of the Kapitza resistance in the heat exchangers, the  $^3\text{He}$

circulation rate  $\dot{m}_3$  and the cooling power. Unfortunately, the cooling power given by the solutions of Frossati turns out to be incorrect at temperatures away from the base temperatures. Here the characteristics of heat exchanger are not correctly taken into account. Takano [32] modified Frossati model by adding the correct boundary conditions which describes the temperature profile along the heat exchanger, the resulting formula cannot be solved analytically and thus do not have the advantage of yielding results quickly and straightforwardly. The resulting solution gives the correct cooling power at all temperatures. The differences between Niinikoski and Frossati analytical model and Takanos numerical results are hardly discernible, but exist. Another method using nodal modeling techniques has been developed [33-34] at CERN using TAK 2000 code, which in addition simulate transient behavior of the refrigerator under varying load condition. In the nodal method, the dilution refrigerator is modeled as a number of discrete nodes which are linked by conductors. A solution is then obtained by solving for thermal equilibrium assuming the heat flow into each node is equal to the heat flow out of each node. The mixing chamber is represented by a node to which the external heat load  $\dot{Q}_m$  and the cooling power are applied. The cooling process is modeled as a negative heat load. The still is represented by a node of constant temperature  $T_s = 0.7K$ . The heat exchanger is modeled by a group of nodes representing the concentrated stream and dilute stream separately. The major input parameters being  $^3\text{He}$  flow rate, the still temperature  $T_s$ , and the heat load on the mixing chamber. However, none of these models combine all the components of the dilution refrigerator as a close circulating system. The present work integrates all components of dilution refrigerator making up a close circulating system and provides more realistic behavior of the system that enables quantitatively the effects of individual components.

# Chapter 2

## Mechanical Components of Dilution Refrigerator

### 2.1 Introduction

The dilution refrigerator has a cryostat that accommodates Internal Vacuum Chamber (IVC) and pumping lines. The IVC contains the dilution insert which consists of four major components: helium evaporator (1K-pot),  $^3\text{He}$  distillation chamber (still), Heat Exchanger (HeX) and Mixing Chamber (MC) as shown figure 2.1. In addition to this, a gas circulating and handling system (GHS), which is at room temperature and comprises of  $^3\text{He}$  and  $^4\text{He}$  gas pipelines, storage system, vacuum pumps and leak detector system is also present and together makes a complete system. Figure 2.2 shows the dilution refrigerator set up developed by us.

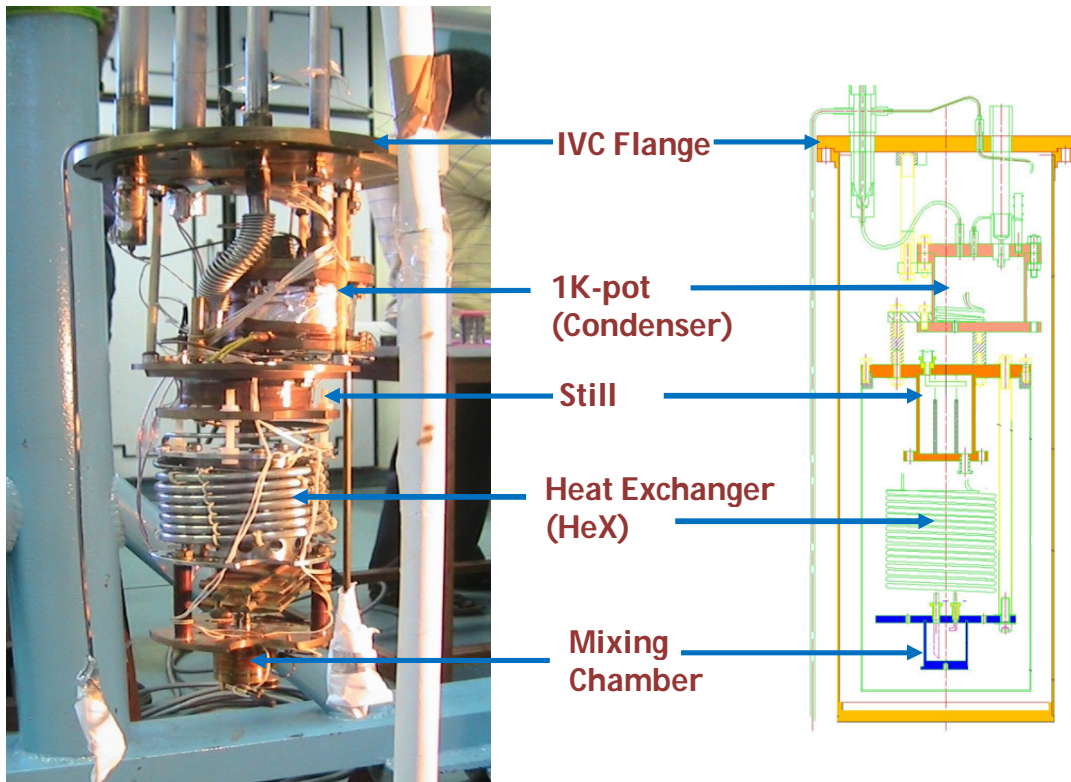


Figure 2.1 Dilution Insert showing different components along with schematic diagram

### 2.1.1 Bath cryostat

The general layout of housing cryostat which has been built is shown schematically in figure 2.3. The system is required to house the dilution insert. This consists of bath cryostat shielded by liquid nitrogen of 80 litres capacity. The liquid helium capacity of the cryostat is about 40 litres with a hold time of about two days. The height of cryostat is 1367 mm with diameter of 382 mm. The top room temperature flange is provided with vacuum port, helium connections and feed through for electrical wiring. The heat load on the helium bath is estimated to be about 0.76 W at 4.2K considering the effect of outer radiation from liquid nitrogen chamber and conduction through pumping lines, needle valves etc. This heat in-leak from different sources is given in table 2.1. The cryostat is designed to obtain a long running time by having a sufficient volume of liquid  $^4\text{He}$  and also by minimising the heat leak by using a reasonably narrow neck.

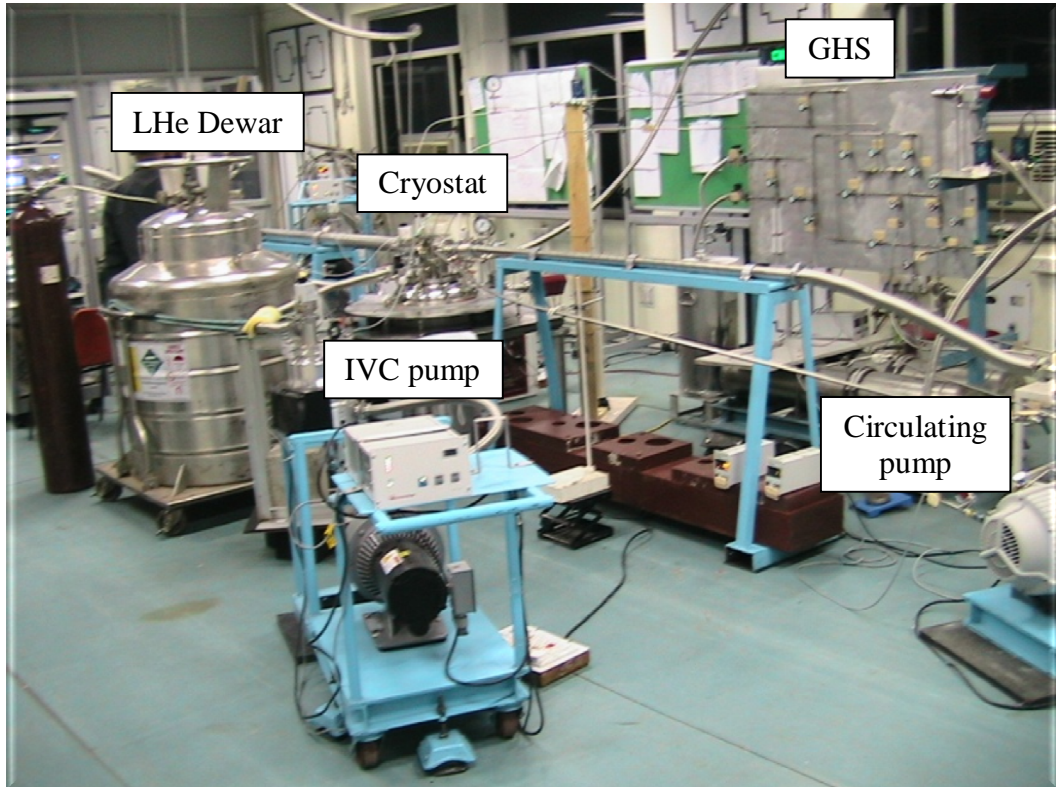


Figure 2.2 Dilution refrigerator set-up developed in the laboratory

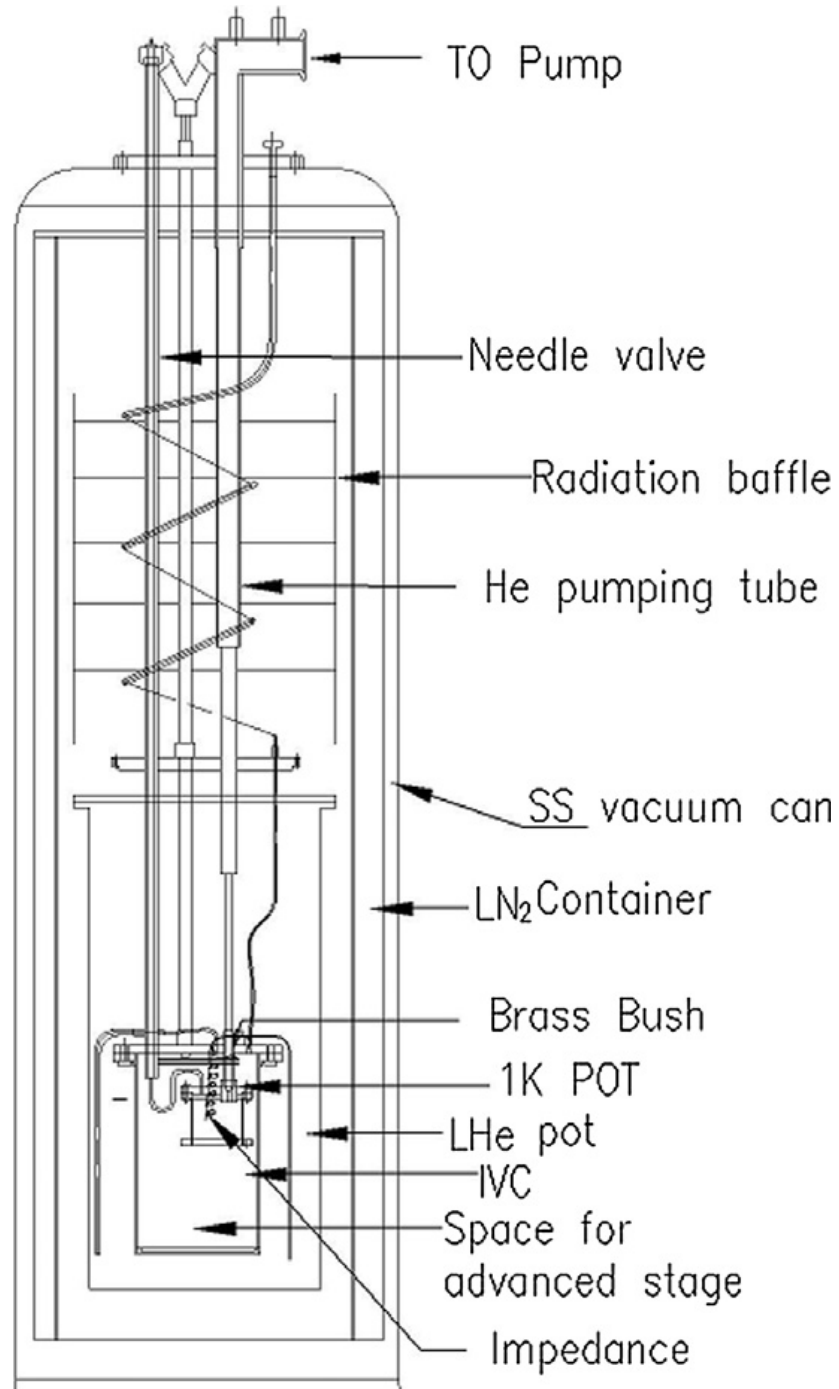


Figure 2.3 General layout of housing cryostat

The cryostat incorporates an IVC, which is centrally positioned for accommodating still, heat exchanger, mixing chamber, pipelines and electrical connections which comprising the dilution insert. This IVC is housed within the helium bath of the cryostat with its top flange immersed in liquid helium. The leak tightness of this demountable flange is ensured with the help of indium o-ring corner seal. The IVC is made of OFE

copper with a height and diameter of 350mm and 130mm respectively. It is evacuated to about  $10^{-6}$  mbar of pressure using turbo molecular drag pump. In order to facilitate this evacuation an activated charcoal is provided with heater arrangement for its regeneration. IVC plays a significant role by way of thermally isolating the sub-kelvin dilution insert from the liquid helium bath at 4.2K. However, at the initial cooling of dilution insert to 4K,  $^4\text{He}$  exchange gas is admitted inside IVC. Brass bushes are hard soldered to the top of IVC flange for carrying thin walled pipe lines, impedance and electrical connections. This provision facilitates removal and replacements of tubes whenever necessary. The Outer Vacuum Chamber (OVC) of the cryostat is maintained below  $10^{-6}$  mabr pressure using of 400L/s turbo molecular drag pump backed by dry scroll pump.

Table 2.1

Heat load to helium bath	
Item	Heat load
Wall and bottom surface of the helium bath	0.0439W
Top flange and radiation baffles (3 nos.)	0.216W
Pumping line (77–4.2 K)	0.00195W
Needle valve	0.5W
Total load	0.764W

Even a slight vibration in cryostat can cause unwanted heating and can result in the performance degradation of the dilution refrigerator. There are three major causes of vibration viz. vacuum pumping lines, circulating gas lines and continuously filled 1K-pot, especially when liquid helium at 4.2K drops into superfluid  $^4\text{He}$  inside the 1K-pot producing turbulence. Vibration isolation and damping are primarily important when working in millikelvin temperature range. In order to eliminate the floor vibration coming

from the surrounding environment and transmitted to the dilution insert, cryostat is mounted on a stainless steel-supported structure with air spring (1.5 bars) and is kept below the ground level as shown in figure 2.4. All lines from the pumps are isolated by lengths of flexible convoluted stainless steel tubing followed by solid tube which are embedded firmly to the wall and ground. The pumping tubes between the room temperature plate and the 4.2K flange pass through number of thermal baffles to which they are soft soldered to make a rigid cage in order to reduce the liquid  $^4\text{He}$  boil-off from the cryostat. Each baffle is perforated and the positions of the perforation alternate at different sides on adjacent baffles to encourage the evolving gas to flow transversely for cooling the tubes and the leads. For mechanical stability, the three main pumping tubes of the still, 1K-pot and IVC form a tripod extending from room temperature flange to the 4.2K flange. To accommodate the cryostat inside the existing laboratory, a 3 meter deep pit had to be excavated which also makes the accessibility to the top surface of the cryostat easy.

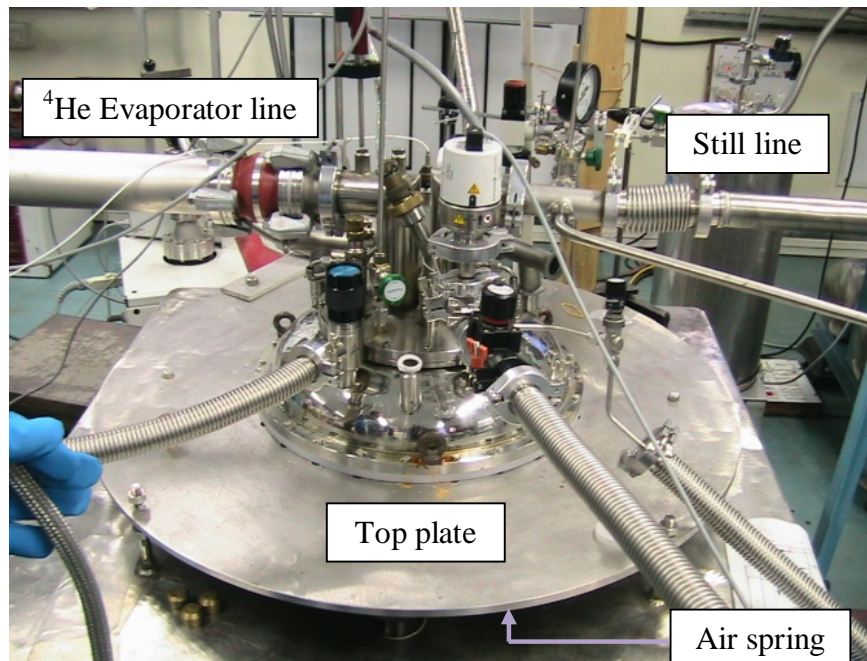


Figure 2.4 Cryostat top plate is mounted on three air springs and all the pumping lines are connected through bellows to reduce vibrations.

### 2.1.2 $^4\text{He}$ Evaporator (1K pot)

The  $^4\text{He}$  evaporator (1K pot) functions primarily to pre-cool the circulating helium isotopic gas mixture and is placed below the IVC flange at slightly off-axis position as shown in figure 2.3. This is continuously filled with liquid helium and has a volume of 99 cc. It is made of OFE copper (figure 2.5) and is suspended from stainless steel IVC flange. It works by evaporative cooling by the way of pumping out the  $^4\text{He}$  vapour from the top of

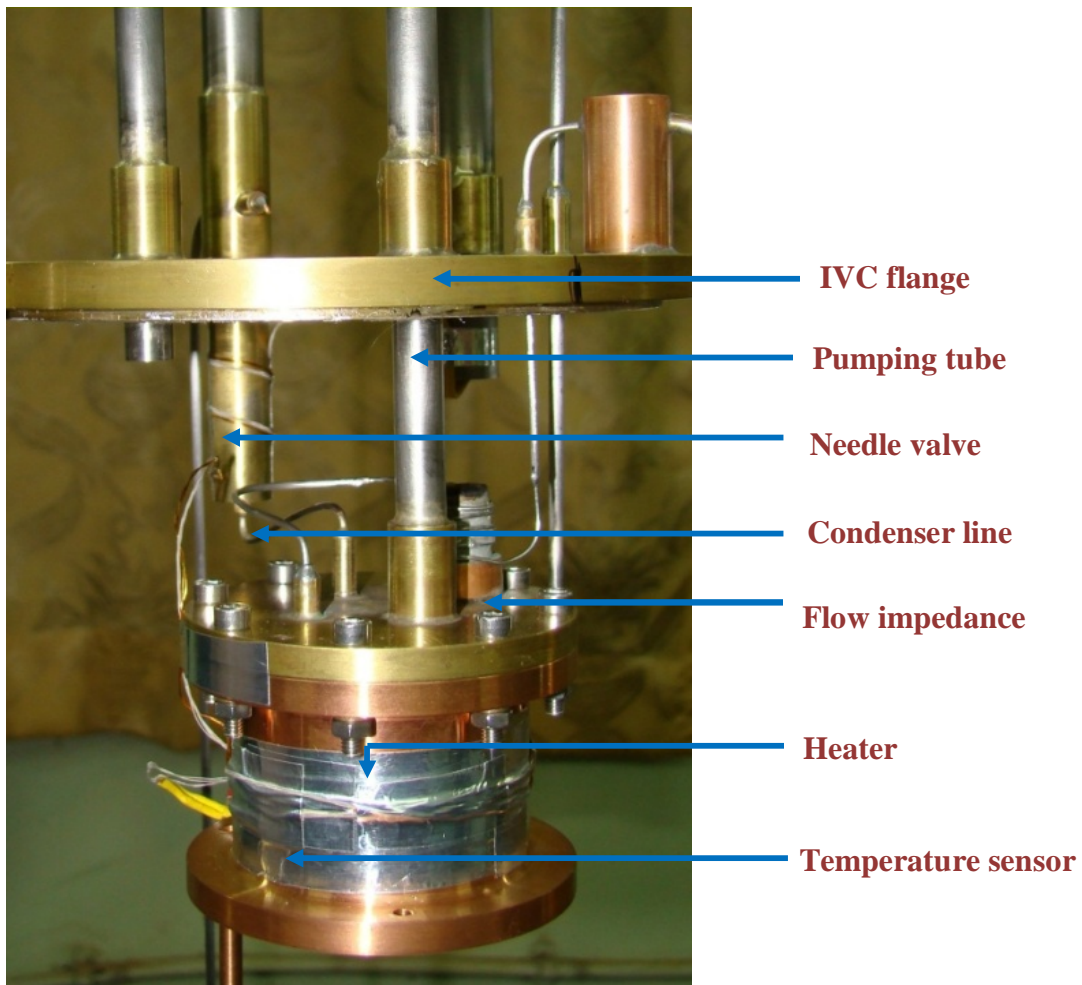


Figure 2.5 Details of 1K pot suspended from IVC flange

the pot. Precision needle valve is used initially to fill up the pot then the permanent flow impedance maintains the liquid helium level inside the pot to replenish the evaporative loss of helium. The automatic cryogenic needle valve with capillary at the end as shown in

figures 2.3 and 2.5 is capable of dealing with the onset of blockage in the capillary. A pumping station comprising of a 250 m<sup>3</sup>/hr roots pump backed by a dry pump was used. Stainless steel bellow connects the pump through vibration damper and gate valve on the top of the cryostat. This flexible link keeps vibration to its minimum. The pumping line are provided with five numbers of thermal baffles to minimise the radiation heat leak without imposing much constraint to the gas flow. The pumping line consists of four sections with different length and diameter. This length and diameter of different sections

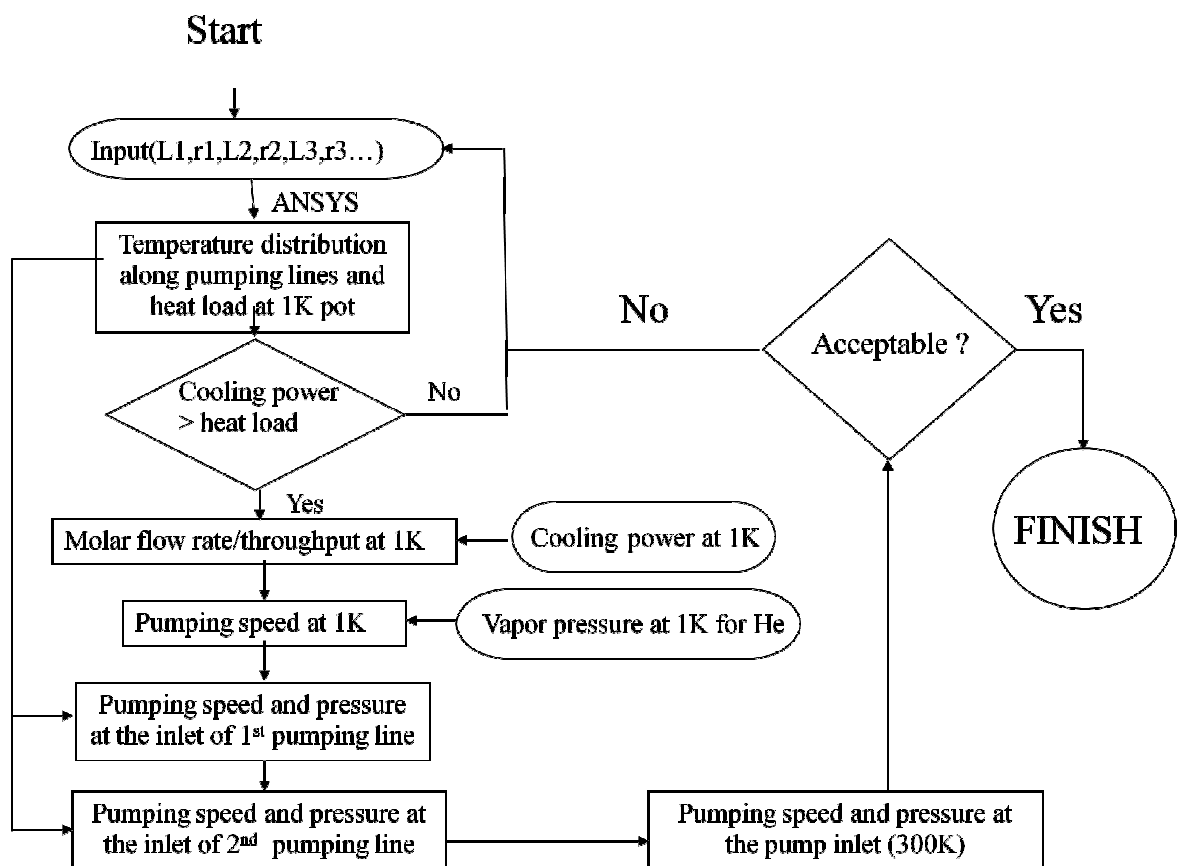


Figure 2.6 Flow chart for pumping line optimisation

of the pumping tubes as well as the positions of baffles are designed to maximise the gas flow with minimum heat conduction. The flow chart for optimisation of pumping tubes is shown in figure 2.6. We have used ANSYS FLOTRAN<sup>TM</sup> CFD module for fluid pressure and temperature distribution inside the pumping line as shown in figure 2.7. A 2.5mm

orifice is provided at the entrance of the pumping line leading to the evaporator to reduce the super fluid film creeping.

Table 2.2

Heat load to 1K pot	
Item	Heat load at 1K pot
Pumping line (4.2–1 K)	1.33mW
Radiation load	$3.363 \times 10^{-5}$ mW
Sensors and Heater wires (8 nos. 38AWG)	$3.2 \times 10^{-5}$ mW
$^3\text{He}$ pre cooling and condensation (4.2–1.0 K)	1.43mW
Total load	2.76mW

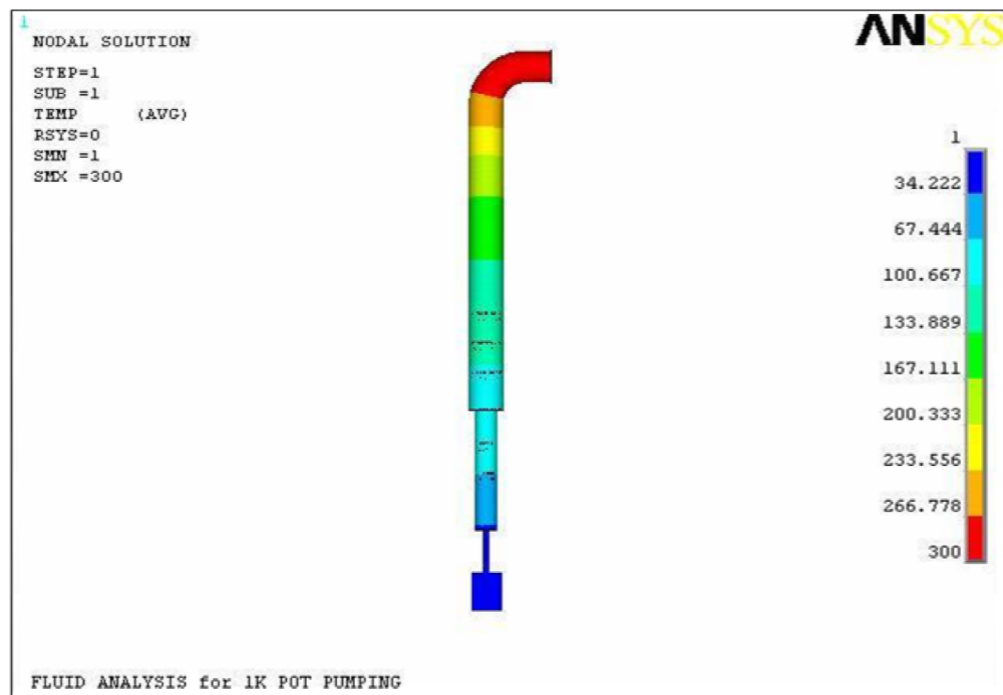


Figure 2.7 Contours of temperature depicting different sections of pumping line

This 1K pot is continuously filled via the flow impedance. The 0.2mm cupronickel capillary impedance was soft soldered to the brass bush of the IVC flange and extends

almost to the bottom of helium bath to admit liquid helium to the pot. Eventually liquid helium is replenished in the 1K pot at a limited rate from the main helium bath through flow impedance. The impedance required is quite high and the total length of the sipper line is limited, so the impedance was constructed by putting a tight-fitting wire into a small stainless tube having 0.2mm diameter with 1 meter length. The impedance was fabricated and tested to maintain the bubble flow for replenishment due to evaporative loss at a given temperature. With too large impedance the evaporator will run dry and with too small impedance the required temperature will not be reached. The design optimisation of 1K evaporator aims to achieve minimum ultimate temperature of evaporator with more cooling power. However the available cooling power is limited by the external heat in leak through the pumping line, the liquid helium supply from the helium bath, the electrical connections and the surrounding media and the values of which are given in table 2.2 The

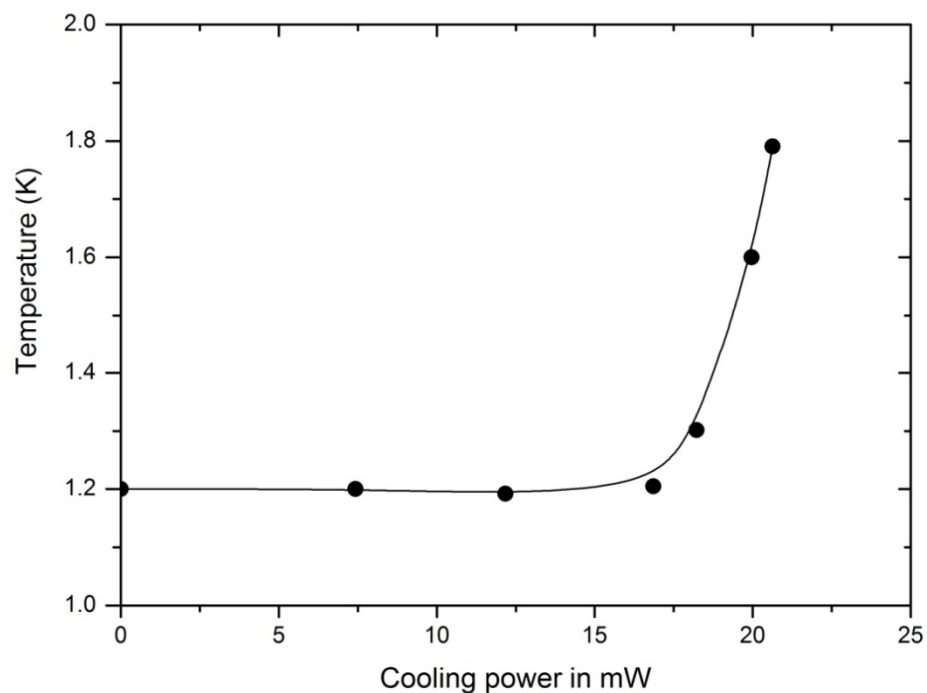


Figure 2.8 Cooling power at different temperatures measured by varying heater power attached to 1K pot ( $^4\text{He}$  evaporator)

short term overload condition due to excessive heat load in the 1K pot is determined by the sizing of the evaporator and its distance from the IVC flange. In the given design, the condensing temperature is about 1.2 K with available cooling power of about 18mW, measured with a 40  $\Omega$  kapton film heater wrapped over the evaporator. This provides a maximum condensing rate of about 180  $\mu\text{moles/s}$  of  $^3\text{He}$ . Variation of cooling power with temperature is shown in figure 2.8. The 1K pot was successfully operated and the temperature maintained for several hours with the lowest temperature of 0.98K have been reached as shown in figure 2.9, This is necessary for operating dilution refrigerator [40].

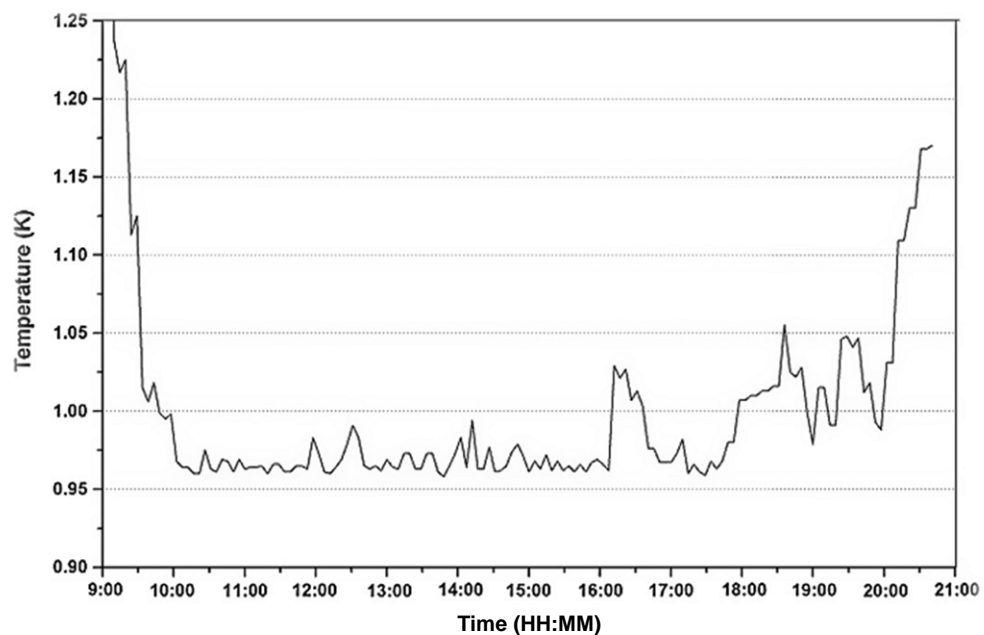


Figure 2.9 Temperature of 1K pot ( $^4\text{He}$  evaporator) over a period of time

However to stabilised the temperature below 1K appeared to be somewhat difficult. The performance was quite satisfactory for the purpose it was been designed for. The base temperature of the pot was measured by Ruthenium Oxide (RX-202A) temperature sensor calibrated between 0.1K and 40K. The flow rate of evaporated  $^4\text{He}$  obtained under different heater power was measured and has been plotted against the pressure drop as shown in figure 2.10. The slope of the curve is proportional to the conductance of the pipe

and was obtained as 30 m<sup>3</sup>/hr. The vertical shift of the measured curve in figure 2.10 is possibly due to error in the pressure measurement.

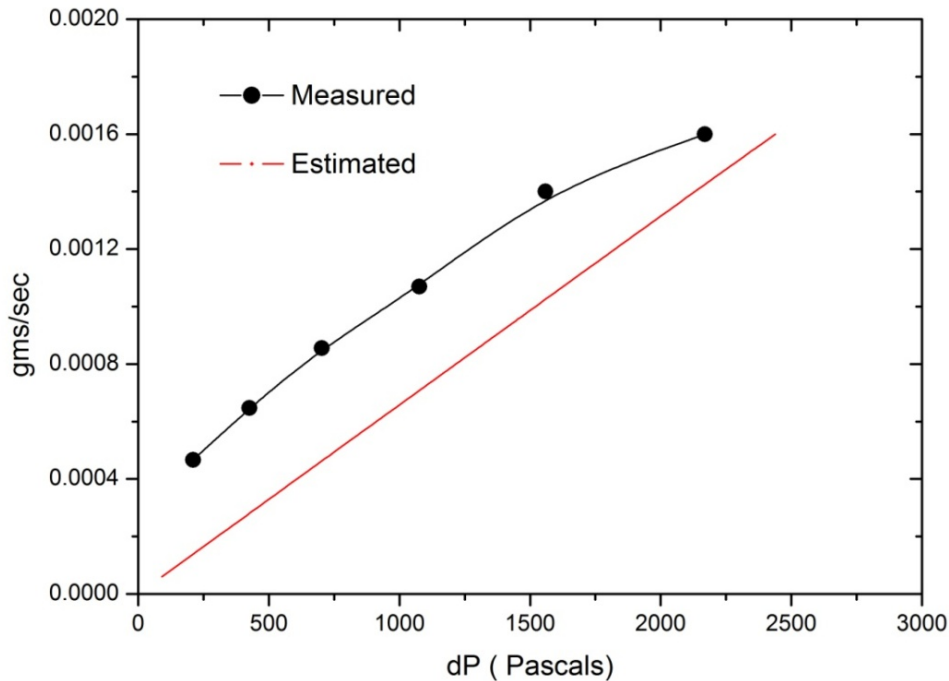


Figure 2.10 Evaporative <sup>4</sup>He mass flow rate vs pressure drop across pumping line measured by varying heater power attached to 1K-pot

When liquid helium is filled in the evaporator and the heat load is smaller than the available cooling power. The liquid helium tends to rise along the connecting line and increase the heat load from the 4K flange. An equilibrium level is reached when the cooling power equals the total heat load. When the external heat source is applied (for example flow of helium isotopic mixture) to the evaporator the liquid level will drop whereby reducing the conduction load and the evaporator remains essentially at the same temperature as before. However at a critical power  $Q_c$ , evaporator temperature increases rapidly until all liquid is evaporated as shown in figure 2.11, for three different impedance values. At external heat load,  $Q > Q_c$ , liquid at the capillary impedance travels progressively further but it vaporises before entering the pot whereas  $Q < Q_c$  liquid reaches

the evaporator and fills it up. As described any change of external heat load is responded with transient change of super fluid level inside the pot within its critical power.

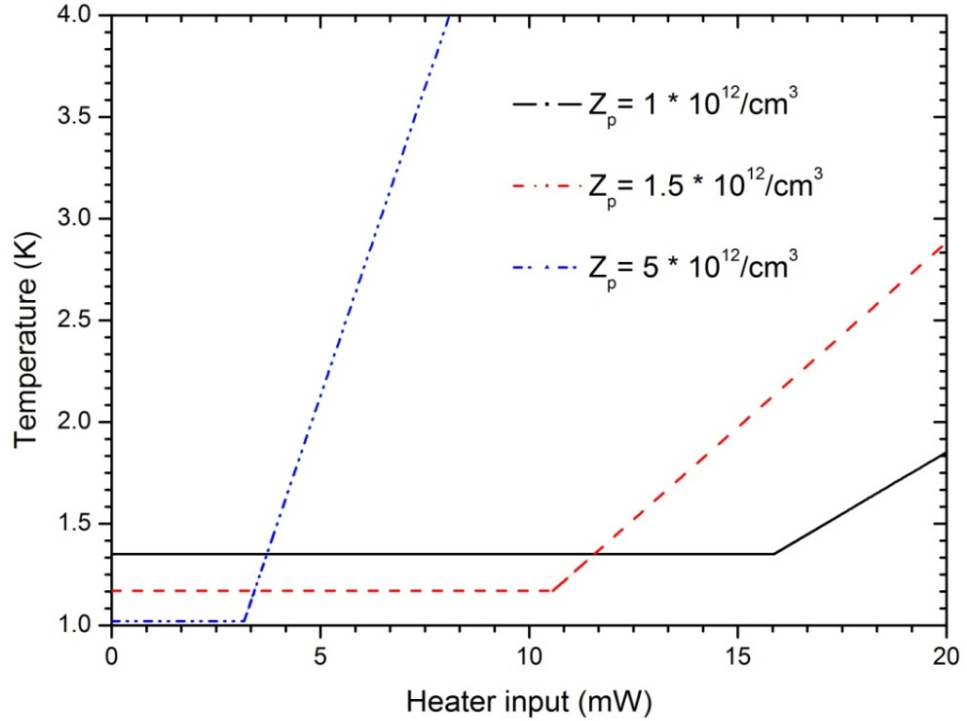


Figure 2.11 Characteristics behaviour of 1K pot for three different impedance values

### 2.1.3 Flow Impedance

In order to maintain the liquid phase in the concentrated phase side of the refrigerator, it is necessary to adjust the flow impedance. It is characterised by a quantity  $Z_p$  and its values is derived from measurement at room temperature using the relation

$$Z_p = \frac{\Delta P}{\eta \dot{V}}, \quad (2.1)$$

where  $\Delta P$  is the pressure drop required to obtain laminar volume flow rate of  $\dot{V}$  of a gas of viscosity  $\eta$ . The volume flow rate  $\dot{V}$  can be written as the product of molar volume  $V_m$  and molar flow rate  $\dot{m}$ . The typical value of impedance required in dilution refrigerator is of the order of  $10^{12} \text{ cm}^{-3}$ .

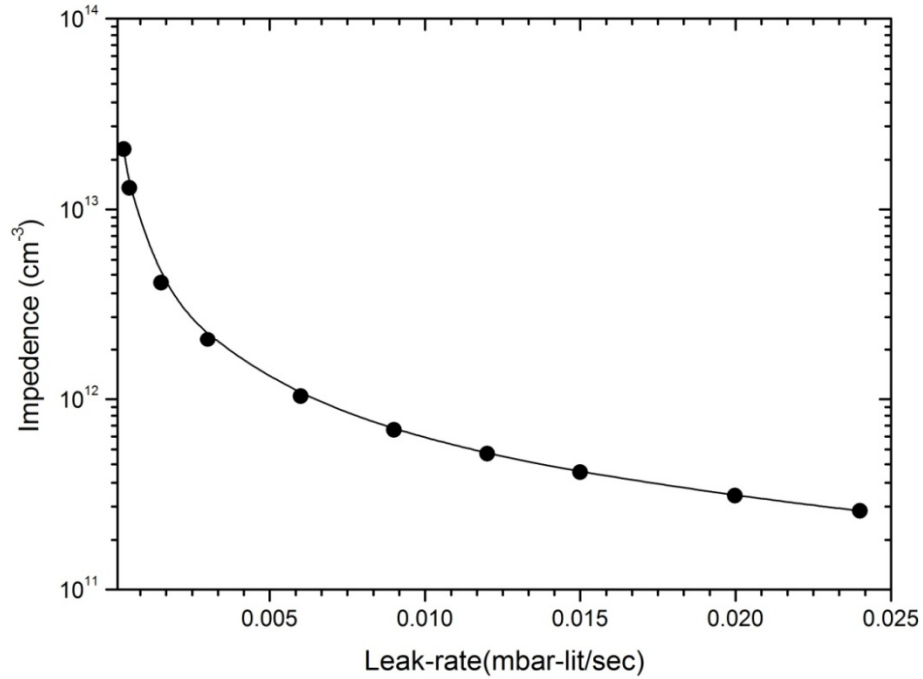


Figure 2.12 Impedance value and corresponding leak rate

It is necessary to establish sufficient pressure (50-200 mbar) for the incoming  $^3\text{He}$  so that it will indeed condense after 1K pot temperature. In fact the pressure everywhere in the concentrated phase must be greater than the vapour pressure of liquid  $^3\text{He}$  at a given temperature. Two flow impedances are introduced into the concentrated liquid  $^3\text{He}$  line between the condenser (1K pot) and the still and between the still and the heat exchanger module. The impedance after the condenser is generally referred as primary impedance and the one below the still is the secondary flow impedance which is required to prevent re-evaporation of  $^3\text{He}$ . Flow impedance is prepared from cupro-nickel capillary (id: 0.2 mm) with a stainless steel wire of 0.16 mm tightly fitted inside it. The impedance is measured by allowing helium gas at room temperature to flow through it, at a pressure of ~1000 mbar and then measuring the leak rate. Variation of capillary impedance with leak rate is given in figure 2.12. As the flow of liquid helium through the capillary driven by the pressure gradient is highly inhomogeneous and complex, the capillary characterization and sizing is in general determined experimentally. Hence to accommodate the impedance

within the limited space inside the dilution refrigerator, several capillary impedances is fabricated with different configurations and minimized dimensions to obtain the desired values. The spiral configuration (dia. 0.5 in.) with overall length of 100 cm is chosen to standardize the impedance and then the leak rates are measured. The detail analysis of the flow inside the capillary is also performed numerically taking into account the fluid property variation with temperature and pressure [40] (see Appendix A).

#### **2.1.4 $^3\text{He}$ Distillation Chamber (Still)**

The still is a container filled with  $^3\text{He}$  and  $^4\text{He}$  solution in dynamic equilibrium with its vapor phase. The vapor phase consists mainly of  $^3\text{He}$  with a small amount of  $^4\text{He}$  depending on the temperature and level of superfluid film creep. It has a large free surface of liquid to facilitate evaporation. The primary drive of the dilution refrigeration process is to pump  $^3\text{He}$  vapour away from the still and to direct it to the condenser after passing it through cold traps. This gas circulation produces continuous cooling in the mixing chamber as it facilitates  $^3\text{He}$  crossing the phase boundary to maintain the equilibrium concentration of  $^3\text{He}$  in the dilute phase. The presence of excess  $^4\text{He}$  in the circulating gas mixture causes phase separation at a relatively higher temperature and may lead to instabilities in the system. This superfluid  $^4\text{He}$  on the concentrated side also causes viscous heating because of phase separation and eventual acceleration of dilute phase due to osmotic pressure. In order to maintain the amount of circulating  $^4\text{He}$  within the desired limit (1-10%), the still is provided with a heater similar to the configuration proposed by Wheatley [19]. This sustains steady-state circulation by ensuring phase separation at a reasonably low temperature. This also, produces the requisite osmotic pressure between the mixing chamber and the still. The picture of still built in the laboratory along with its essential features are shown schematically in figure 2.13. The still utilizes a short length

of heated cupro-nickel tube and employs copper webs and brass baffles between its different sections. Pumping is entirely from the top of the still. The baffles re-condense  $^4\text{He}$  and prevent it from being sucked into the pumping line. The tube is heated with manganin wire to restrict the flow of super fluid  $^4\text{He}$  film on its wall. The vapor mixture flowing from the still shows the characteristics of thermal equilibrium within the still. When the heating rate is low the  $^4\text{He}$  film flow is apparently undiminished, however in a rather small range of heater power called critical power, the  $^4\text{He}$  film flow stops. The  $^4\text{He}$  film flow is linearly dependent on the smallest cross-section along its flow path above liquid. In our design of still, the film crosses a tube of minimum diameter of 3 mm before it reaches the heater. The thickness  $t$ , of a helium film at a height  $h$  (in cms) above the bulk liquid level is given by [35]

$$t(\text{nm}) \cong 30 h^{-1/4} \quad (2.2)$$

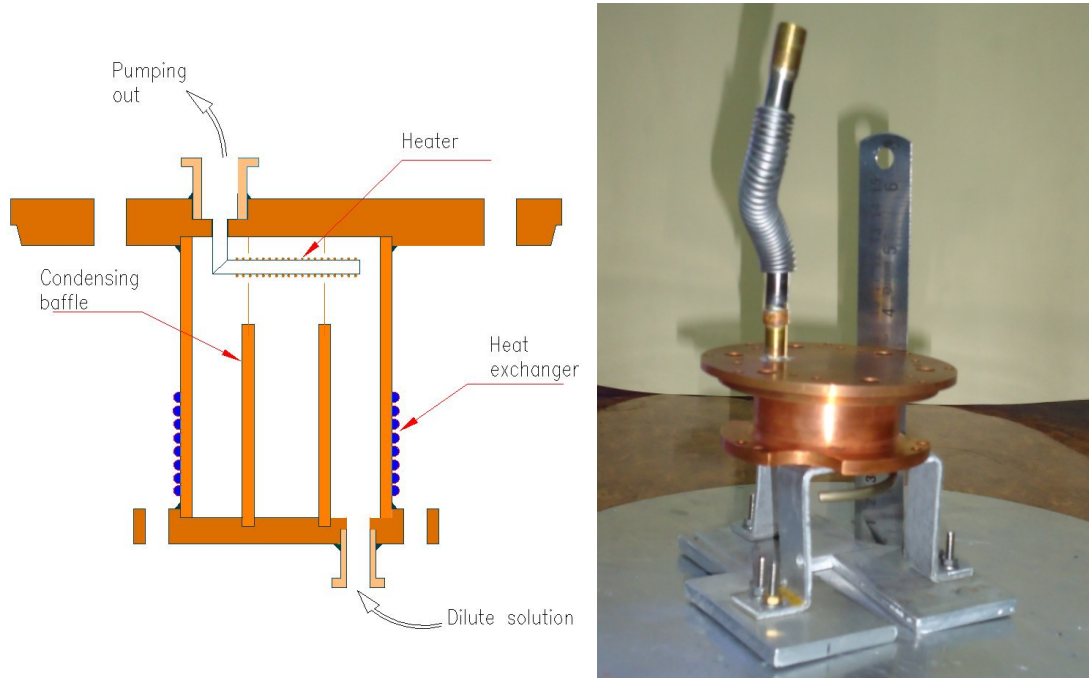


Figure 2.13 Schematic of still and its photograph

However  $t$  depends on the cleanliness and the smoothness of the tube surface.  $^4\text{He}$  film flow has been widely studied but the results are varied. The condition of the surface

over which the film flows causes wide variations in flow rates. For a typical critical velocity of  $^4\text{He}$  film,  $v_{crit} \sim 30$  cms/sec, volume flow rate creeping through the tube of radius  $R$  is obtained as

$$\dot{V} = 2 R \pi t v_{crit} \quad (2.3)$$

Taking the density of  $^4\text{He}$  as  $\rho$ , Molar flow rate,  $\dot{m} = \dot{V} * \rho / M_4$ , where  $M_4$  is molecular weight of  $^4\text{He}$  i.e. 4 gms/mole.

The amount of heat required to vaporize the  $^4\text{He}$  film is equal to the difference in the enthalpy of  $^4\text{He}$  between  $T_s$  (still temperature) and  $T_\lambda$  plus the heat of vaporization at  $T_\lambda$ . The critical heater power to evaporate the  $^4\text{He}$  film under different level of liquid inside the still is thus calculated and is shown in figure 2.14. This heat used to evaporate the film is absorbed by the still when  $^4\text{He}$  re-condenses.

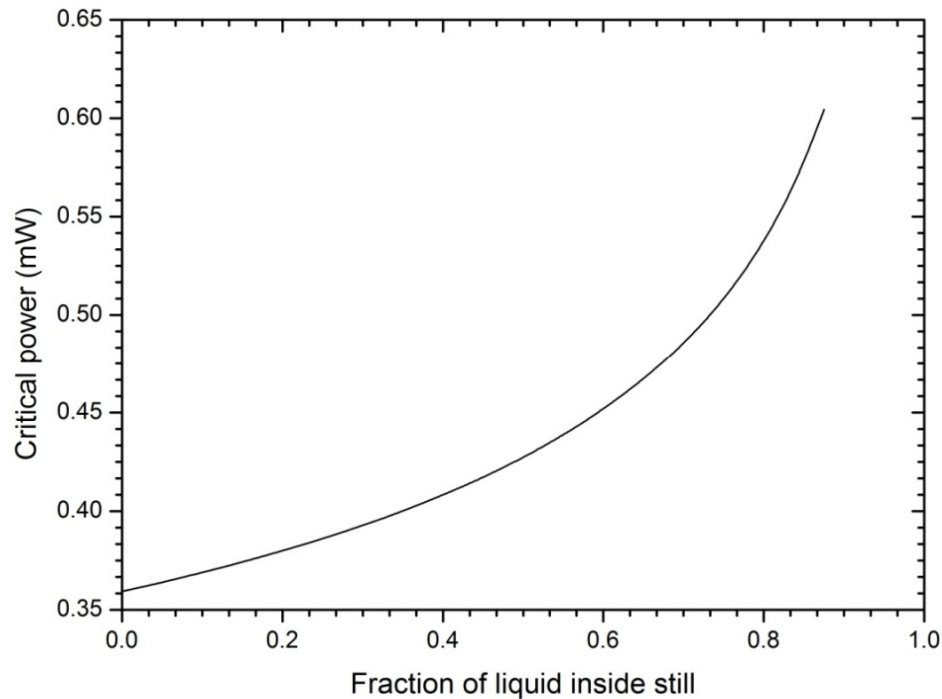


Figure 2.14 Minimum heater power required to vaporise superfluid  $^4\text{He}$  film creep under different liquid levels inside the still

Still is a cylindrical enclosure of size 32mm ID and 48 mm height made of OFHC (CDA-101) grade copper. It has a volume of  $\sim 40$ cc with large liquid free surface. It is

supported by three numbers of hanger rods made of G10 from the 1K pot. A separate set of support rods are used to hang the continuous heat exchanger from the bottom flange of the still. A thermal shield is anchored to the top flange and surrounds all the cold parts below to reduce the heat of radiation. Other parts like electrical leads and capillaries are heat sunk at the still as well. Pump-out line socket and other fittings on the ports of the still top flange are hard soldered while the remaining pump-out line is soft soldered. A Ruthonium oxide temperature sensor is mounted in the still flange to monitor its temperature. Owing to large thermal gradient at the entrance of the dilute stream into the still and this becomes a critical part of the refrigerator. Hence this part of the still is made smooth and polished with great care taken to reduce any asperities. The pumping line for  $^3\text{He}$  circulation from still is designed taking into consideration minimum heat conduction. This is ensured by increasing the sizes of the tube towards the higher temperature similar to 1K pot. Total pumping line is about 6 meter long of which about 4.5 meter is inside the cryostat. The theoretical pressure drop against different molar flow rate is calculated (see figure 2.15) and accordingly,  $35 \text{ m}^3/\text{hr}$  scroll pump is connected for gas circulation.

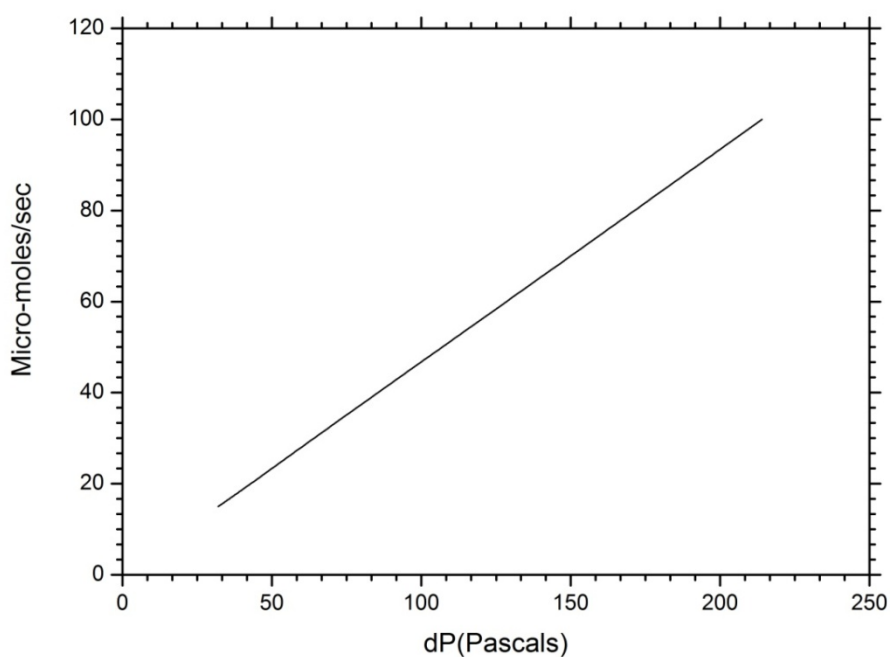


Figure 2.15 Molar flow rates under different pressure across still pumping lines

### 2.1.5 Heat Exchanger (HeX)

Heat exchanger plays the key role by reducing the temperature of the incoming concentrated  $^3\text{He}$  to a temperature close to that of the mixing chamber by exchanging heat with the returning dilute solution. Operation of dilution refrigerator requires an efficient heat exchanger and achieving the lowest temperature is primarily dependent on its performance. To ensure the maximum possible heat exchange between the concentrated and dilute phase, the effective surface area, flow rate and tube sizes are optimized. Since thermal boundary resistance between liquid helium and HeX wall increases with the decrease of temperature, so it demands very large surface area to achieve low temperature. The surface area for cooling the  $^3\text{He}$  below 100mK is selected considering different mixing chamber temperatures. Additional thermal contribution from fluid viscosity and heat conduction along the fluid were considered during the design of HeX. Viscous heating increases as we decrease the tube diameter whereas thermal conduction through fluid decreases. However thermal conductivity and coefficient of viscosity of liquid helium increases as the temperature gets lowered. Because of the gradual decrease in the concentration of  $^3\text{He}$  from the mixing chamber to the still, the average weight density of the fluid increases from the mixing chamber to the still. Whereas the temperature of the fluid increases as it moves towards the still. This condition is likely to induce convective instability which limits the performance of the heat exchanger. However convection is damped by viscosity and thermal conduction of the fluid. The high impedance due to smaller tube diameter in the dilute stream requires larger osmotic drive for  $^3\text{He}$  atoms to diffuse through the column of superfluid  $^4\text{He}$  and reach to still. The pressure drop of the  $^3\text{He}$  in the dilute phase is calculated and found to be much less than the change in the osmotic pressure from the mixer to the still so that the diffusion of  $^3\text{He}$  to the still is not impeded. The HeX is optimized keeping in mind all these factors which determine its

performance. However the HeX had to be small enough to be accommodate in the limited space inside the IVC. It is also desirable to have a small liquid volume to minimize the  $^3\text{He}$  requirements. A tubular continuous counter flow heat exchanger as shown in figure 2.16 was designed and developed and is placed below the still inside the IVC (figure 2.1). The main parameters of this HeX are given in table 2.3. It is made of two thin walled cupro-nickel capillary tubing with brass header. The inner concentrate side tube is of 3mm inner diameter and has a length of 2.4 mts which is inserted inside the 5mm diameter outer tube having a length of about 2 mts, and carries dilute stream. The inner tube is spirally wound inside the outer tube and both the tubes are wound in helical shape as shown in figure 2.16. The spiral provides a large area for heat exchange while allowing a low impedance path for dilute flow along the annular space. The spiral layers are gently separated and bound with braided insulating sleeving to tie the whole structure together while at the same time providing turn-to-turn thermal insulation. The heat exchange has volume of 40cc on the dilute side and 16cc on the concentrated side. The flow impedance were measured for both the dilute and concentrate channel as shown in figure 2.17 using the scheme described in section 2.1.3. The critical region of the heat exchanger is the hottest side of the dilute channel where it enters the still because of the large thermal gradient. This section is made separately and has no obstructions. The returning concentrated phase is lightly connected to this critical region by soft solder at discrete positions before joining fully to reduce thermal gradient.

As opposed to counter flow heat exchangers in which the temperatures of the counter-flowing streams change continuously with the distance, the sintered exchanger's temperature changes in steps. The two sintered exchanger are placed after the continuous exchanger. These sintered exchangers are introduced into the dilution refrigerator to provide a large surface area of contact requires for lowering the temperature further. This

step exchanger consists of blocks containing two cavities into which a high surface area material is sintered. The two exchangers are connected together with short length of low thermal conductivity tubing so that the incoming stream passes through one cavity and the exit stream passes through the other cavity of each block.

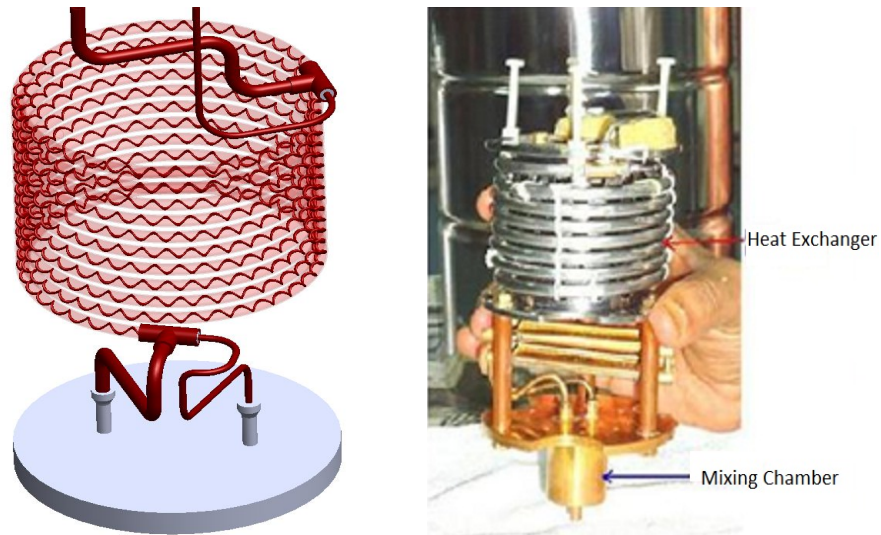
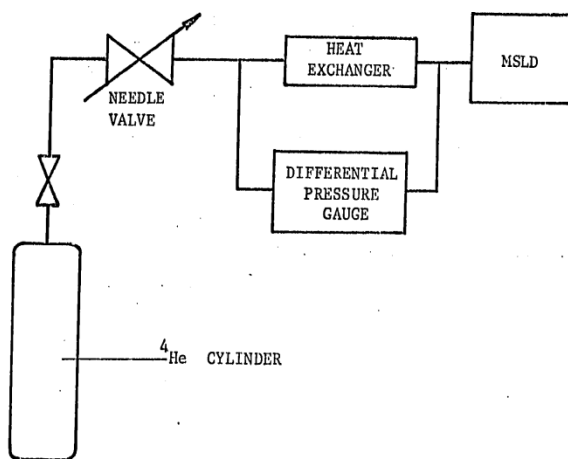


Figure 2.16 3D- Model of HeX and its photograph showing with mixing chamber



Scheme



Measurement

Figure 2.17 Scheme as well as measurement of flow impedance in both dilute and concentrate channels of HeX

Table 2.3: Parameters of tubular helical HeX

	Concentrate stream	Dilute stream
Tube size (mm)	Length: 2400 I.D: 3.0, W.T: 0.3	Length: 2090 I.D:5.0 W.T: 0.4
Surface area (cm <sup>2</sup> )	181	226
Impedance (cm <sup>-3</sup> )	$9 \times 10^8$	$5 \times 10^8$

### 2.1.6 Mixing Chamber (MC)

Mixing chamber is the coldest part of the dilution refrigerator where the interface between concentrated and dilute phase boundaries is situated. The <sup>3</sup>He rich concentrated phase floats above the <sup>4</sup>He rich dilute phase due to the weight difference of the two types of atom. Because of the finite solubility of <sup>3</sup>He in superfluid <sup>4</sup>He at very low temperature the dilute solution contains about 6.4 % of <sup>3</sup>He. Since the vapour phase is continuously removed from the still, to maintain the equilibrium <sup>3</sup>He concentration in the dilute phase, <sup>3</sup>He moves across the interface in the mixing chamber and thereby produces cooling. The size of the connecting tube leading to the mixing chamber is same as that of the tube of the last heat exchanger. The concentrate stream of <sup>3</sup>He enters the mixing chamber via a 6mm diameter tube. The mixing chamber is made of gold plated OFE copper. The free volume inside the mixing chamber is about 10cc and about half of this volume is occupied by dilute phase in normal operation. It is rigidly held in position by fixing it to the heat

exchanger and is provided with calibrated Ruthenium Oxide temperature sensor and manganin heater (560  $\Omega$ ).

### **2.1.7 Gas Handling System (GHS)**

The gas handling system is an important part of the dilution refrigerator having four main systems, the gas storage system, gas circulation system, vacuum system for OVC and IVC and the pumping system for 1K pot. This GHS involve a large collection of pumps, pipes, gauges and valves whose layout is shown in figure 2.18. It is laid out in such way that the four operations namely gas cleaning, condensation, normal circulation and recovery of  $^3\text{He}$  gas are facilitated during different stages of operation. The system includes liquid nitrogen cooled trap, storage tank (dump), precision pressure gauges along with pumps and valves needed to conveniently operate the refrigerator. A bypass valve as shown in the circulating scheme in figure 2.18 is provided to short circuit the two sides of the refrigerator. It prevents to build a large pressure difference across the impedance, which can block the flow of helium mixture during initial condensation stage. Provision is also made for connecting the subsystem via precision metering valve to a mass spectrometer leak detector. This is useful for leak testing, measurement of the  $^3\text{He}$  content of the circulating gas and as an aid in diagnosing refrigerator performance. A relief valve located in the subsystem shunts the  $^3\text{He}/^4\text{He}$  mixture into the storage tank in case a blockage of the refrigerator occurs, and also allows unattended operation for extended period of time. The arrangement of valves permits circulation of the mixture through the nitrogen-cooled charcoal traps prior to its admittance to the refrigerator, thereby ensuring that no contaminants reach the dilution unit. The charcoal traps are pumped out at room temperature between runs. The purpose of different valves will become apparent when the various procedures necessary for the operation of the refrigerator will be discussed later in

section 2.2. As the cooling power of the dilution refrigerator is dependent on the  $^3\text{He}$  circulation rate, the GHS is characterised by the circulation rate it can achieve and the pump it employs.

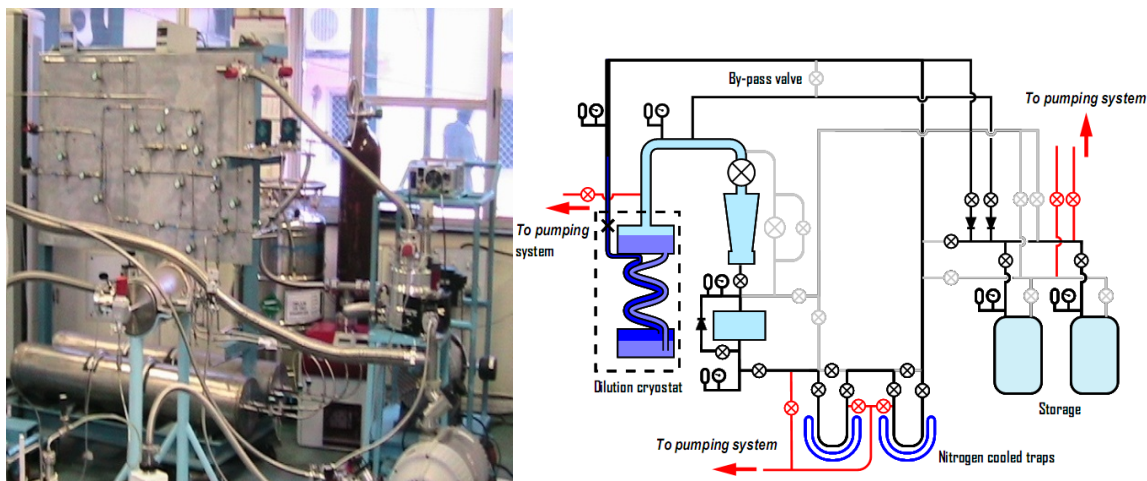


Figure 2.18. Gas circulation and handling system along with schematic flow diagram

The pumping is provided by 10 L/sec helium sealed scroll pump (Edwards model no. XDS35i) which provides a maximum of about 200 micro-moles/sec circulation rate. Interconnection to the pump/purge subsystem is provided by way of a needle valve permitting one to flush the piping network and the vacuum space during start up and to admit exchange gas whenever and wherever necessary in a well controlled fashion. A quick-connect fitting is provided to connect a mass spectrometer leak detector directly to the vacuum space. In order to minimise the vibration the gas handling system is firmly bolted to the floor and physically isolate from the cryostat. In addition, all the tubes are embedded in the concrete of the room for a considerable length. All interconnecting lines are isolated by lengths of flexible convoluted stainless steel tubing followed by a solid tube embedded firmly with ground. The high pressure side of the pump is connected to stainless steel tube of 0.125'' diameter bore which is immersed in the main liquid  $^4\text{He}$  bath and its lower end is connected to the flow-limiting capillary and is immersed inside the 1K

pot. The lower pressure side of the circulating pump is connected to the still by tubes of varying diameter with radiation traps in between them. The gas pressure of the circulating and returning  $^3\text{He}$  is measured by a precision gauge and flow rate is also measured during the operation.

### 2.1.8 Electrical System and Data Acquisition (DAQ)

In order for the refrigerator to operate properly it is necessary to monitor the temperature at several crucial points in the unit. These points are 1K pot, still and mixing chamber. The temperature measurements are diagnostic in nature rather than absolute. All sensors are mounted to their respective position using threaded screws. 36 gauge and 38 gauge manganin wires are used for the sensors and all wires are anchored to the intermediate temperature posts leading to the 300K plate of the cryostat to limit the thermal conduction.



Figure 2.19 Instrumentation rack and Labview based Graphical User Interface for monitoring different parameters of DR

Four numbers of heaters are provided to the activated charcoal trap in IVC, 1K-pot, still and mixing chamber respectively. The cryostat along with the tubing attached to it is grounded electrically. The readings from three numbers of flow sensors and two numbers of pressures are monitored continuously. The LabView based data acquisition software is developed for recording the data continuously as shown in figure 2.19. The heater current

is directly applied from two numbers of Lakeshore temperature controllers (model 336) and one ac bridge controller which is used for the mixing chamber temperature and heater.

## **2.2 Operation of Dilution Refrigerator**

A dilution refrigerator uses a mixture of  $^3\text{He}$  and  $^4\text{He}$  to reach temperature in the millikelvin range. However running a dilution refrigerator under certain regimes with optimum performance is rather tricky and is more of an art than a science. This section discusses the normal procedure for the preparation of the run, the introduction of the mixture into the system and cooling of the refrigerator down to the base temperature. This is mainly divided into five steps; charging of  $^3\text{He}$  /  $^4\text{He}$  mixture into the storage tanks, preparation for run, condensing the mixture, circulating the mixture and finally shutting down and dumping the helium mixture back to storage.

### **2.2.1 Preparation for Run**

The following steps are followed before the actual run of the dilution refrigerator.

- The Outer Vacuum Chamber (OVC) of the cryostat is evacuated using turbo-molecular pump which is backed by rotary pump for several days. The OVC vacuum level reached to about  $2 \times 10^{-5}$  mbar.
- The liquid helium chamber as well as Inner Vacuum Chamber (IVC) is purged and filled with pure helium gas.
- Liquid nitrogen is filled in the outer jacket of the cryostat for about three days before the actual dilution refrigeration operation. The OVC vacuum improved to  $4.2 \times 10^{-6}$  mbar.

- The IVC is leak checked with a mass spectrometer leak detector (MSLD) by spraying helium in the liquid helium chamber, 1K pot and tubing, condenser line and still pumping line. It was found to hover around  $10^{-8}$  mbar-liter/sec.
- Any obstruction in the 1K pot is checked by attaching the mass spectrometer leak detector to the pumping line and spraying helium bath inlet with  $^4\text{He}$  and verifying that helium passed through.
- The room temperature impedance of the assembled dilution insert is measured by connecting MSLD in the still pumping line and passing helium gas at  $\sim 1000$  mbar to the condenser side. If all the impedances are clear, a leak indication should result. This test requires some time for the helium to diffuse through all of the associated capillary tubing and impedances. The leak rate was  $1.39 \times 10^{-2}$  mbar-liter/sec corresponding to an impedance of  $\sim 10^{11} \text{ cm}^{-3}$ .
- The impedance of the cold valve connected to 1K pot is also estimated in both the closed and crack open condition to ensure that the required impedance of about  $2 \times 10^{12} \text{ cm}^{-3}$  is achieved. It is performed by measuring the leak rate by connecting MSLD in the 1K pot pumping line.
- Liquid helium is filled in the helium chamber and subsequently the pressure in the OVC further reduced to  $3.7 \times 10^{-7}$  mbar whereas IVC pressure reached to  $5.2 \times 10^{-6}$  mbar. The liquid helium transfer is carried out very slowly to avoid thermal shocks and to conserve liquid helium. When about 40L of liquid helium is transferred, the liquid level rises to about 200mm above the IVC flange and then the transfer stops. Throughout the liquid helium transfer the IVC pressure is monitored and found to reduce continuously. Large leaks in the

IVC would have manifest themselves in case of an increase of the pressure. The cryostat is allowed to remain at 4.2K for sufficient time to cool all the components to 4.2K.

- IVC is leak checked again for any cold leak and leak rate is found to be of the order of  $10^{-7}$  mbar-liter/sec.
- Thermal exchange gas is given in the IVC at about 3 to 5 mbar pressure and is left overnight for thermal stabilisation of all the components to 4.2K temperature.
- The helium gas is pumped out of the IVC to achieve vacuum better than  $10^{-6}$  mbar.
- After the liquid helium transfer, the condenser lines are checked again for the overall impedance to ensure a clear path for circulating  $^3\text{He}$ .
- 1K pot pump is turned on and the gate valve opened. The cold needle valve is adjusted and temperature is maintained to about 1.5K-1.6 K in the evaporator.
- Pure  $^4\text{He}$  gas is passed in both condenser and still pumping lines by opening the by-pass valve to about 500 mbar pressure.
- The IVC is again leak checked for any super leak and leak tightness is found to be to the tune of  $10^{-6}$  mbar-liter/sec under super fluid environment of liquid  $^4\text{He}$ .
- After closing the by-pass valve the circulating pump is switched on to circulate the  $^4\text{He}$ . This is to ensure any abnormality and leaks in the system. The MSLD is continuously connected to the IVC to monitor both leak rate and gas

pressure. The temperatures of the dilution insert reduced to about 1.7K which is evident from the still and mixing chamber temperature sensors.

- 1K pot pump is turned off and the circulating  $^4\text{He}$  is expelled from the system.

### 2.2.2 Charging of Isotopic Helium Gas Mixture

- The gas handling system is thoroughly leak checked by connecting it with MSLD (figure 2.20) after pressure retention test.

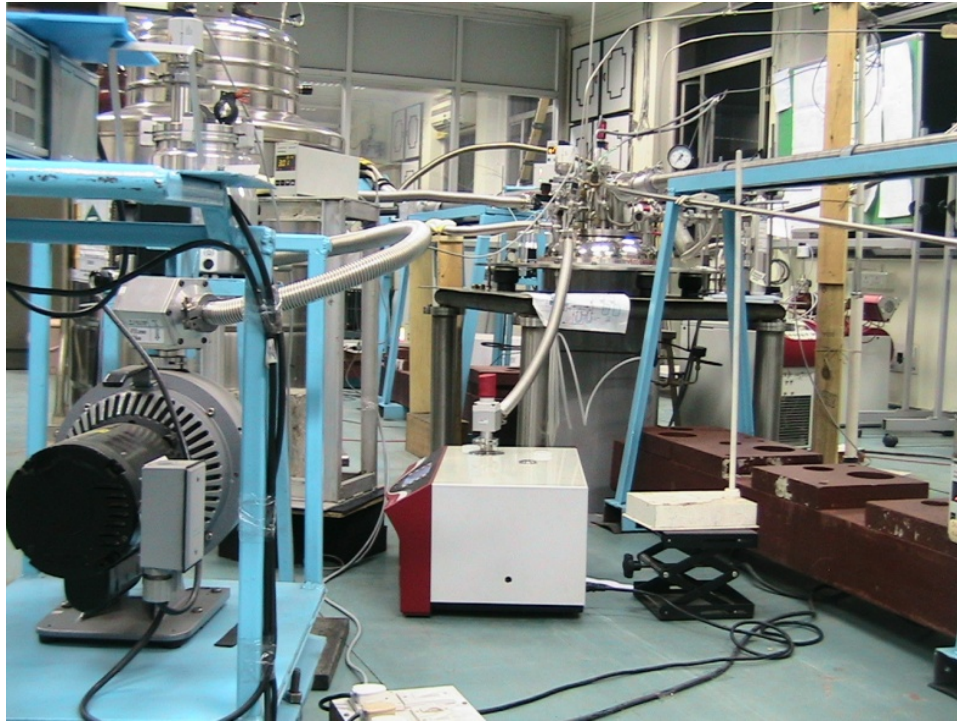


Figure 2.20 MSLD connected for leak testing of different joints and interfaces

- All the lines of GHS are purged with pure helium gas.
- The necessary amounts of  $^3\text{He}$  and  $^4\text{He}$  is estimated on the basis of the volume of the various parts of the dilution refrigerator, including a considerable part of the condensing line which will also be filled with liquid  $^3\text{He}$ . The liquid volume is

estimated to be 90cc of which 25 % were  $^3\text{He}$  and the total number of moles required is about 3. Gas mixer of helium isotopes ( $^3\text{He}/^4\text{He}$ ) is prepared with molar ratio of 1:3 and stored in two storage tanks with capacity of 43L each at pressure of 800 mbar. It is easily determined that a pressure of 600 mbar of  $^4\text{He}$  is needed in the two storage tanks. In a similar fashion 25% of  $^3\text{He}$  corresponds to 200 mbar in the tanks.

- Mixer gas is cleaned by circulating several times through liquid nitrogen cooled charcoal traps. Circulation is slow enough to allow the gas sufficient time inside the trap to achieve thermal equilibrium with the trap. Any contained moisture or air in the mixture gas condenses and trapped in the charcoal.

### **2.2.3 Condensation of Isotopic Helium gas mixture**

The condensation phase is where the bulk of the mixture is taken from the dump i.e. storage tanks and condensed into the mixing chamber.

- 1K pot pump is turned on and the gate valve opened and pot temperature is monitored for stabilization it to about 1.5-1.6K. The needle valve is opened to maintain a constant pressure. If at any point in time this pressure drops to zero, the needle valve is opened so that the 1K pot will not get empty and warm up.
- After stabilization of 1K pot temperature, the mixer gas is passed through both condenser and still pumping line by opening the by-pass valve (see figure 2.18) from the storage tanks. The mixture gas is passed through cold traps before entering the cryostat. Since there is a constriction on the condensing side i.e. concentrate channel of the dilution refrigerator, a by-pass valve is opened to short circuit the condensing side and the still side of the refrigerator to prevents a large pressure difference across the impedance. So the mixer gas is admitted from both the lines simultaneously in a

controlled manner, to avoid large flow through the 1K pot. The by-pass valve is always open until you start to condense the mixture. Initially gas pressure is about 700 mbar and it gradually decreased as the gas condenses. This is passive condensation.

- When the passive condensation is not taking any more gas out of storage tanks, circulating pump is switched on to start active condensation. This ensures no more gas is remaining in the tanks. The mixer condenses further which is evident from the reduction of pressure in the condenser side to about 100 mbar.

#### **2.2.4 Normal Circulation**

Once the mixture condenses, normal circulation starts slowly, initially through a small valve and then by opening the large valve. The objective is to pump the  $^3\text{He}$  from the still, re-pressurise it with the mechanical pump and to re-condense it in the condenser. This circulation causes the mixing chamber to cool below 1K.

- When the condensing pressure remains steady indicating no more condensation, normal circulation is started and the by-pass valve is closed. Initially gas is sucked through a small control valve using the scroll pump at the exits of the still and finally through a large VAT valve.
- As the normal circulation begins, temperature started to decrease and takes about three hours to reach the base temperature of about 45mk. During refrigeration operation the liquid helium re-filling is done two times without any major disturbance to the temperatures. Once the mixing chamber temperature goes to sub-Kelvin, the still heater is turned on using still power. The temperature of the still is increased and the first signs of cooling are observed at the inlet of heat exchanger. The cooling progresses downward towards the mixing chamber along with phase boundary and finally settles in the mixing chamber. The process can be much slower

if insufficient heat is supplied to the still or if the capillary is partly blocked. This makes it necessary to alter the still heater power in order to find the optimum cooling rate.

- Different performance tests is carried out and cooling power of 6 micro-watts is obtained at 50mK. The temperature of the mixing chamber is altered by adjusting the still heater power and by applying power to the mixing chamber heater.

### **2.2.5 Shutdown and Gas Recovery**

In order to terminate operation, the gaseous  $^3\text{He}$  and  $^4\text{He}$  is stored in the storage tank. This is accomplished by connecting both the condenser and still sides of the dilution unit to mechanical pump and exhausts the mixer gas into two storage tanks. The 1K system is then turned off. The pumping is continued until the temperature indicates that the refrigerator is totally above 4.2K. After all the mixture is pumped out, the gas handling system is isolated from the cryostat and the  $^4\text{He}$  exchange gas is added to the IVC to aid warming.

## Chapter 3

# Thermodynamics and Model Simulation under Steady State

Design and fabrication of a dilution refrigerator involves several mechanical challenges and requires a thorough understanding of the thermo-dynamical process occurring at sub-kelvin temperature. The cooling power ( $Q_m$ ), and mixing chamber temperature ( $T_m$ ), are two important parameters of the dilution refrigerator. The cooling power of the dilution refrigerator is obtained from Eq. (1.1), which is primarily dependent on mixing chamber temperature and the temperature of the  $^3\text{He}$  that enters the mixing chamber as discussed in chapter 1. Regardless of the method of calculation used, the available cooling power depends on heat dissipated from external sample insert and the residual heat load, which may slowly decrease with time and approaches a constant value. I have developed a computer program which enables us to have a clear understanding of the underlying phenomena of the cooling process and also enables the characterization of the each components of the dilution refrigerator responsible for satisfying performance. It identifies the different factors required for optimal design and the various means by which the overall performance of a dilution refrigerator can be improved. In addition, mathematical model provides a better understanding of the factors responsible for the efficiency of each component and the performance of the system as a whole.

Several mathematical models have been developed and published earlier as discussed in chapter 1. But none of these models consider all components making up the dilution refrigerator under a closed cycle. The present work attempts to address this matter

and simulate more realistic behavior of the dilution refrigerator. Here each components of the dilution refrigerator are mathematically modeled and are mutually dependent.

In the framework of this thesis, a dilution refrigerator has been built at Helium Technology & Low Temperature Physics Laboratory, VECC to test the results of the numerical simulation and develop technology relevant to dilution refrigerator.

### **3.1 Factors Degrading Refrigerator Performance**

There are several intrinsic factors which degrade the performance of dilution refrigerator and precautions need to be taken to minimize their effects. The convective instability of the dilute side of the refrigerator and the presence of superfluid on the concentrated side are two major factors, among many, that greatly reduce the refrigerator's performance. Hence many experimental observations were rather disappointing and have deviated from the actual values. As sometimes during the operation the temperature at different locations oscillates more abrasively towards the colder ends near the MC. Such fluctuations are generally accompanied by a degraded performance of the refrigerator apart from being a nuisance. Improper design may add to viscous heating and thermal conduction along the liquid column in the dilute channel and prevents from reaching the desired temperature. Hence it is important to understand and identify possible sources of instabilities and consider them right at the design stage.

#### **3.1.1 Convective Instability in Dilute Side**

Convective instability of the dilute phase of the dilution refrigerator returning from the mixing chamber to the still was a problem in earlier refrigerators as suggested by H London and discussed by Hall, Ford and Thompson [8]. They have found that refrigerator started to cool satisfactorily but as the temperature approaches 200mK a catastrophe

occurred in the device which prevented further cooling [8]. The convective instability results from the higher density of the dilute phase in the still as compared to the mixing chamber, since the concentration of lighter  $^3\text{He}$  component in the still is smaller. Convective instabilities are damped by the viscosity of the dilute phase and by the diffusion of  $^3\text{He}$  through super fluid column of  $^4\text{He}$ . If the tube diameter is made reasonably smaller the convection effect will be sufficiently reduced. H London estimated that the critical inner diameter of the dilute phase tube should be of the order of 1mm for the typical conditions [8]. Hence later refrigerators have not experienced this instability since the dilute phase tube inner diameters were kept less than 1mm. Peshkov used a 1mm inner diameter dilute phase tube and found it necessary to have a loop in it to prevent instabilities [41]. The loop provided a region where the density gradient was in the proper direction i.e. the heavier liquid was at the bottom part of the loop. The conditions for the existence of convective instability and for the gravitational waves are closely related [42]. The gravitational forces is damped by the effect of viscosity and thermal conductivity of the fluid as discussed by Wheatley and is most likely at intermediate temperature around 100mK[19]. Convection in the super fluid can do more than increase the effective heat conduction between different parts. A convective eddy in the super fluid might interrupt the uniformity of  $^4\text{He}$  chemical potential  $\mu_4$  and hence there is a distribution of osmotic pressure that drives the  $^3\text{He}$ . Under non-uniformity of  $^4\text{He}$  chemical potential, acceleration of the super fluid occurs and affects the entire dilute side. It is this effect which most seriously affects the overall refrigerator performance and cannot be avoided.

### **3.1.2 Improper Pressure Distribution in Concentrate Side**

Another type of instability, which was pointed by Wheatley, Vilches and Abel [14], can occur when the pressure on the concentrated  $^3\text{He}$  side of the refrigerator falls below the

vapour pressure of the liquid. If the liquid pressure head below the still is too small, then a bubble of  $^3\text{He}$  vapour can form. This  $^3\text{He}$  vapour is forced downward by the action of increased pressure and condenses inside the heat exchanger releasing a large heat load. It may be possible for this condition to exist where a vapour column remain continuously between the still and heat exchanger. Therefore flow impedance is placed to prevent re-evaporation of  $^3\text{He}$ . Similarly, below  $^4\text{He}$  evaporator main flow impedance (primary impedance) is required to establish sufficient pressure head for the incoming  $^3\text{He}$  so that it condenses at that temperature.

### 3.1.3 Effect of $^4\text{He}$ in Concentrate Side

Super fluids  $^4\text{He}$  enters the concentrate side of the dilution refrigerator either by being pumped from the still and circulate it with  $^3\text{He}$  or by creeping from the mixing chamber up the walls of the interconnecting tubing on the concentrate side [43]. Circulated  $^4\text{He}$  will degrade the performance of the dilution refrigerator because heat of separation is released when the temperature falls below the phase separation temperature within the heat exchanger. It also forms a column of superfluid along the inner tube of heat exchanger on the concentrate side. Due to the temperature distribution along the heat exchanger superfluid  $^4\text{He}$  will see different temperatures at different regions along the length of tube. However superfluid helium has a tendency to accelerate whenever chemical potential  $\mu_4$  becomes non-uniform and can lead to vigorous movements. Initially when the refrigerator starts the total amount of circulating gas contains rather high fraction of  $^4\text{He}$ , which sometimes produce violent relaxation oscillations leading to sudden increase of condensation pressure followed by a surge of pressure in the vapour over the still. Moreover the cooling capacity of the refrigerator, which depends on the number of  $^3\text{He}$  atoms diffusing across the phase boundary, is reduced in presence of  $^4\text{He}$  during the

circulation. Since the pumps used for circulation are normally run at near capacity, the amount of  $^3\text{He}$  circulation eventually decreases. Wheatley developed special  $^4\text{He}$  film flow suppressing still to study the effect of circulated  $^4\text{He}$  [19]. Experiment, in which the circulated gas was replaced by pure  $^3\text{He}$  source, resulted in the mixer temperature decreasing from 13mK to 10mK [44].

### 3.1.4 Composition of Isotopic Helium Gas Mixture

The amount of isotopic gas mixture of  $^3\text{He}$  and  $^4\text{He}$  needed to fill the refrigerator is calculated from the volume of all components, including the room temperature parts of the dilution refrigerator. The quantities of  $^3\text{He}$  and  $^4\text{He}$  are estimated assuming that at equilibrium,  $^3\text{He}$  completely fills one side of refrigerator, called the concentrated side and phase separation occurs in the mixing chamber.  $^4\text{He}$  along with some fraction of  $^3\text{He}$  must then fill the rest of the refrigerator up to the still, where liquid-gas phase separation occurs. The  $^3\text{He}$  and  $^4\text{He}$  ratio is selected in such a way that in all conditions of operation, phase separation occurs in the mixing chamber. Too much of  $^3\text{He}$ , shifts the interface towards the dilute side of heat exchanger and the mixing chamber is flooded with pure  $^3\text{He}$ . In such a case the refrigerator would fail to operate. Whereas in the other extreme case of low quantity of  $^3\text{He}$  it may not be as quite as serious. In this case dilute solution completely fills the mixing chamber and is further diluted from its equilibrium value. The mixer is then said to be starved for  $^3\text{He}$  and dilution takes place in the concentrated side of the heat exchanger. Still this will cause the mixer to cool although the effective length of heat exchanger is shortened and leads to performance degradation. Moreover, the position of interface in the mixing chamber affects the time constant of the mixer for temperature stabilisation. Since pure  $^3\text{He}$  has a much higher specific heat than the dilute  $^3\text{He}$  on volume

basis so more  $^3\text{He}$  in the system gives higher time constant, which is desirable for maintaining very uniform temperature in the mixer.

### 3.1.5 Flow Impedance across Heat Exchanger

Designing of heat exchanger demands low flow impedance to reduce viscous heating and small size to economise the amount of  $^3\text{He}$  needed and to get a short thermal time constant. Viscous heating is more serious in the dilute side than the concentrate side and it increases with decreasing temperature. To keep the viscous heating of the two streams in the heat exchanger equal, one needs  $d_d \sim 1.7 d_c$  [1], where  $d_d$  and  $d_c$  are the diameters of dilute and concentrate channel of heat exchanger. Wheatley et al. [13, 14, 19 and 44] have explained arguments that the practical lower limit for  $T_m$  is due to viscous heating and conduction of heat to the mixing chamber through dilute phase. Frossati[30,45] has discussed these problems by considering viscous heating and heat conduction for the concentrated and dilute streams for a tube diameter  $d$ , with  $Q_{\text{visc}} \propto d^{-4}$  (assuming Poiseuille flow) and  $Q_{\text{cond}} \propto d^2$ , the sum of the two is

$$Q_{\text{visc}} + Q_{\text{cond}} = a d^{-4} + b d^2, \text{ where } a \text{ \& } b \text{ are constants.} \quad (3.1)$$

Yielding an optimal channel size

$$d_{\text{opt}} = \left(\frac{2a}{b}\right)^{1/6} \quad (3.2)$$

Since viscosity and thermal conductivity in both concentrated and dilute streams increase with decreasing temperature, their limiting influence becomes more and more severe as temperature goes lower. However, larger impedance of flow channel of dilute stream results in the requirement of higher osmotic pressure difference to drive the flow of dilute  $^3\text{He}$  from mixing chamber to the still.

### 3.1.6 Residual Heat Load

The residual heat load in the mixing chamber happens to be a thermal constraint of the dilution refrigerator, when all external sources of heat are removed and is independent of  $^3\text{He}$  circulation rate. The minimum temperature in dilution refrigerator for a given flow  $\dot{m}$  is decided by the residual heat load besides other factors. The flow dependent heat leak is much higher and can be minimised by appropriate design of the heat exchangers and mixing chamber. In practice, flow dependent heat brought to the mixing chamber by viscosity ( $\dot{Q}_{visc}$ ) and by conduction ( $\dot{Q}_{cond}$ ) is negligible compared to the incoming load from concentrate stream. However at very low temperature this becomes prominent because of the  $1/T^2$  dependence of helium viscosity and  $1/T$  dependence of the thermal conductivity of the liquids. The residual heat leak is likely to come from the exchange gas in the IVC, radiation, vibrations, conductions along the supports etc. Part of this leak generally decreases with time because of absorption of residual gas on cold surfaces, or thermal equilibrium of low diffusive materials. Precaution concerning vibration damping is also important for reduction of residual load.

Thermal conduction along the support structures can be reduced by choosing materials with low thermal conductivity, minimizing the cross section of the structure, maximizing its length and by good heat sinking. In addition to conduction in solids, heat can also be transported through substances which have condensed on the surface of a solid body. If  $^4\text{He}$  is used as exchange gas in the IVC, a superfluid film of  $^4\text{He}$  may cover the cold surfaces and conducts heat. This mobile film creeps to the warmer regions of the machine where it then evaporates. The vapour re-condenses at the colder surfaces, which creates an enormous heat load. This may be avoided by pumping on the vacuum space of

the IVC for a sufficiently long time and using  $^3\text{He}$  as an exchange gas instead of  $^4\text{He}$ . This does not become super fluid at temperatures typically encountered in dilution refrigerator.

Structural relaxation and creep in the material give rise to time dependent heat load [35]. Structural relaxation is the time dependent reduction of stress at constant deformation. Creep is defined as the tendency of material to deform permanently resulting from long exposure to level of stress below the material yield stress. Internal stress introduced from manufacturing process may already be present in the sample before cool down. Stress caused by mechanical loads, such as in support structures, may also relax with time and give rise to a time dependent heat release.

Both eddy current heating of a conductor, vibrating in magnetic field (for example Earth field) and dissipative structural damping of vibrational movement in the cold mass give rise to a heat load on a very low temperature dilution refrigerator. A great increase in heat dissipation can be observed in samples which are simultaneously subjected to vibration and a constant mechanical load such that vibration induces stress beyond the elastic limit [46]. In addition the vibration of the cryostat may lead to swaying of phase boundary inside the mixing chamber. The viscosity of  $^3\text{He}$  at millikelvin temperature range is considerable and may lead to substantial heating under mechanical vibration or movements.

Conduction through residual gas in the IVC is another source of residual heat in dilution refrigerator. Gas particles which do not stick to a surface bounce around in the vacuum space and collide both with hot and cold surfaces. Energy is exchanged during these gas-wall collisions. The resulting heat flux depends among other parameters on the pressure of residual gas. The heat load due to conduction of residual gas is minimized by incorporating large number of thermal shields and thereby preventing the gas particles

from travelling from hot to cold parts in straight trajectories. This also reduces the radiative heat to the mixing chamber. However, the total amount of gas inside the IVC is minimized by improving the vacuum and implementing charcoal traps. Furthermore, the surfaces inside the vacuum vessels of IVC should be carefully cleaned to remove contaminations with a high vapour pressure.

## 3.2 Numerical Modeling

Numerical modeling is a useful tool for simulation of thermal behavior of the dilution refrigerator. It is mandatory for the initial design of dilution refrigerator as it greatly reduces the risk of any serious design flaws. In modelling the dilution refrigeration process we encountered the inherent difficulties of dealing with the varying properties of circulating  $^3\text{He}$  and  $^4\text{He}$  fluids. The fact that these properties vary with both temperature and concentration make them more difficult to thoroughly consider using analytical approach. A numerical model which takes into account these varying properties and deals with the design and optimization of a dilution refrigerator just by putting required input data, turns out to be a somewhat complex assignment. To address this problem we have developed an integrated simulation tool SIDFO (Simulation of Integrated Dilution Refrigerator for Optimization) to design, characterize and optimize dilution refrigerator under steady state condition. Moreover, the data of thermodynamic properties are not available for all temperatures and composition of  $^3\text{He}$  /  $^4\text{He}$  and are compiled and interpolated wherever necessary from various literatures. Some of the features that the present computer programme SIDFO offers are as follows.

- Temperature dependence fluid properties.
- Materials with different Kapitza resistances and its dependence on temperature
- Viscous heating and axial conduction through fluid

- Transient behavior during start-up
- Variation under different still heater settings
- Temperature and pressure at different locations
- Design of individual components and selection of circulating pump
- Convective instabilities on dilute side
- Effect of superfluid  $^4\text{He}$  on concentrate side
- Osmotic pressure which drives  $^3\text{He}$  from MC towards still
- Position of phase separation interface under different operating conditions and gas compositions.

While some numerical analyses of the thermo-dynamical processes related to dilution refrigeration have been published as discussed in section 1.4, we set forward a different approach for simulating a complete and closed cycle of dilution refrigerator based on enthalpy balance. The simulation identifies different abnormalities, which may arise during operation and cannot be easily accounted for by any other models. In addition, the simulation also takes into account the effect of arbitrary flow rates and of varying  $^4\text{He}$  concentration in the circulating gas on the resulting performance. The interplay between the still power and flow rate on the cooling power and the mixing chamber temperature is also investigated. The possibility of the gravitational convective mixing in the dilute solution returning from the mixing chamber to the still is studied for a given design, utilizing the variation of temperature and  $^3\text{He}$  concentration along the dilute side. The simulation results are compared with the results obtained experimentally and are found to comply well. This section discusses the details of numerical modelling, the various factors accountable for optimal design and the different means by which the overall performance of a dilution refrigerator can be improved are also covered in detail.

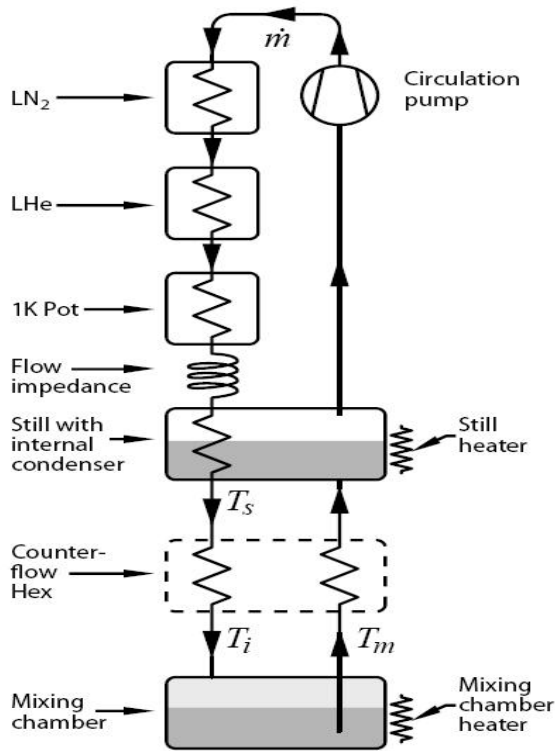


Figure 3.1 Schematic flow diagram of dilution refrigerator used in simulation

For the sake of computational convenience, the dilution system is considered as being composed of four distinct units viz.  $^4\text{He}$  evaporator (1K pot), Still ( $^3\text{He}$  distillation chamber), heat exchanger and mixing chamber. The numerical schemes are framed to couple all these units together considering interactions between them (see Appendix B). The schematic flow of closed and complete system of the dilution refrigerator under which present simulation is based is shown in figure 3.1. This allows a more accurate diagnosis of the dilution process than the analysis of separate units. The performance study is essentially based on determining the cooling power at mixing chamber temperatures as a function of still heater power. The circulating flow rate  $\dot{m}$  and the  $^3\text{He}$  concentration  $x$  is controlled by the still heater for a given still design. In consequence the condensation of the circulating gas is affected and its condensing temperature is calculated iteratively for a

given flow rate as follows below. The meanings of the symbols used in the calculation are described at the beginning under List of symbols.

1. Assume base temperature of pot,  $T_{pot}=1.2K$
2. Compute the maximum possible heat transfer  $\Delta H_{max}$ . ( $=H_{4.2K} - H_{T_{pot}}$ )
3. Obtain the enthalpy reduction of the circulating mixture  $\Delta H = \Delta H_{max} \varepsilon$
4. If  $\Delta H < Q_c$ , go to step 5 else calculate the pot temperature from the measured cooling power at  $Q = \Delta H$ , and go back to step 2.
5. Obtain temperature  $T$  of the circulating gas from enthalpy reduction  $H = H - \Delta H$
6. Find the viscosity  $\eta$  and the volume flow rate  $\dot{V}$  at Temperature= $T$  and  $^3\text{He}$  concentration  $x$
7. Calculate the viscous heating inside the flow impedance  $Z_p$ ,  $\Delta H = Z_p \eta \dot{V}^2$  and the pressure drop  $\Delta P = Z_p \eta \dot{V}$
8. Calculate the condensation temperature and pressure from the enthalpy  $H = H + \Delta H$ .

### 3.2.1 Still and Molar Flow Rate

Gas is circulated by the evaporation in the still and produces cooling by maintaining the equilibrium concentration of  $^3\text{He}$  in dilute phase within the mixing chamber. The selection of the appropriate still power for a given flow rate with the minimum amount of  $^4\text{He}$  is made through simulation. The presence of  $^4\text{He}$  in the circulating gas tends to cause phase separation at higher temperatures in the concentrated side, hence reduces the cooling power. The least amount of  $^4\text{He}$  in the circulating gas occurs when the still heater power is just enough to suppress the film creep and is defined as the critical heater power  $Q_{hc}$ . The critical power of the still is computed to have the lowest percentage of  $^4\text{He}$  in the circulating, gas below which the  $^4\text{He}$  flow rate remains almost constant and depends only

on the creep rate. The vapour pressure and  $^3\text{He}$  concentration in the vapour above still is determined from the energy balance for a given still power. For a pump of a given throughput, the vapour pressure thus obtained determines the amount of helium circulating through the pump. The control volume representing the still for calculation is shown in figure 3.2 and satisfies the following conditions.

1. Energy balance
2. Same chemical potential of  $^4\text{He}$  in both MC and still i.e.  $\mu_4(\text{MC}) = \mu_4(\text{Still})$
3. The flow is limited by the pump throughput,  $\dot{Q} = S_p \times \Delta P$

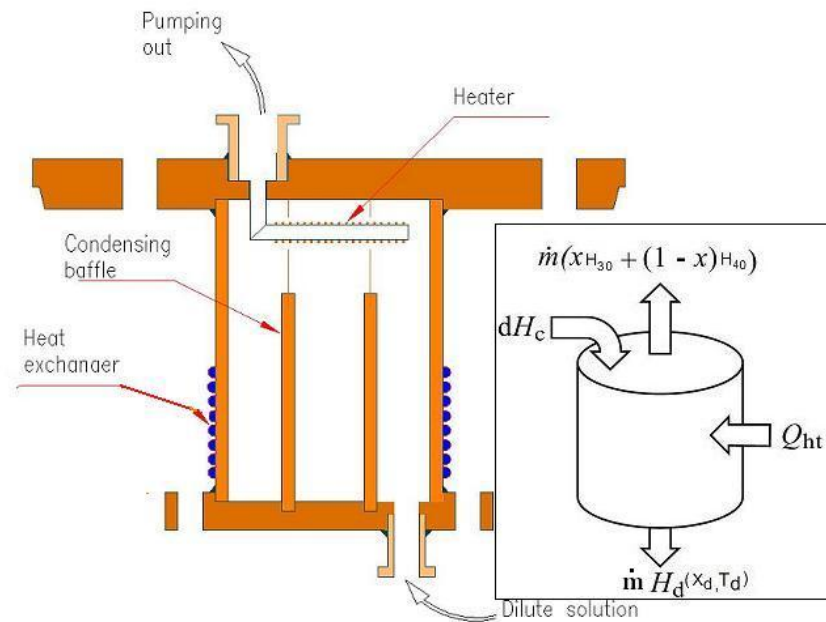


Figure 3.2 Schematic diagram of still and its control volume showing flow lines into and out of it

The energy balance is given by

$$Q_{ht} + dH_c - \dot{m}[H_{30} x + H_{40}(1-x) - H_d(x_d, T_d)] = 0 \quad (3.3)$$

The superfluid component of  $^3\text{He} / ^4\text{He}$  mixture in dilute stream from MC to the still is

driven by chemical potential gradient of  $^4\text{He}$ . The superfluid equation of motion is expressed by

$$\frac{\partial \vec{v}_s}{\partial t} = -\vec{\nabla} \mu_4 \quad (3.4)$$

Where  $v_s$  the superfluid velocity,  $t$  is time and  $\mu_4$  is the chemical potential of the  $^4\text{He}$  component of the mixture [36]. There are no viscous drag terms in Eq. (3.4) so that the superfluid component flows with no viscosity which is true for low enough superfluid velocities unlike normal component of the mixture is primarily driven by pressure gradient. All viscous effects are associated with the normal component of the mixture. It is also assumed that all the flow is hydrodynamic and that the thermal and mass diffusion effects can be neglected. In steady flow, the superfluid velocity does not change in time.

Therefore by Eq. (3.4), the chemical potential of the  $^4\text{He}$  component of the mixture must be same across dilute channel from MC to still. Hence  $^3\text{He}$  concentration in the dilute solution and in the still is computed by exploiting the equilibrium condition expressed by

$$\mu_4 = \mu_4^0(T) - \Pi(T, x_3) V_4 = \text{constant} \quad [28]. \quad (3.5)$$

where,  $V_4$  is the molar volume of  $^4\text{He}$  in the solution and is approximated by

$$V_4 = 27.58 - 3.3 \times 10^{-3} \text{ cm}^3/\text{mole}. \quad (3.6)$$

The effective enthalpy flux in a  $^3\text{He}/^4\text{He}$  fluid stream is given by [47]

$$(\dot{m}H)_{eff} = \dot{m}_3 H_{os} + \dot{m}_4 \mu_4 \quad (3.7)$$

Where  $H$  and  $H_{os}$  are the enthalpy and osmotic enthalpy respectively of the fluid per mole of  $^3\text{He}$ .  $\dot{m}$ ,  $\dot{m}_3$ , and  $\dot{m}_4$  are the molar flow rate of the mixture,  $^3\text{He}$  and  $^4\text{He}$  respectively.

The osmotic enthalpy is a property of the incoming stream. The expression for the effective enthalpy flux works equally well for non-superfluid mixtures both gaseous and liquid. Since chemical potential  $\mu_4$  is the same across dilute channel and  $\dot{m}_4 = 0$  under steady flow, osmotic enthalpy plays a role completely analogous to the enthalpy. The

osmotic enthalpy must be used to describe the enthalpy in the dilute side whereas in the MC, the enthalpy of  $^3\text{He}$  in saturated dilute solution is used.

The gradual decrease of  $^3\text{He}$  concentration along the dilute channel towards the still is computed from Eq. (3.5) & (3.6). The still heater power is estimated for various mixing chamber temperatures under steady flow condition. The applied heater power  $Q_{ht} > Q_{hc}$  decides the ultimate temperature and cooling power by controlling the circulation flow rate and the  $^4\text{He}$  concentration. With reduction of the heater power i.e.  $Q_{ht} < Q_{hc}$ , the total flow decreases, although, the steady superfluid films creep will result in an overall increase of the  $^4\text{He}$  concentration. The vapour pressure above the liquid surface is estimated from the still temperature  $T_s$  and the  $^3\text{He}$  concentration  $x_s$  in the liquid phase using the following relation [13]:

$$P_v = \frac{\left(8.3143 T_s x_s e^{(-2.7/T_s)}\right)}{(27.58 m^*(x_3)^{1.5}) x_v 10^{-6}} \quad (3.8)$$

The change in flow rate is computed iteratively until the pressure at the pump inlet becomes sufficient to maintain the desired volume flow for a given pump capacity. The numerical process to determine the flow rate, temperature and  $^3\text{He}$  concentration in the vapour phase involves the following steps:

1. Assume still temperature  $T_s = T_{pot}$
2. Initialize  $^3\text{He}$  concentration in the liquid phase at still  $x_s = x_m$
3. Calculate the  $^4\text{He}$  chemical potential at the still  $\mu_{4s}$  for  $T = T_s$  &  $x = x_m$
4. Calculate  $^4\text{He}$  chemical potential for saturated mixture  $\mu_{4m}$  for  $T = T_m$
5. If  $\mu_{4s} \neq \mu_{4m}$  then reduce  $x_s$  and go to step 3 else go to step 6
6. Calculate  $^3\text{He}$  concentration in the vapour phase,  $x = x_v(T_s, x_s)$
7. If  $x_v = x$ , go to step 8 else reduce  $T_s$  and go to step 2

8. Calculate vapour pressure  $P_v(T_s, x_s)$
9. Assume pressure at the pump inlet as  $P_o$
10. Calculate flow rate for given pump line diameter
11. Obtain pump inlet pressure  $P_i$  from its pumping speed.
12. If  $P_i = P_o$ , go to step 13 else  $P_o = P_i$  and go back to step 10
13. Print still temperature  $T_s$ , mass flow rate  $m$ ,  $^3\text{He}$  concentration  $x_s$ , vapor pressure  $P_v$ .

It is necessary to ensure that the pressure at all locations on the concentrate side to be larger than the vapour pressure as discussed in earlier section. The total pressure  $P_c$  at point on the concentrate side at an elevation  $h_c$  above the phase boundary in the MC is given by

$$P_c = P_s + \rho_d g h_d - \rho_c g h_c + Z_d \eta_d \dot{V}_d + Z_c \eta_c \dot{V}_c \quad (3.9)$$

Here  $P_s$  is the vapour pressure over the still,  $\rho_d$  is the average mass density of dilute solution,  $h_d$  is the elevation of the interface in the still above the phase boundary in the MC,  $\rho_c$  is the density of the concentrated  $^3\text{He}$  and  $Z_d$ ,  $\eta_d$  and  $\dot{V}_d$  are respectively the impedance factor, viscosity and volume flow rate of the dilute side while  $Z_c$ ,  $\eta_c$  and  $\dot{V}_c$  represent the same quantities for the concentrate side up from MC to the point in question. It is required that  $P_c > P_{\text{sat}}(T)$ , vapour pressure at temperature  $T$ . The program continuously calculates the pressure at all the points along the concentrate side to ensure the desired condition.

### 3.2.2 Cooling Power and the Continuous Counter-Flow HeX

The cooling power at a given mixing chamber temperature is mainly governed by the molar flow rate, the incoming concentrated  $^3\text{He}$  temperature,  $T_i$ , from the HeX and the presence of  $^4\text{He}$  in the circulating mixture. The temperature  $T_i$  primarily depends on the

molar flow rate  $\dot{m}$  and the mixing chamber temperature,  $T_m$ , for a given heat exchanger design.  $T_i$  is virtually independent of the still temperature, whereas the  $^4\text{He}$  concentration increases with molar flow rate. Basically the total molar flow rate  $\dot{m}$  and the  $^3\text{He}$  concentration  $x$  are controlled by the associated mechanical system of still and heater power. In the present simulation, the flow rate and the  $^3\text{He}$  concentration are calculated for our still design for various still heater powers. The generalized cooling power  $Q_m$  in the MC with a molar flow rate  $\dot{m}$  and  $^3\text{He}$  concentration  $x$  is given by the energy balance in the MC as put forward by Radebaugh [28]

$$Q_m = \dot{m} \left[ xH_1[T_m] - \left( \frac{(x-x_i)H_{30}[T_i]}{1-x_i} + \frac{x_i(1-x)H_1[T_i]}{1-x_i} \right) \right] \quad (3.10)$$

It is assumed that the phase boundary between the dilute and the concentrated phase is isothermal and that its temperature  $T_m$  is equal to that of the dilute solution in the mixing chamber. Due to the presence of  $^4\text{He}$  in the circulating mixture the amount of pure  $^3\text{He}$  available for refrigeration is reduced to  $\dot{m} \left( \frac{x-x_i}{1-x_i} \right)$  and the dilute solution already separated out at  $T_i$  will contain  $\dot{m} x_i \left( \frac{1-x}{1-x_i} \right)$  moles of  $^3\text{He}$  and thus the expression for cooling power in the MC is obtained assuming a negligible quantity of  $^4\text{He}$ . Therefore the above Eq. (3.9) for  $x=1$  reduces to:

$$Q_m = \dot{m}(H_1[T_m] - H_{30}[T_i]) \quad (3.11)$$

This is the simplified expression used by several authors [6, 16, 30, 31, and 33] for the cooling power calculation. In practice,  $^4\text{He}$  will always be present under both higher and lower flow rates. The film creep effect enhances the  $^4\text{He}$  percentage in the circulating gas below the critical heater power. Also, above the critical power  $^4\text{He}$  concentration begins to increase with the heater power. Given that the cooling power degrades with the increase of  $^4\text{He}$  concentration in the circulating  $^3\text{He}$ , we find out the optimum heater power for minimizing the circulating  $^4\text{He}$  percentage. The simple expression for the enthalpies of

the dilute and concentrated phases given the linear variation of the specific heat below 50mK [6, 33] are approximated by:

$$C_c(T)=22 T \text{ J/(mole-K)} \text{ and } C_d(T)=106 T \text{ J/(mole-K)} \quad (3.12)$$

The fact that the chemical potentials of the concentrated and dilute phase in the MC must be equal, results in the following expressions for the enthalpies neglecting an integration constant,  $H_c(0)=0$ .

$$H_l(T)=95 T^2 \text{ J/(mole-K}^2) \text{ and } H_{30}(T)=11 T^2 \text{ J/(mole-K}^2) \quad (3.13)$$

The saturated  $^3\text{He}$  concentration at temperature  $T_i$  is given by [31]

$$x_i = 0.0648(1 + 8.4T_i^2 + 9.4T_i^3) \quad (3.14)$$

Hence the cooling power/molar flow rate below 50mK from Eq. (3.9) is reduced by using Eq. (3.12) and Eq. (3.13) respectively.

$$Q_m/\dot{m} = (C_1 - T_i^2 C_2 - T_i^3 C_3 + T_i^4 C_4 + T_i^5 C_5)/C_0 \quad (3.15)$$

Where,

$$C_0=0.935-0.544 T_i^2 - 0.609 T_i^3$$

$$C_1=88.37 T^2 x$$

$$C_2=(5.31+x (6.37 + 51.44 T^2))$$

$$C_3=57.56 T^2 x$$

$$C_4=51.44 x -44.63$$

$$C_5=57.56 x -49.94$$

While in some reported works the ideal condition, assuming  $x=1$  has been taken to study the effect of  $^4\text{He}$  in the circulating gas, we have rather chosen to consider the generalized expression for the cooling power (Eq. (3.9)). However, if we do indeed limit ourselves to the special case of  $x=1$  then our results reproduce those of other workers.

We have made a spiral coiled type heat exchanger manufactured from Cu-Ni tube. This avoids the difficulty of including the very complex behavior of the heat exchange

across sinters which is not only temperature and concentration dependent but also varies with the geometry.

The temperature  $T_i$  of the incoming  $^3\text{He}$ , at the exit of the HeX depends on the performance of the heat exchanger and is a strong function of the Kapitza resistance between the wall and the fluid. To ensure the maximum possible heat exchange between the concentrated and dilute phase effective surface area, flow rate and tube sizes have been optimally determined using SIDFO for improved performance.

An analysis of the continuous counter-flow heat exchanger is based on two coupled differential equations corresponding to the dilute and concentrated phases.

Dilute phase:

$$S_d \frac{d}{dx} \left( k_d \frac{dT_d}{dx} \right) + \mu V_d^2 \frac{dZ_d}{dx} + \frac{dA}{dx} \frac{(T_c^4 - T_d^4)}{4 R_{kt}} = \dot{m} C_d \frac{dT_d}{dx} \quad (3.16)$$

Concentrated phase:

$$S_c \frac{d}{dx} \left( k_c \frac{dT_c}{dx} \right) + \mu V_c^2 \frac{dZ_c}{dx} + \frac{dA}{dx} \frac{(T_c^4 - T_d^4)}{4 R_{kt}} = \dot{m} C_c \frac{dT_c}{dx} \quad (3.17)$$

where the three terms on the LHS represent the axial thermal conduction, viscous heating and radial heat exchange respectively. The thermal conductivity and viscosity both increase with decreasing temperature for  $^3\text{He}$  in both the dilute and concentrated phases. The viscous heating from the liquid flow is proportional to the flow impedance and depends on the geometry of the tubes used. Since the heat exchanger material has a thermal conductance much greater than the Kapitza conductance, thermal gradient across the heat exchanger body is neglected. This means that we can take the temperature on either sides of the heat exchange material separating the concentrated and dilute solution as being the same. The heat is transferred via two Kapitza resistances in series, consisting of Kapitza resistance between the concentrated  $^3\text{He}$  and the heat exchanger wall, and that between the wall and the dilute  $^3\text{He}$ . The small difference between the heat exchange

surface area corresponding to concentrate and dilute side is neglected and the average Kapitza resistivity  $R_{kt}$  is obtained from the sum of the two Kapitza resistances in series. The continuous variation of the temperature and  $^3\text{He}$  concentration along the dilute side is obtained by assuming a constant chemical potential of the  $^4\text{He}$  in the dilute side of the heat exchanger. Since these equations cannot be solved analytically, we solve them numerically with somewhat simplified assumptions and appropriate boundary conditions: a) the thermal conduction term is neglected, b) the effective surface area per unit length of the exchanger is taken as constant, c) the heat transfer rate along a length of  $dx$  is given by  $\Delta Q = \frac{p(Tc^4 - Td^4) dx}{4 R_{kt}}$ , and d) at the entry of the dilute side  $T_d = T_{mc}$ .

Frossati et al. [30] and later Takano [32] have solved the above Eq. (3.16) and Eq. (3.17) assuming perfect continuous heat exchanger and thus neglected the first two terms. Using the specific heat relation from Eq. (3.12), the above equations reduce to

$$T_c \frac{dT_c}{dx} = 4.8 T_d \frac{dT_d}{dx} \quad (3.18)$$

$$T_c \frac{dT_c}{dx} = \frac{0.01 p (Tc^4 - Td^4)}{\dot{m} R_{kt}} \quad (3.19)$$

Frossati solved Eq. (18) and Eq. (19) by assuming the warm end temperatures of the HeX (both dilute and concentrated sides) to be far from  $T_{mc}$  and obtained the relation of cooling power:

$$Q_m/\dot{m} = 95 T_m^2 - \frac{505.78 \dot{m} R_{kt}}{p} \quad (3.20)$$

Takano alternatively assumed  $T_d(0) = T_m$  during integration of Eq. (3.18) and found the relation for cooling power to be:

$$Q_m/\dot{m} = \frac{(106 \text{ Cons} - 128) T_m^2}{\text{Cons} - 1.5} \quad (3.21)$$

$$\text{where } \text{Cons} = \text{Exp} \left[ \frac{0.036 p \dot{m} T_m^2 - 0.00085 Q_m R_{kt}}{R_{kt} \dot{m}^2} \right]$$

The complete solution involving the parameters affecting the performance of the heat exchanger is indeed a difficult problem in terms of numerical convergence and formulation. In the present simulation the heat balance Eq. (3.16) and Eq. (3.17) are numerically solved to obtain the temperature distribution along the length of the heat exchanger on both dilute and concentrated sides by subdivision into  $N$  small sections of length  $dx$ . The input to the first section on the concentrated side is taken from the still heat exchanger output. The lowest temperature in the dilute side of the HeX is assumed to be the MC temperature  $T_m$ . The outlet temperature of one section happens to be the inlet temperature of the next section. Thus the temperature of different sections are related by

$$T_{n+1,c}(\text{input})=T_{n,c}(\text{output})$$

$$T_{n+1,d}(\text{input})=T_{n,d}(\text{output})$$

The input to the first section in the concentrated side is still temperature  $T_s$ . The mixer temperature is taken as the input temperature on the dilute side of the last,  $N^{\text{th}}$  section.

$$T_{1,c}=T_s, \text{ still temperature}$$

$$T_{N,d}=T_m, \text{ mixing chamber temperature}$$

By balancing the change in enthalpy in each sections and using the temperature dependent properties of liquid helium, the heat exchanger problem is solved by iterative numerical process. The heat transfer between the two phases is limited by Kapitza thermal boundary resistance and not the thermal conductivity of the heat exchanger material. To achieve the given base temperature of the mixer and maintaining a constant chemical potential across the dilute side, the concentration of  $^3\text{He}$  flowing through the dilute side was obtained through several iterations. The presence of excess  $^4\text{He}$  in the circulating gas and the resulting phase separation along with thermal effects are probed by the program and presented here.

Convective instability that may grow in the dilute stream for a given geometry of the HeX is already discussed. To study and estimate this instability, two layers of fluid separated vertically by a distance  $z$  are considered. The fluid layer is driven by the gravitational force vertically downwards. The driving force per unit volume for the gravitation wave between two layers can be written as

$$F = g (\rho_2 - \rho_1) = g \left( \frac{d\rho}{dz} \right) z \quad (3.22)$$

It can be written as

$$F = \rho g \left( \frac{1}{\rho} \frac{d\rho}{dT} \right) \frac{dT}{dz} z = \rho g \beta \left( \frac{dT}{dz} \right) z \quad (3.23)$$

Where,  $\beta$  and  $g$  are coefficient of thermal expansion and acceleration due to gravity respectively.  $\rho_1$  and  $\rho_2$  are the solution density  $\rho$  of the fluid at temperature  $T$  and  $T + dT$  respectively.  $\frac{dT}{dz}$  is the temperature gradient along the  $z$  direction ( along the tube axis).

Gravitational wave Equation can be written as

$$\rho g \beta \left( \frac{dT}{dz} \right) z = -\rho N^2 z \quad (3.24)$$

Where  $N$  is the frequency of the gravitational wave and  $N = \sqrt{g \beta \left( \frac{dT}{dz} \right)}$

The conditions for the existence of convective instability and for the gravitational waves are closely related [42]. For exponentially growing wave  $N^2 < 0$ . The gravitational force is opposed by the viscosity and the thermal conductivity of the fluid. From the dispersion relation of plane gravitational wave propagating through a classical one component fluid it can be written the condition for the growing wave [42]  $WR \cong G P > 1$

Where  $G = \frac{N^2 d^4}{\nu^2}$  and  $P = \frac{\nu}{\chi}$  are the Grashof and Prandtl numbers for one component fluid.  $d$  is the characteristic length perpendicular to the tube axis and to the plane of the flow,  $\nu = \mu/\rho$ , viscosity of the fluid. Here  $d$  is taken as the radius of the heat exchanger tube. Therefore  $WR$  can be written as

$$WR = \frac{N^2 d^4}{\nu \chi} = \frac{g \beta d^4}{\nu \chi} \left( \frac{dT}{dz} \right) \quad (3.25)$$

Or

$$WR = \frac{g \beta d^4}{\nu \chi} \left( \frac{dT}{dz} \right) = \frac{\rho g \beta C_{\mu_4} d^4}{\mu k} \left( \frac{dT}{dz} \right) \quad (3.26)$$

where  $\chi = \frac{k}{C_{\mu_4}}$  k and  $C_{\mu_4}$  are thermal conductivity and the specific heat at constant chemical potential of  $^4\text{He}$  respectively.

$$\text{Since } \beta = \frac{1}{\rho} \frac{d\rho}{dT}$$

For the dilute solution [19]

$$\beta \approx 0.53 \left( \frac{dx}{dT} \right)_{\mu_4} \quad (3.27)$$

where, x is the mole fraction of  $^3\text{He}$ . Value of k,  $C_{\mu_4}$  and  $\mu$  are taken for dilute solution of  $^3\text{He}$ . The dimensionless parameter,  $WR$  responsible for growing wave is calculated under a given flow conditions and geometry of the HeX. This probes the convective instability in circulating fluid of DR along dilute side.

Effect of superfluid  $^4\text{He}$  on the concentrated side of HeX is already discussed. Excess  $^4\text{He}$  in concentrated stream will form a column of superfluid along the inner tube of heat exchanger and is in dynamic equilibrium with concentrated  $^3\text{He}$ . Due to the temperature distribution along the tube superfluid  $^4\text{He}$  will see different temperature of concentrated  $^3\text{He}$  at different regions along the length of the tube. The  $^3\text{He}$  will flow through the superfluid column. One end of the column is at temperature  $T_L$  and saturated with  $^3\text{He}$  at this temperature. The resultant partial potential for  $^4\text{He}$  at zero pressure is  $\mu_4(T_L, x_L, 0)$ . Other end of the column is at temperature  $T_H$ , saturated with  $^3\text{He}$  at this temperature and a pressure P.  $T_H$  is greater than  $T_L$ . The superfluid does not accelerate if

$$\mu_4(T_L, x_L, 0) = \mu_4(T_H, x_H, 0) + V_4 P \quad (3.28)$$

Where,  $V_4$  is molar volume of  $^4\text{He}$ .

Eq. (3.28) provides the maximum transient pressure across a non-accelerating column of superfluid with temperatures  $T_H$  and  $T_L$  respectively along the concentrated side.

However at higher temperatures, it is possible for the  $^4\text{He}$  from the MC to diffuse up the incoming  $^3\text{He}$  stream to cause some dilution above the MC. If the velocity of the incoming  $^3\text{He}$  stream is high,  $^4\text{He}$  will be prevented from diffusing up as high as the heat exchanger. Expressed analytically, the stream leaving the heat exchanger will be pure  $^3\text{He}$  for  $\frac{m_3 L V_m}{D S_c} \gg 1$  whereas for  $\frac{m_3 L V_m}{D S_c} \ll 1$  the stream will have the same composition as the concentrate phases in the mixer [28]. In this expression  $L$  is the length of tubing from the HeX to the MC,  $V_m$  is the molar volume of the incoming stream,  $D$  is the diffusion coefficient of  $^4\text{He}$  in  $^3\text{He}$  and  $S_c$  is the cross-sectional area of tube. In practice, something between the two extremes most likely will occur.

Considering the known impedances for both dilute and concentrated sides, the viscous heating and the pressure drop across the heat exchanger have been calculated. The computation ensures that the pressure difference in the dilute side is reasonably less than the osmotic pressure to maintain continuous flow of  $^3\text{He}$  from MC to Still.

The viscosities of the concentrated and dilute phases are assumed to vary with temperature as;

$$\eta_c = (1.8 \cdot 10^{-6}) / T^2 \text{ Pa-sec} \quad (3.29)$$

$$\eta_d = (5 \cdot 10^{-7}) / T^2 \text{ Pa-sec} \quad (3.30)$$

The iteration starts with an initial guess value of the warm end temperature of the dilute side and calculates the final  $N^{\text{th}}$  temperature which successively converges towards the mixing chamber temperature to within an accuracy of  $\pm 1\text{mK}$ . During each iteration, the temperature increment  $\Delta T$  of the dilute side (warm end) continuously changes depending on the difference between the final  $N^{\text{th}}$  temperature and desired mixing chamber temperature ( $T_m$ ). The  $^3\text{He}$  concentration  $x$  is calculated iteratively in a similar

way for each section of the dilute side assuming constant  $^4\text{He}$  chemical potential. The enthalpy of each section for both dilute and concentrated sides is successively obtained from the energy balance and the corresponding temperature is iteratively calculated until an accuracy of  $\pm 1\text{mK}$  is reached. The enthalpy data is taken from Radebaugh's compilations [28] and in the case of the dilute solution the enthalpy is a function of mixer temperature due to its dependence on concentrations. The results so obtained are also influenced by the number of sections which heat exchanger is divided into. The computer program was modified to incorporate variable number of sections depending on the temperature gradient. The conduction heat load to the mixing chamber arising from the finite temperature gradient at the junction is calculated for both concentrated and dilute sides. The expression for the Kapitza resistivity coefficient ( $T^3$ -dependent) between helium and the HeX wall is taken from literature [49]. The following numerical steps were followed for the HeX simulation;

1. Divide the heat exchanger into N sections of equal length  $dx$
2. Assume the exit temperature of the first section on the dilute side  $T_{1d}$
3. Calculate the  $^4\text{He}$  chemical potential at the mixing chamber  $\mu_{4m}$  at  $T=T_m$
4. Assume the  $^3\text{He}$  concentration on the dilute side  $x_{id}=x_m$
5. Find the  $^4\text{He}$  chemical potential  $\mu_{4i}$  at  $T=T_{id}$  &  $x=x_{id}$
6. If  $\mu_{4i} = \mu_{4m}$  go to step 8, else reduce  $x_{id}$  and go back to 5
7. Find the volume flow rate on both dilute  $V_{id}$  and concentrated side  $V_{ic}$
8. Calculate the enthalpies and pressure drop on both dilute and concentrated sides over the  $i^{\text{th}}$  section using energy balance
9. Find temperatures and concentration on both dilute and concentrated sides from corresponding enthalpies.
10. Repeat steps 4-9 for  $i=1$  to  $n$

11. If  $T_{nd}=T_m$  go to step 13 else reduce  $T_{1d}$  and go back to step 4
12. Calculate the thermal conduction load at the mixing chamber on both dilute  $Q_d$  and concentrated sides  $Q_c$  from the temperature gradients at the  $n^{\text{th}}$  section
13. Print  $T_{nc}$ ,  $T_{1d}$   $Q_c$  &  $Q_d$ .

### 3.3 Results and Discussion

The cooling power per unit molar flow rate is calculated and compared with the Frossati and Takano models. The cooling power shown in figure 3.3 is normalized with respect to the maximum upper bound cooling power  $Q_{m,\text{max}}$  at MC temperature  $T_m$  and is given by Eq. (3.11) with  $T_i=T_m$

$$Q_{m,\text{max}}=\dot{m}[H_d(T_m,x)-H_{30}(T_m)] \sim \dot{m}84T_m^2\text{watt} \quad (3.31)$$

The MC temperature  $T_m$  is normalized to the base temperature of the dilution refrigerator in the absence of any heat leak i.e. where  $Q_m=0$ . Figure 3.3 shows the expected temperature squared relationship at higher temperatures.

Since we are assuming an integrated closed system, the boundary conditions are fixed by the ancillary components unlike in the Frossati, and Takano models [30, 32 and 50]. The warm-end temperature on the concentrated side of the HeX is obtained from the output of still module and the cold-end dilute side is assumed to be at the mixing chamber temperature  $T_m$ . Unlike analytical expressions for helium enthalpies (Eq. 3.13) used by others, the present method used the data of Radebaugh compilation [28] at all temperatures during the calculation. Figure 3.4 reveals that towards the higher temperatures the maximum cooling power computed from compiled data somewhat lower than that obtained from  $T^2$  dependent relationship (Eq. 3.31). This finding stems from the fact that small but finite linear temperature dependencies of enthalpies occur towards

relatively higher temperatures. Consequently  $T^2$  -dependence of enthalpies will approximate the energy balance during HeX calculation.

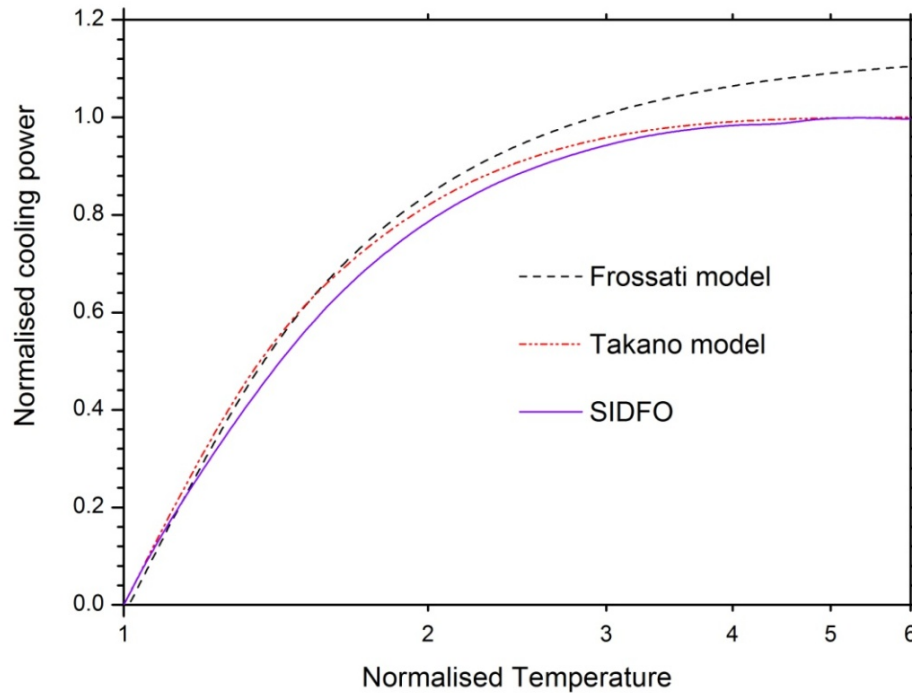


Figure 3.3 Normalized cooling power versus normalized temperature based on Frossati, Takano and the present model

From figure 3.5 we see that the presence of  $^4\text{He}$  in the circulating gas reduces the cooling power from its maximum value for  $x=1$ . The present simulation takes into account variation of  $x$  during calculation under different mixing chamber temperatures and flow rates. At higher mixing chamber temperatures the incoming  $^3\text{He}$  tends to attain the MC temperature very closely as shown in figure 3.6 and the same cooling power given by Eq. (3.31) is obtained.

The molar flow rate for  $^3\text{He}$  and  $^4\text{He}$  with different heater powers is shown in figure 3.7(a). The maximum flow rate for the present design is about  $150 \mu\text{moles/sec}$ , which is decided by the pump and the size of its connecting tubes. Assuming clean and smooth metal surface, the superfluid film creep at the entry of the still pumping line is calculated to be about 2-3 micro moles/sec on the basis of its geometry. To vaporize this

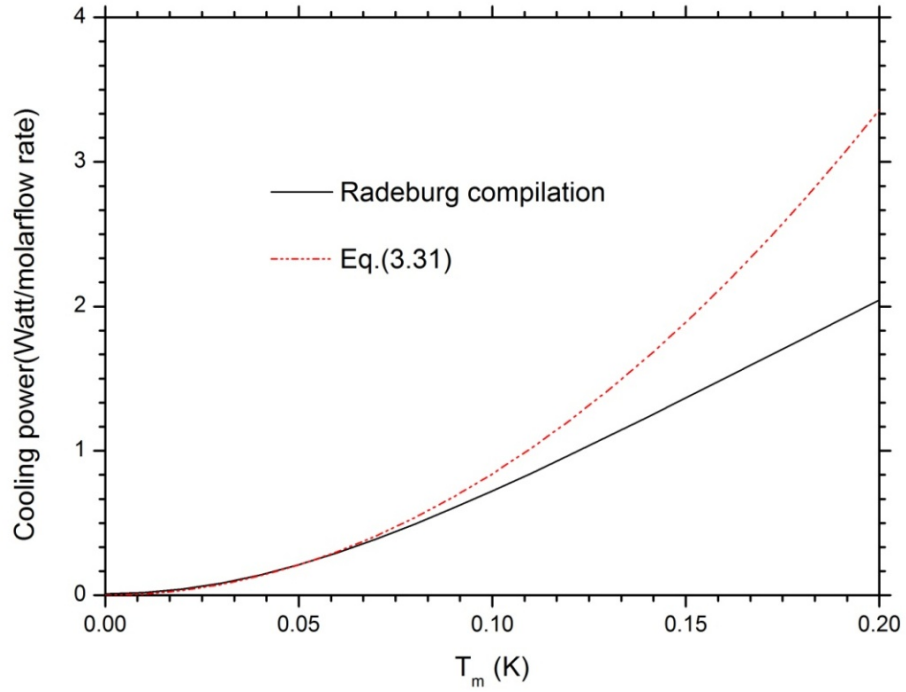


Figure 3.4 Comparison of the maximum cooling power for  $T_i=T_m$

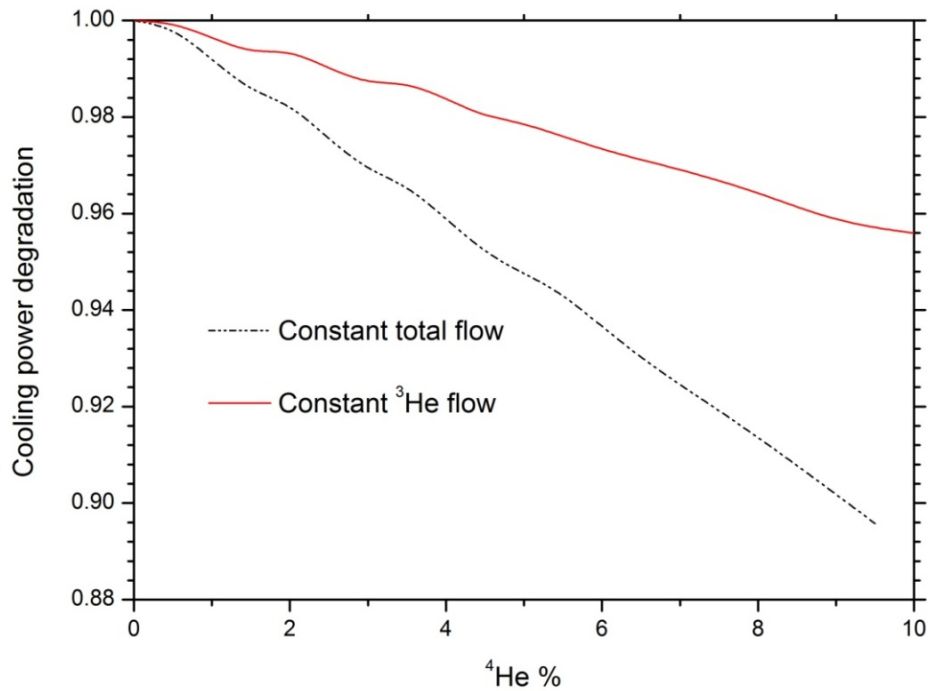


Figure 3.5 Degradation of cooling power with  $^4\text{He}$  percentage in the circulating flow

film flow, the required heat input amounts to the difference in enthalpy of  $^4\text{He}$  between still temperature  $T_s$  and  $T_\lambda$  coupled with the heat of vaporization at  $T_\lambda$  [48]. As such the

estimated critical power,  $Q_{hc}$  of the still turns to be 0.4-0.5mW. Owing to the large thermal conductivity of the superfluid, the  $^4\text{He}$  flow rate remains nearly constant below the critical power and is largely commensurate with the film creep rate [19, 48] as seen in Figure 3.7(a). The total molar flow rate at the critical heater power is about 20  $\mu\text{moles/sec}$  with traces of  $^4\text{He}$  concentration, and increases with increasing still heater power. The measurement is carried out for total flow rate ( $\text{He}^3 + \text{He}^4$ ) using Hasting make flow meter

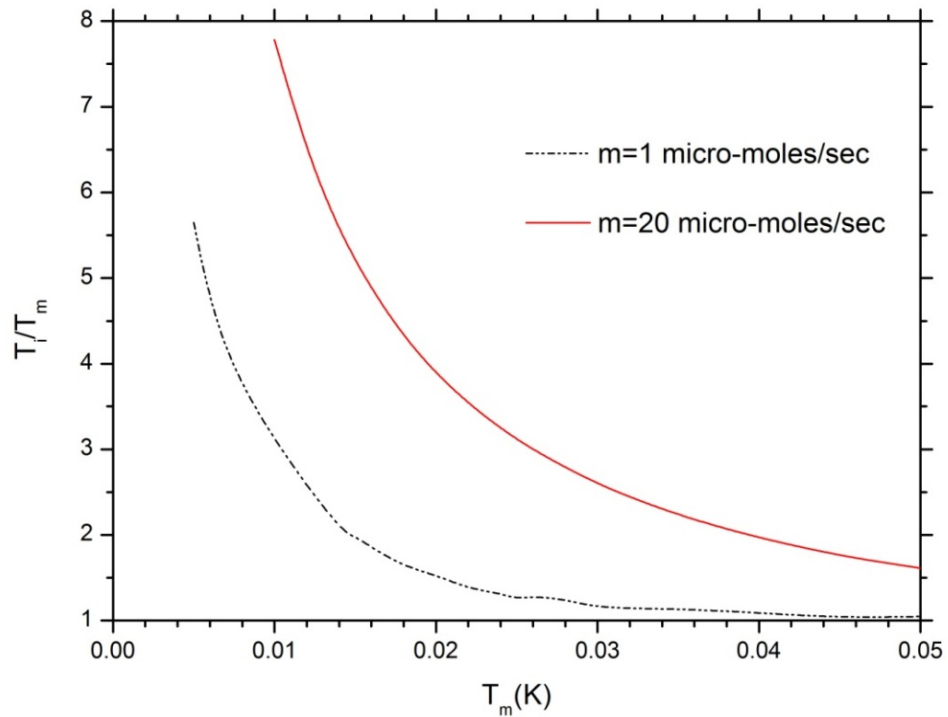


Figure 3.6 Decrease of incoming  $^3\text{He}$  temperature  $T_i$  with MC temperature for a given flow rate  $\dot{m}$

under different still heater power as shown in figure 3.7(b). It is observed that measured flows are more than the calculated values for all the heater settings. This may be due to due to the additional heat load to the still which is not considered during simulation. The measurement may also involve an error in the flow measurement which is calibrated to  $\pm 1\%$  of FS. Though the effect of superfluid creep on flow rate is not visible in the measurement at lower still power.

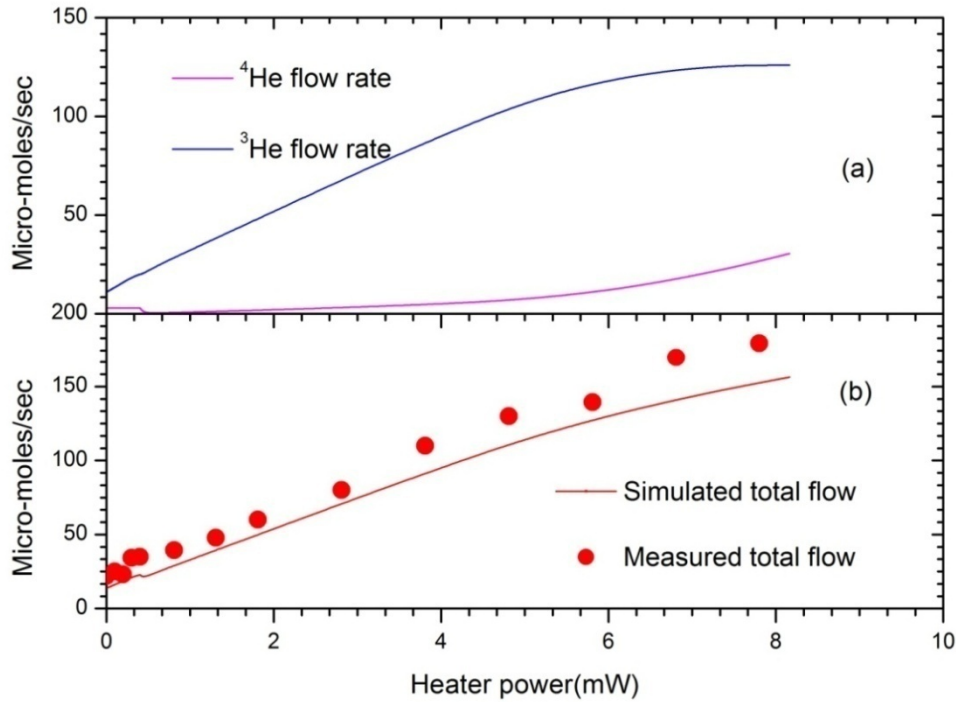


Figure 3.7 (a)Variation of molar flow rate on still heater power showing the film suppression effect and (b) comparison with measurement for total flow ( $\text{He}^3 + \text{He}^4$ )

The continuous counter flow heat exchanger below the still has about  $80 \text{ cm}^2$  of geometrical surface area over a length of 1 meter where heat transfer occurs. Figure 3.8 shows the effect of molar flow rate on the minimum temperature which largely depends on the heat exchange surface area. This minimum temperature may not be achievable in practice since the flow required may not be realized due to high heat load on the still. For the given surface area, a higher circulation flow rate arising from increased heater power may result in the positive effect of more  $^3\text{He}$  atoms crossing the phase boundary. This is likely to offset the negative effect of an increasing heat load to the mixing chamber from the increased temperature of the incoming concentrated stream (figure 3.6). Ultimately the residual heat load decides the minimum temperature achieved during operation of the dilution refrigerator. The steady state behavior of the dilution refrigerator under different still heater settings is experimentally studied. The mixing chamber temperature under ten

different heater settings are measured while giving sufficient time to reach equilibrium in between measurements. This is plotted in figure 3.8 which clearly indicates optimum flow

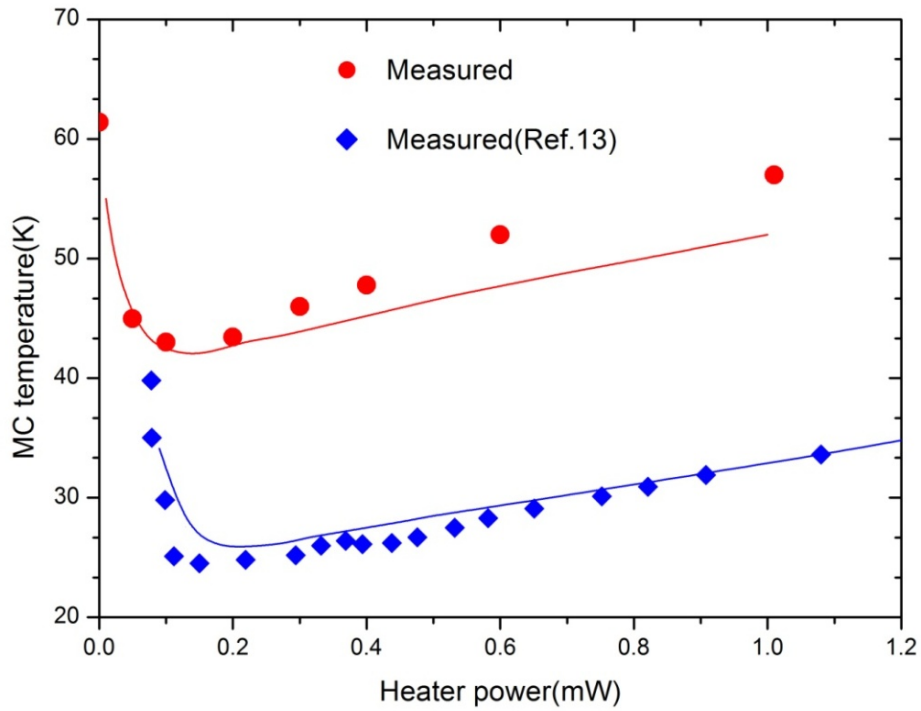


Figure 3.8 Comparison of simulation and measurement of mixing chamber temperature under different still heater powers.

condition. Uncertainties in the temperature measurement do not amount to more than  $\pm 0.5\text{mK}$  and was calibrated upto 25 mK. In figure 3.8, the results from the numerical simulation are given as solid lines. The reduction of geometric surface area of the HeX especially under high circulation flow rate necessitates, to fits the experimental data by choosing an appropriate ratio between the effective and the geometric surface of the HeX ( $S_{\text{eff}}/S_{\text{geom}}$ ) as well as residual heat load  $Q_{\text{mr}}$  to the MC[32, 34]. This indicates that the part of the surface area does not participate in heat exchange between dilute and concentrate side of the refrigerator. So the simulations are carried out assuming a suitable ratio of  $S_{\text{eff}}/S_{\text{geom}}$  and the residual heat load  $Q_{\text{mr}}$ . The cooling power against different MC temperatures are calculated and plotted in figure 3.9 along with a measured data. During the measurement still power remains same at  $\sim 0.4\text{mW}$ . However, Kapitza resistance and

its variation with temperature add another uncertainty for predicting the cooling power of refrigerator.

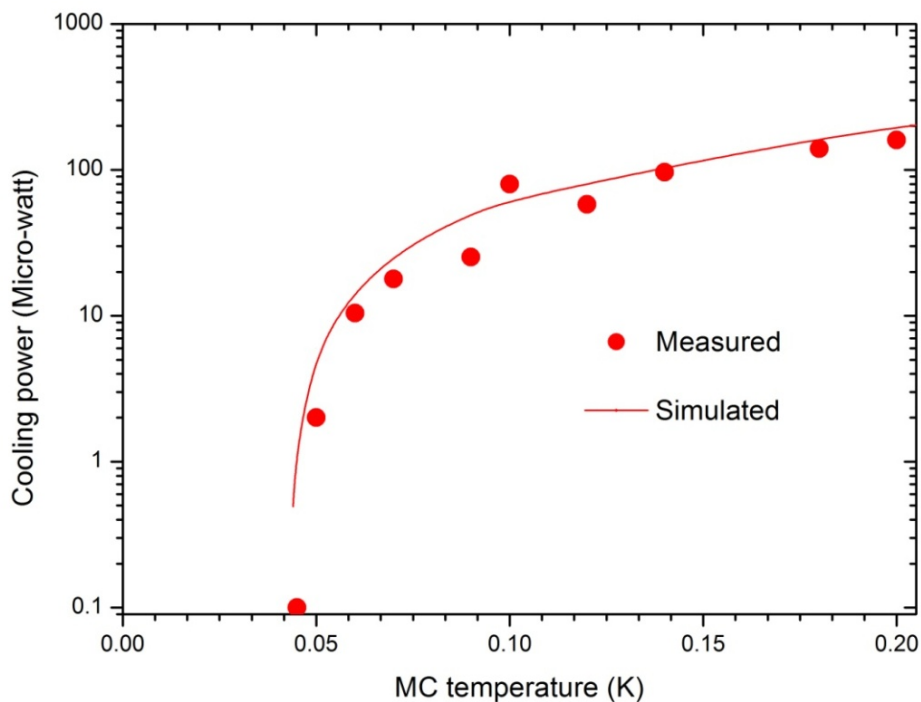


Figure 3.9 Comparison between simulation and measurement for applied power  $Q_m$  to the mixing chamber under different MC temperature for still power of 0.4mW

The degradation of cooling power beyond a certain flow rate is attributed to viscous heating and the increase of  $^4\text{He}$  in the circulating gas. Moreover, in the case of high flow rate, the maximum heat exchange between the concentrated and dilute phases is constrained by the Kapitza conductance. The viscous heating is virtually independent of MC temperature and is found to be 5-6 micro-watts at a molar flow of 150 micro-moles/sec assuming concentrated and dilute flow impedances of  $8 \times 10^9 / \text{cm}^3$  and  $1 \times 10^7 / \text{cm}^3$  respectively. It is interesting to note that the lower cooling power at higher MC temperature say, 100mK endow with the lowest temperature whereas higher still power is appropriate to obtain more cooling power at higher MC temperature.

The temperature of the still provides the primary information about molar flow rate under steady state situation and their relationship is presented in figure 3.10(b) along with experimental data. The figure 3.10(a) shows that the flow rate of  $^4\text{He}$  tends to increase with the still temperature. Evidently, the measure of  $^4\text{He}$  concentration at 0.6K, temperature becomes minimum corresponding to a critical power of about 0.4mW.

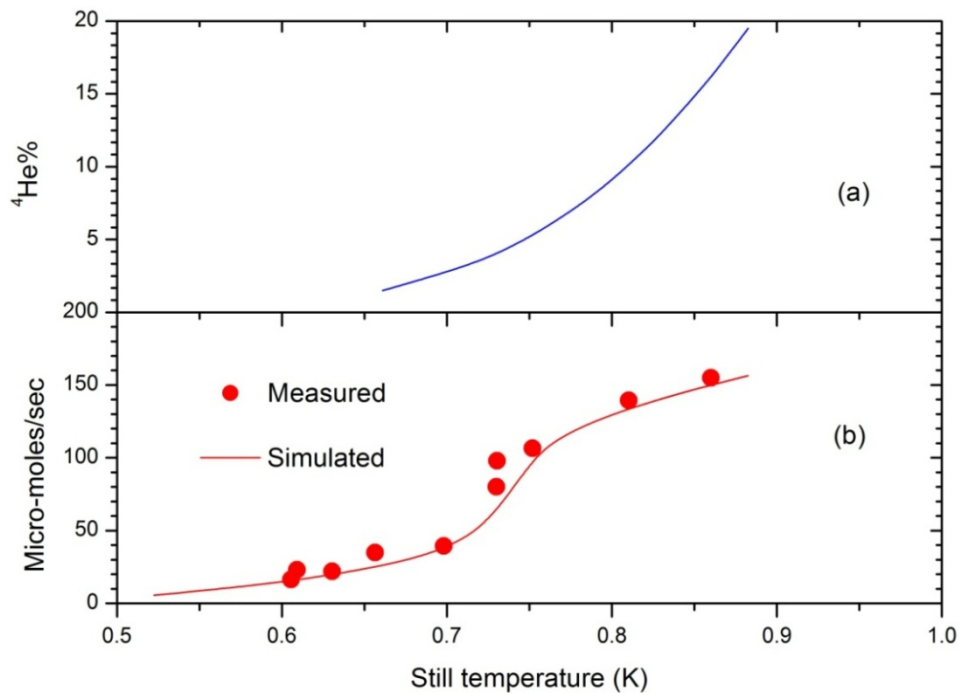


Figure 3.10 Relation between the total molar flow rate, the  $\text{He}^4$  concentration in the circulating gas and the still temperature  $T_s$ .

The variation with flow rate of the osmotic pressure difference between the mixing chamber and still for different mixing chamber temperatures is shown in figure 3.11. This figure indicates that to maintain a continuous flow of  $^3\text{He}$  through the dilute channel, the osmotic pressure difference ( $\Delta\pi$ ) between the mixing chamber and the still should be maintained higher than the pressure drop across the dilute side of the refrigerator which primarily depends on the dilute-side impedance of the heat exchanger. It can be seen from Figure 3.11 that the osmotic pressure remains almost constant for flow rates varying between 40 micro-moles/s and 120 micro moles/s (50mK-80mK). Model simulation

reveals that the osmotic pressure decreases for both higher and lower flow rates. For a design temperature of 50mK, the maximum pressure drop across the dilute side of the HeX is less than 1 mbar for an impedance of  $1 \times 10^7 / \text{cm}^3$ . For temperature of more than 80mK the osmotic pressure difference decreases sharply at lower flow rates which necessitates operation at a higher flow rate for a higher mixing chamber temperature and vice versa (higher flow rate from higher still power giving higher osmotic pressure). For lower temperatures (10mK) the still power is comparatively less, with the lower flow rate being sufficient to maintain adequate osmotic pressure.

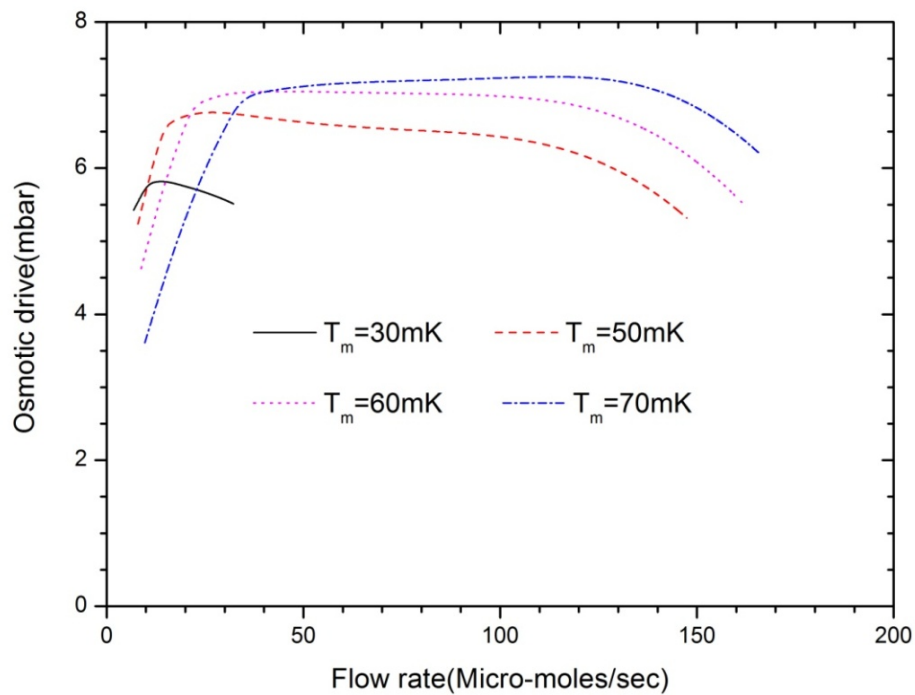


Figure 3.11 Variation of osmotic pressure across mixing chamber and still with molar flow rate for various mixing chamber temperatures

A proper pressure distribution on the concentrated side of circulating mixture is maintained by flow impedance as mentioned earlier in section 2.1.3. These impedances settle the circulation of  $\text{He}^3$ . However very high impedance could result temperature rise due to isenthalpic expansion of the liquid. In our design the circulation rate varies from about 10-150  $\mu\text{moles/sec}$  and accordingly the impedances are fixed. The pressure at the

condenser relative to vapour pressure  $P_{\text{sat}}$  is plotted for different condensing temperatures ( $T_{\text{pot}}$ ), under three different still power settings is shown in figure 3.12. In our case the condensing temperature is about 1.2 K with measured cooling power of about 18mW which could provides the maximum condensing rate of about 180  $\mu\text{moles/sec}$ .

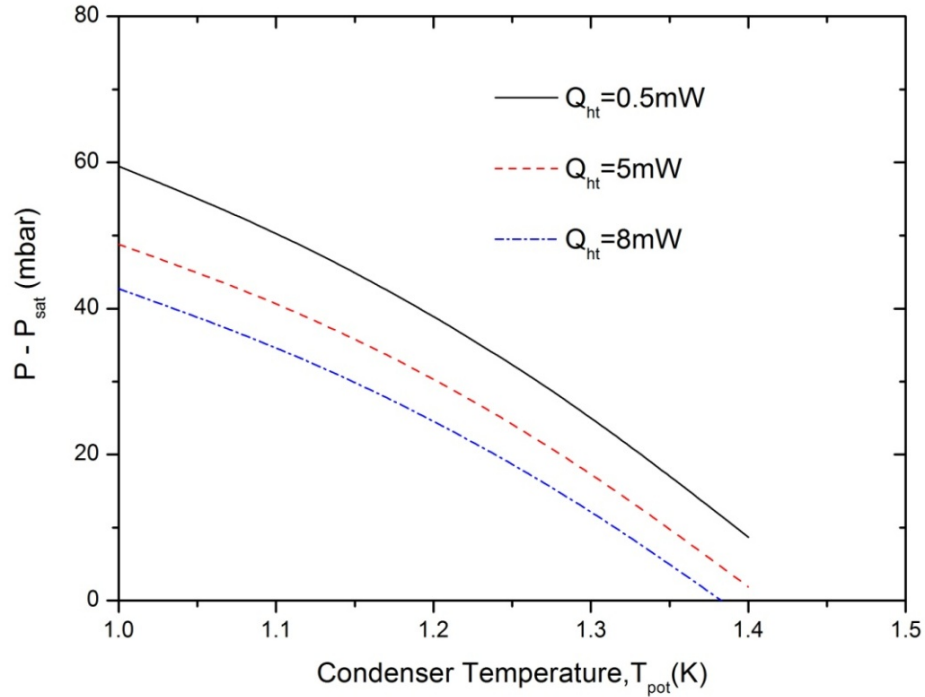


Figure 3.12 Required pressure margins with respect to  $\text{He}^3$  vapour pressure before still under three different heater settings

It is estimated that about 70 mbar of pump discharge pressure is required in maximum flow condition to maintain pressure along the concentrate channel of the DR without exceeding the vapour pressure at any location. Whereas total pressure head to maintain continuous flow for different still heater settings is shown in figure 3.13 with maximum  $\Delta P = 40$  mbar at still power of 8mW. The condensing temperature has a little effect on the  $\Delta P$  with marginal increase at lower temperature owing to viscosity increase. The pressure head  $\Delta P$  increases about 20 mabr with increase of still power which is

provided by the increase of pump discharge pressure with flow rate. This enables to maintain almost negligible pressure before mixing chamber.

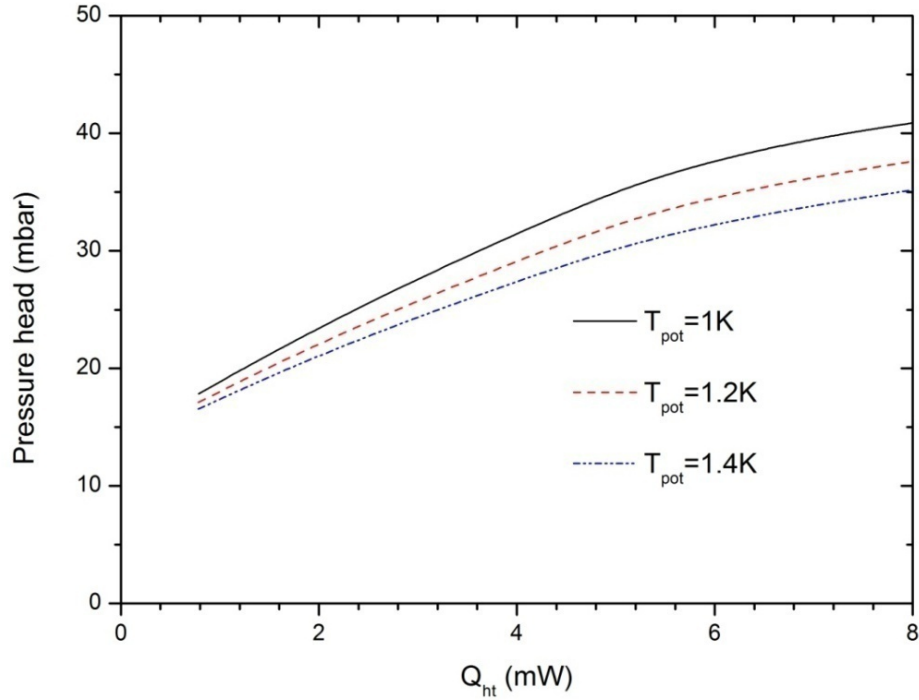


Figure 3.13 Variation of total pressure head with still heater power under three different pot temperatures

The typical temperature distribution along the heat exchanger is determined for a flow rate of 20  $\mu\text{moles/sec}$  and  $T_{\text{MC}} = 50\text{mK}$  and shown in figure 3.14. Using the temperature distribution along the HeX in the dilute side, parameter  $WR$  defined by Eq. (3.26) is determined. The convective instability is damped if the parameter,  $WR$  is kept well below 1.0 as discussed by Whitely J.C [19] and Warkentin P.A [42]. This parameter is plotted in figure 3.15 (b) as a function of temperature of dilute stream. The dilute phase of  $^3\text{He}$  is heated by exchanging the heat with the concentrated phase of  $^3\text{He}$ , as it moves from mixing chamber side to the still side along the outer tube of the heat exchanger.

It is seen from the figure 3.15(b), that the value of  $WR$  increases with the diameter of the outer tube. It also increases with the temperature for a known diameter. This is due

to the fact that the temperature gradient,  $\left(\frac{dT}{dz}\right)$  and also the term  $\frac{1}{T}\left(\frac{dT}{dz}\right)$  increase along the higher temperature side near still of the dilute stream. In figure 3.15(a) the parameter,

$\frac{\rho g \beta C_{\mu_4} T_d}{\mu k}$  designated as '*par*' which is responsible for the convection to occur is plotted

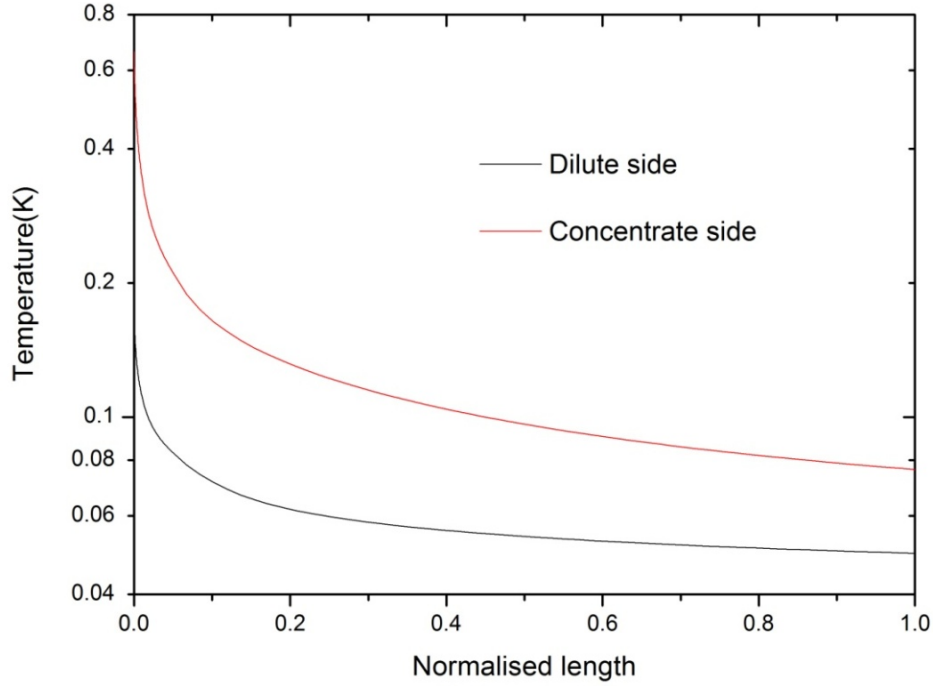


Figure 3.14 Typical temperature profile along the HeX for  $T_{mc}=50mK$

as a function of temperature of dilute stream for diameter of 4 mm. It is observed that convective instability is most likely to grow in the vicinity of 100 mK. So, one can choose the tube of lower diameter at the mixing chamber side and higher diameter at the still end. Choosing the of higher diameter of tube in dilute side one can decrease the viscous heating of the fluid, but possibility of growing convective instability occurs much earlier. It imposed the low temperature limit in the dilution refrigerator.

The Eq. (3.28) is solved numerically by considering a number of superfluid columns connecting concentrated  $^3He$  of different  $T_L$  and  $T_H$ . These  $T_L$  and  $T_H$  are taken from the temperature distribution as shown in figure 3.14. Whereas  $^3He$  concentration at

these two temperatures is determined from the solubility curve. The maximum transient pressure across a non accelerating column of superfluid connecting saturated solution at

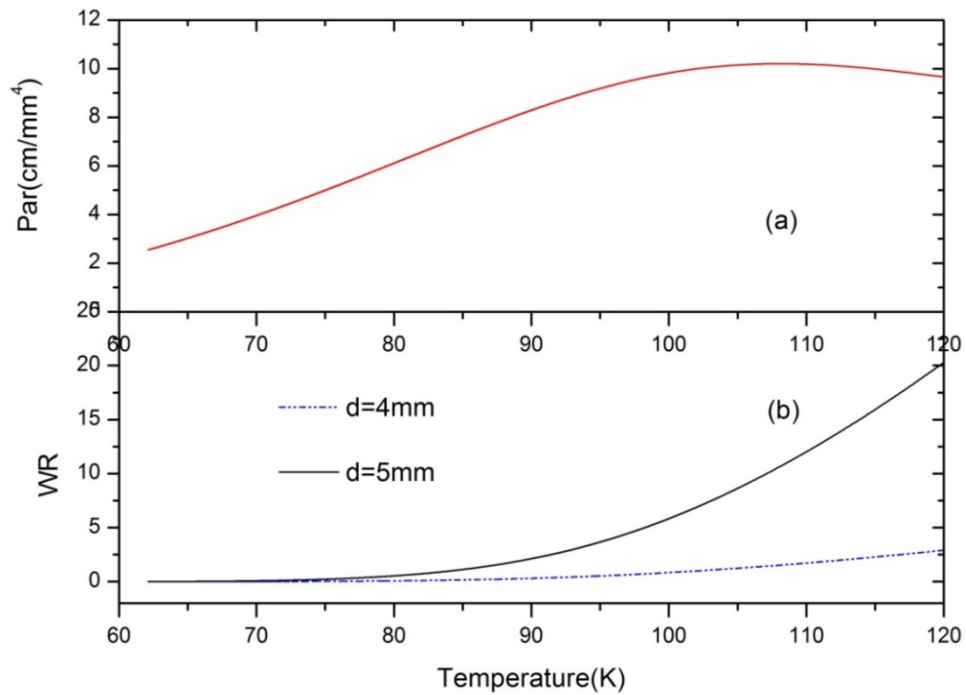


Figure 3.15 Parameters responsible for the convection instability to grow as a function of temperature along the dilute channel

two temperatures  $T_L$  and  $T_H$  along the concentrated side of the heat exchanger tube is calculated and presented in Table 3.1. This table shows that the maximum build up pressure increases as connecting temperatures  $T_L$  and  $T_H$  increases. At lower temperature the build up pressure is below the pressure available to drive  $^3\text{He}$  through the system. Substantial pressure builds up at higher  $T_H$  and it may be comparable to the largest pressure anywhere in the system. This substantial pressure difference may drive  $^3\text{He}$  with an abnormally high speed against the action of viscosity. To preclude the formation of superfluid column one can maintain very high the  $^3\text{He}$  flow through the heat exchanger. Convective instability in the superfluid may also interrupt the uniformity of chemical potential ( $\mu_4$ ) and it affects in the distribution of osmotic pressure that drive the  $^3\text{He}$  through the superfluid in the dilute stream of the heat exchanger.

Table 3.1

---

Pressure in torr and temperature in Kelvin

---

$T_H$ \ $T_C$	0.61	0.46	0.39	0.32	0.23	0.12
0.46	97	--	--	--	--	--
0.39	145	48	--	--	--	--
0.32	169	73	24	--	--	--
0.23	192	95	46	22	--	--
0.12	219	123	74	50	28	--
0.10	240	143	95	71	48	21

---

# Chapter 4

## Thermodynamics and Model Simulation of Transient Phenomena

### 4.1 Introduction

It is important to have a detailed study and analysis of the dilution refrigerator during cool down before reaching its steady state condition. Such a study allows an insight into the various parameters responsible for optimal functioning of the machine. It takes few hours for condensation of the isotopic gas mixture in the refrigerator which occurs at 1.2-1.5 K. For a predetermined gas composition at this temperature,  $^4\text{He}$  becomes superfluid and  $^3\text{He}$  begins to condense. As the normal circulation starts, phase separation initiates at the high temperature end of the concentrated channel of the heat exchanger and eventually the interface propagate towards the mixing chamber. All these phenomena are primarily governed by the effectiveness of the condenser and heat exchanger, initial isotopic gas composition, still heater power and the circulating system. The time variation of all these attributes to reach a stable steady-state condition of the dilution refrigerator with optimum base temperature and desired cooling power necessitates the numerical modelling and simulation under transient conditions.

Achieving the steady state condition of a dilution refrigerator primarily relies on the condensation of the circulating gas mixture in the 1 K pot and the occurrence of phase separation within the mixing chamber. Inside the 1K pot, at the temperature range of 1.2 K – 1.5K,  $^4\text{He}$  becomes superfluid while  $^3\text{He}$  gas at temperature and pressure remains in the

liquid phase. With the passage of time, the temperature of the still gradually falls thereby reducing the vapour pressure substantially, this will result in low flow rate which will prevent the circulating gas from causing phase separation. The transient process of cool-down and subsequent phase separation is simulated by extending steady state simulation program SIDFO [39]. It incorporate the stages of development preceding the steady state condition and obtain the base temperature from a homogenous mixture of liquid  $^3\text{He}$  and superfluid  $^4\text{He}$  [38]. The consequences of several relevant thermodynamic parameters and the composition of isotopic mixture for successful operation of dilution refrigerator are discussed in this chapter. The selection of still heater power and still temperature to set up the right conditions during cool-down for optimal performance of the DR have also been explored.

## 4.2 Process Simulation

To study the operation of dilution refrigerator during transient conditions, SIDFO is extended by introducing a time variable. This analysis is based on a mass and energy balance approach involving time-dependent relationship between pressure, volume, temperature and  $^3\text{He}$  concentration. In the simulation subtle changes occurring in the process of cool down phenomena ahead of reaching base temperature turns out to be rather complex. Formulation for the simulation process requires fundamental understanding of the various stages of cooling and the continuous change of fluid properties with change of temperature and  $^3\text{He}$  concentration. The  $^3\text{He}/^4\text{He}$  mixture in a given proportion is introduced into the system at about 700-800 mbar of pressure and continuously cools down by exchanging heat in the 1K pot. Eventually, both helium isotopes gets condense into a homogenous mixture. The simulation is carried out by stringing together each component of the system and numerically solving them [38]. Additional auxiliary

structured modules are added to modify the process flow sheet easily with minimal recoding. The computer program is made modular which means that the code which represents each piece of equipment is assembled into one sub-routine. The simulation helps to diagnose and identify the system performance as well as control and run for a variety of input conditions. The primary goal of the simulator is to calculate values of temperature, pressure and  $^3\text{He}$  concentration of the  $^3\text{He}/^4\text{He}$  mixture over time with reasonable accuracy for a set of probable input conditions. It is desirable to have phase separation in the mixing chamber for optimal performance. Hence the program precisely locates the position of the phase-separation interface during cool-down under different operating conditions. The phase separation temperature and  $^3\text{He}$  concentration in the separated mixture for a given composition of mixture is also calculated using a separate auxiliary module in the program.

#### **4.2.1 Process Description**

The dilution refrigerator is assumed to consist of five distinct units which are interconnected to make a complete and closed system as discussed earlier in section 3.2 and the schematics of the process flow is given in figure 3.1. The room-temperature circulating pump extracts the mixture from the still and returns it to the dilution unit through successive cooling stages at 77K and 4K temperatures before it enters the condenser. Simulation relies on the experimental data with a condensation temperature of 1.2 K with a cooling power of about 18mW [40].

As the gas mixture condensed and fills the colder section of the refrigerator, normal circulation starts to pump out the vapour from still.  $^3\text{He}$  content of the circulating gas increases as the time progresses and the  $^4\text{He}$  largely settles down inside the dilute channel starting from MC to still. This ensures continuous circulation and maintains dynamic equilibrium at low temperature. This sucked gas is pushed back into the cryostat

through the discharge port of the pump. The concentrated mixture leaving the condenser is further cooled by the still before it is directed to the main heat exchanger. The heat exchanger plays the key role of reducing the temperature of the incoming concentrated  $^3\text{He}$  to a temperature close to that of the mixing chamber by exchanging heat with the returning dilute solution from the MC. Finally, the concentrated  $^3\text{He}$  mixture enters the MC where the interface between the concentrated and dilute phases occurred.

The transient cool-down of dilution refrigerator comprises of following discrete steps.

1. Filling of the dilution insert with the homogenous mixture of  $^3\text{He}/^4\text{He}$  with a concentration ranges from 25% to 40% of  $^3\text{He}$
2. The condensation of gas mixture by heat exchange with the 1K pot.
3. The circulation of the mixture by pumping thereby reducing the vapour pressure at the still and bringing down the temperature further.
4. Maintaining the still temperature thru still heater to ensure adequate flow and initiation of phase separation.
5. The phase separation interface gradually reaches the mixing chamber and cools further to the base temperature by dilution of  $^3\text{He}$  atoms in  $^3\text{He}/^4\text{He}$  mixture.

For optimal performance of the dilution refrigerator, the total amount of mixture and ratio of  $^3\text{He}/^4\text{He}$  in the mixture must be tuned in order to obtain phase boundaries within the MC at desired position. This transient simulation helps to diagnose and avoid phase transition in the HeX and avoid degradation of cooling power. While considering the  $^3\text{He}/^4\text{He}$  ratios inside the dilution refrigerator, the dead volume of the circulating pump presumed to be negligible compare to the total volume of the closed circulating system. After the occurrence of the phase separation, osmotic drive facilitates the continuous flow of  $^3\text{He}$  across the phase boundary within the MC and produces desired cooling effect.

## 4.2.2 Numerical Model

Each component of the dilution refrigerator is conveniently represented in the form of a control volume as already described in the chapter 3. It is important to determine the position of the phase separation for possible sets of operating conditions. The circulation rate is effectively controlled by the still heater and this in turn controls the heat extraction rate in the MC. Because of the large specific heat of the dilute  $^3\text{He}$  returning from the MC to the still coupled with marginal thermal load from the incoming concentrated phase keeps the still on cooling. It is fair to assume that the heat capacity of the metallic part is negligible compared with the solution. A realistic way is to consider the volume of the still and mixing chamber to be fairly large compared to the total volume of the interconnecting pipe lines.

Analysis for the heat exchanger is based on two coupled differential Eq. (3.16) & Eq. (3.17) corresponding to the dilute and concentrated sides of the exchanger. The details of the equations are already described in chapter 3. As earlier, these heat balance equations are numerically formulated in order to yield the temperature distribution along the length of the heat exchanger on both dilute and concentrated sides. This is achieved by subdividing the exchanger into N number of small sections of length dx. The effective length of the heat exchanger is determined from the position of phase separation. The input to the first section on the concentrated side is taken from the still heat exchanger output. The calculation starts with an initial guess temperature on the warm end of the dilute side and calculates the final  $N^{\text{th}}$  temperature on both dilute and concentrated side of the HeX. The outlet temperature of one section is taken to be the inlet temperature of the next section. Thus the temperatures of successive sections are related by

$$T_{n+1,c}(\text{input})=T_{n,c}(\text{output})$$

$$T_{n+1,d}(\text{input})=T_{n,d}(\text{output})$$

The input to the first section in the concentrated side is still temperature  $T_s$ .

$$T_{1,c}=T_s, \text{ still temperature}$$

The guess temperature at the warm end of dilute side of the HeX is continuously varied to satisfy energy conservation in the MC for a time interval,  $\Delta t$ . The enthalpy difference between the outgoing dilute and incoming concentrated mixture measures the cooling of the mixing chamber as  $^3\text{He}$  atoms cross the phase boundary and enters into the dilute phase. The total moles in the concentrated and dilute phase are computed along with the corresponding specific heat that is used for finding the change of temperature.

$$T_m = T_m - \frac{Q_m \Delta t}{C_c(T_m)n_c + C_d(T_m,x_d)n_d} \quad (4.1)$$

The temperature of the mixture  $T_{N,d}$  obtained from the heat exchanger module must be equal to the MC temperature  $T_m$ . By balancing the change in enthalpy in each sections of the HeX and using the properties of two liquid phases, a solution is obtained for each time step by iterative numerical process.

The Kapitza resistivity between liquid helium and the HeX wall is taken from literature [49]. The viscosity of the concentrated and dilute phase is assumed to varies with temperature as given by Eq. (3.29) and Eq. (3.30) respectively.

The temperature and  $^3\text{He}$  concentration in the still is determined from the energy balance for a given heater power. The available cooling inside the still is given by

$$Q_s = Q_{ht} + dH_c - \dot{m}([xH_{30} + (1-x)H_{40}] - H_d(x_d, T_d)) \quad (4.2)$$

The number of liquid moles inside the still is obtained from the  $^3\text{He}$  concentration and its liquid volume as:

$$n_s = \frac{rr V_{mc}}{27.58 + 7.6 x_s + 1.65 x_s^3} \quad (4.3)$$

The  $^3\text{He}$  concentration  $x_s$  in the still is computed exploiting the equilibrium condition expressed by Eq. (3.5)

Next temperature following the time increment  $\Delta t$  turns out to be

$$T_s = T_s - \frac{Q_s \Delta t}{C_d(T_s, x_s) n_s} \quad (4.4)$$

The vapour pressure above the liquid surface is estimated from the still temperature  $T_s$  and the  $^3\text{He}$  concentration  $x_s$  in the liquid phase using Eq. (3.8).

The pressure at the inlet of the pump is calculated from the pressure drop across the still pumping lines, and the flow rate is iteratively computed until the pressure at the pump inlet becomes sufficient to maintain the flow for a given speed.

The phase separation temperature for a given composition of the  $^3\text{He}/^4\text{He}$  solution is obtained from the phase diagram of  $^3\text{He}/^4\text{He}$  solutions. The solubility curve for a dilute solution is given by [31]

$$\frac{x_l}{(x_l + y_l)} = 0.0648 * (1 + 10 * T^2) \quad (4.5)$$

And the solubility curve for the concentrated solution is given by [31]

$$\frac{y_u}{(x_u + y_u)} = 0.85 * T^{1.5} * \text{Exp}[-0.56/T] \quad (4.6)$$

$$x_l + x_u = m x \quad (4.7)$$

$$y_l + y_u = m (1 - x) \quad (4.8)$$

Total number of moles of  $^3\text{He}$  and  $^4\text{He}$  remain the same after phase separation. Two mass conservation Eq. (4.7) & (4.8) defining the moles of  $^3\text{He}$  and  $^4\text{He}$  and the solubility Eq. (4.5) & (4.6) governing the  $^3\text{He}$  concentrations are used to find phase separation temperature and the  $^3\text{He}$  concentration in the phase separated mixture.

The volume of the still containing liquid immediately after the initial filling and before circulation begins is written by

$$V_s = r r V_{mc} \quad (4.9)$$

If the system is filled with  $n$  moles of  $^3\text{He}$  and  $^4\text{He}$  with concentration  $x_i$  then

$$n V^i = V_{mc} + V_s + V_{hx} + V_c \quad (4.10)$$

where  $V^i = 27,58 + 7.6 x_i + 1.65 x_i^3$  is the molar volume of the initial mixture and  $V_{hx}$  is defined as

$$V_{hx} = (S_d + S_c) * L \quad (4.11)$$

where  $V_{hx}$  is the liquid volume inside the HeX and  $V_c$  is the liquid volume within the condenser.

Computer program continuously calculates the moles of  $^3\text{He}$  and  $^4\text{He}$  for both dilute and concentrated side along the HeX. While cooling down, the fraction of change in liquid level inside the still relative to the initial level is designated by  $h_s$  whereas the fraction of the mixer volume occupied by dilute solution is represented by  $h_m$ . By neglecting the volume of the room temperature gaseous mixture,  $h_m$  and  $h_s$  are obtained by solving the following equations

$$(1 - h_m) * \frac{V_{mc} x_{3u}}{V_{mu}} + h_m * \frac{V_{mc} x_{3l}}{V_{ml}} + h_s * \frac{V_s x_s}{V_{ms}} + n_{3c} + n_{3d} + n_{3s} = n * x_0 \quad (4.12)$$

$$(1 - h_m) * \frac{V_{mc}}{V_{mu}} + h_m * \frac{V_{mc}}{V_{ml}} + h_s * \frac{V_s}{V_{ms}} + n_c + n_d + n_s = n \quad (4.13)$$

The Eq. (4.12) represents the total number of moles of  $^3\text{He}$  in the system and the Eq. (4.13) gives the total number of moles of the solution. All the molar volumes  $V_{mu}$ ,  $V_{ml}$  and  $V_{ms}$  are functions of  $^3\text{He}$  concentration, which continuously varies as cooling, occurs. Initially, phase separation occurs inside the HeX at a length  $L_{sep}$  from its warm end side then  $h_m=1$  and the above two equations can be re-written as

$$\left[ V_{mc} + \frac{V_{hx}(L-L_{sep})}{L} \right] * \frac{x_{3l}}{V_{ml}} + V_{hx} * \frac{L_{sep}}{L} * \frac{x_{3u}}{V_{mu}} + h_s * \frac{V_s x_s}{V_{ms}} + n_{3c} + n_{3d} + n_{3s} = n * x_0 \quad (4.14)$$

$$\left[ V_{mc} + \frac{V_{hx}(L-L_{sep})}{L} \right] * \frac{1}{V_{ml}} + V_{hx} * \frac{L_{sep}}{L} * \frac{1}{V_{mu}} + \frac{V_s}{V_{ms}} + n_c + n_d + n_s = n \quad (4.15)$$

The above four auxiliary equations are used in separate module and is called from the main program in each time step to calculate  $h_m$  and  $h_s$ , two diagnostic parameters help to examine the position of the phase separation within the mixing chamber and liquid volume inside the still respectively.

### **4.2.3 Solution Method**

The actual solution of the temperature at a given point in time and position is based on the known states at previous times. The temperature at the warm end of the dilute side of the HeX remains unknown, while the energy conservation condition is defined at the cold end side for each time step. This presents a problem because with a downwind scheme the entire state at the warm ends is required as a boundary condition. Therefore an iterative method of solution was used. The method uses a guess temperature at the warm end of the dilute side of HeX , and iteratively solves for the lower temperatures close to the MC. These temperatures are compared with the temperature obtained from the energy conservation inside the MC. The temperature error was used to update the guess value of warm end temperature, and the iterative procedure is continued leading to convergence.

The complete solution in transitory stages involving the parameters affecting the performance of heat exchanger happens to be rather difficult in terms of numerical formulation and convergence. However, convergence of numerical solution while maintaining a constant chemical potential across the dilute side was obtained through several iterations. Considering the measured impedances for both dilute and concentrated sides, viscous heating and pressure drop across the heat exchanger have been estimated. The computation ensures that the pressure difference across the dilute side is reasonably less than the osmotic pressure to maintain continuous flow of  $^3\text{He}$  from MC to Still.

The numerical convergence is obtained through successive iteration by using a suitable relaxation factor to speed up the convergence with an error of less than 1mK. The fluid properties for the concentrated and dilute mixture are exploited as the phase transitions interface in the inner tube moves down the heat exchanger. The results thus obtained are also affected by the number of sectional increments which the heat exchanger is divided into. The computer program was modified to incorporate time-dependent discretisation of heat exchanger depending on the temperature gradient.

In general, the solution of the equations necessitates an under-relaxation technique for convergence keeping the iteration process stable without losing any information or compromising the precision of outcome. Thus for a given iteration  $k$ , the guess temperature takes the values in accordance with the following relationships.

$$T_k = T_{k-1} + \Delta T_m * \omega \quad (4.16)$$

$$\Delta T_m = (\Delta T_{m, k-1} + \Delta T_{m, k}) * 0.5 \quad (4.17)$$

$T_k$  is the temperature of the current iteration  $k$ , and  $w$  is a relaxation factor between 0 and 1 and was varied during simulation to improve the stability of the solution and the speed of computation.  $\Delta T_m$  is the difference of MC temperature obtained from energy conservation and output from HeX module. The Eq. (4.17) is used to update  $\Delta T_m$  after each iteration until the comparison indicates that the two most recent temperatures are within some tolerance limit, usually  $\pm 1\text{mK}$ . The solution converges smoothly to the desired accuracy after several iterations. The size of the numerical time step relative to the size of the numerical space step is chosen carefully to preserve system stability. Furthermore, increasing  $\Delta t$  to get faster simulations implies that an increase in  $dx$  is also required to maintain stability and thus a loss of spatial resolution is manifested tending the solution to diverge.

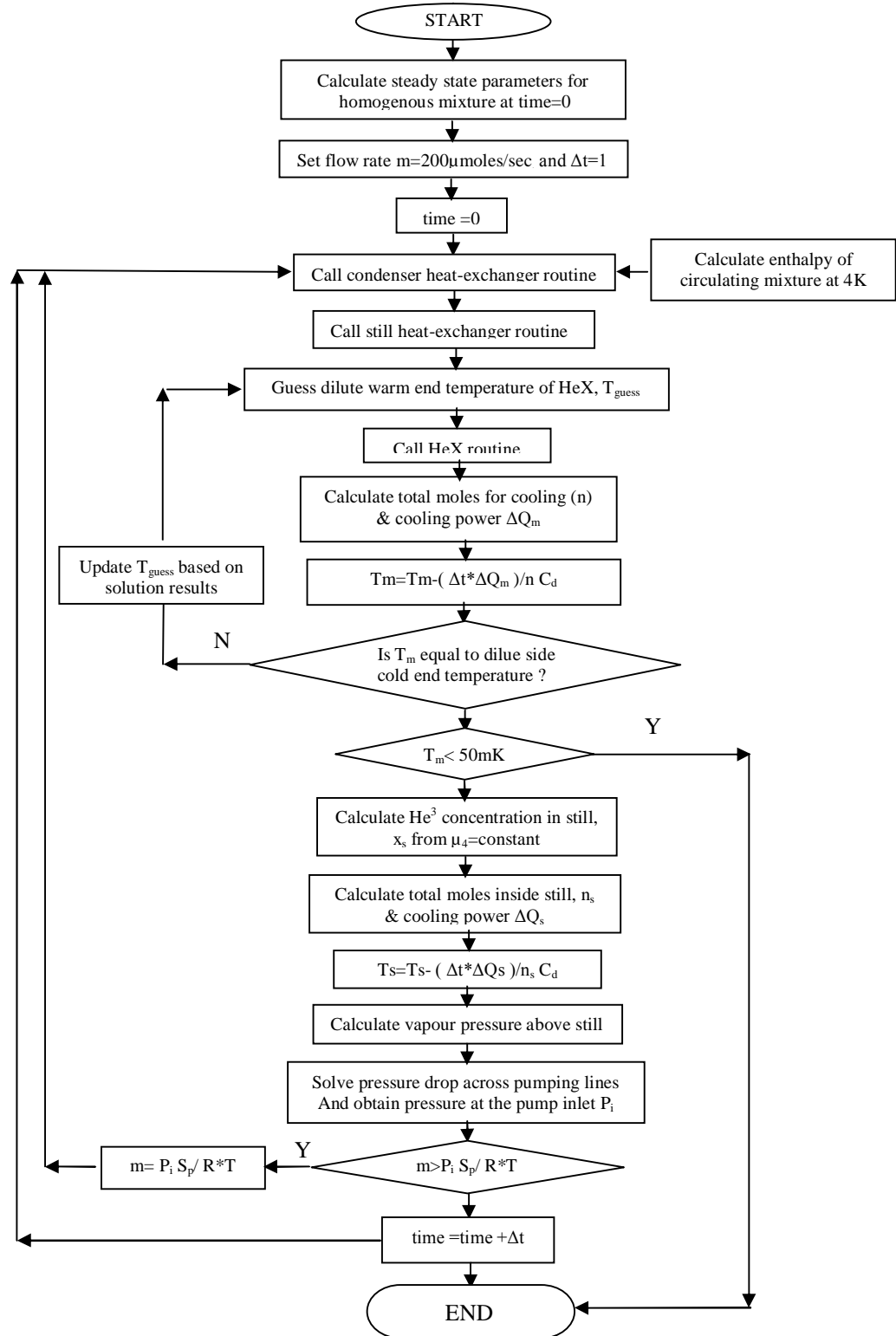


Figure 4.1 Algorithm used in transient simulation for extended SIDFO. It involves sub-routines for each components making up the complete dilution refrigerator

Most of the input/output (I/O) is made via files to keep the tedious process of data entry minimum. We present a flow sheet in figure 4.1 of the process simulation coupled with the mass and energy balance used in the model. Owing to the sensitivity of the process to small changes in temperature in the thermo-physical region of interest all calculations were done in double precision.

### **4.3 Results and Discussion**

The MC temperature variation with time during cool-down under four different still temperatures is shown in figure 4.2. This illustrates the simulated results obtained from the numerical computations carried out. It is found that for a typical still temperature of 0.6 K, it takes about three hours after the beginning of circulation, to reach the operating condition, which agrees well with the times reported elsewhere for operating machines [48, 51, and 52]. However, calculation assumes a zero residual loads and negligible specific heat of the metallic components. For comparison the measurement performed during experimental run is also shown alongside. During operation it was seen that as the rate of cooling decreases still power is varied and the still warmed to about 0.7K however, MC continues to cool. The still power was readjusted manually to maintain its temperature to about 0.6K as MC smoothly cools down. The figure shows that there is a noticeable change in slope of the temperature profile during the first couple of hours. This indicates that the entire HeX becomes effective and the cooling occurs at a faster rate causing a sharp decrease in temperature. Finally, the cooling rate becomes very slow as the MC temperature reduces further. It can be seen from the profile that, neither higher still temperature (~0.8K) nor lower still temperatures (~0.4K) results in tangible phase separation. At relatively high temperature large amount of vapour will be produced having significant amount of  $^4\text{He}$  in the circulating mixer that give rise to higher flow rate. This

high flow with large quantity of  $^4\text{He}$  tends to ensue instability in the condenser and phase separation is impeded, while a relatively low still temperature produces a small amount of  $^3\text{He}$  circulation which is hardly sufficient to generate phase separation. Since, we need to arrive at a situation where adequate flow of  $^3\text{He}$  with minimum amount of  $^4\text{He}$  in the circulating gas to occur, during the measurement, an optimum still temperature was maintained.

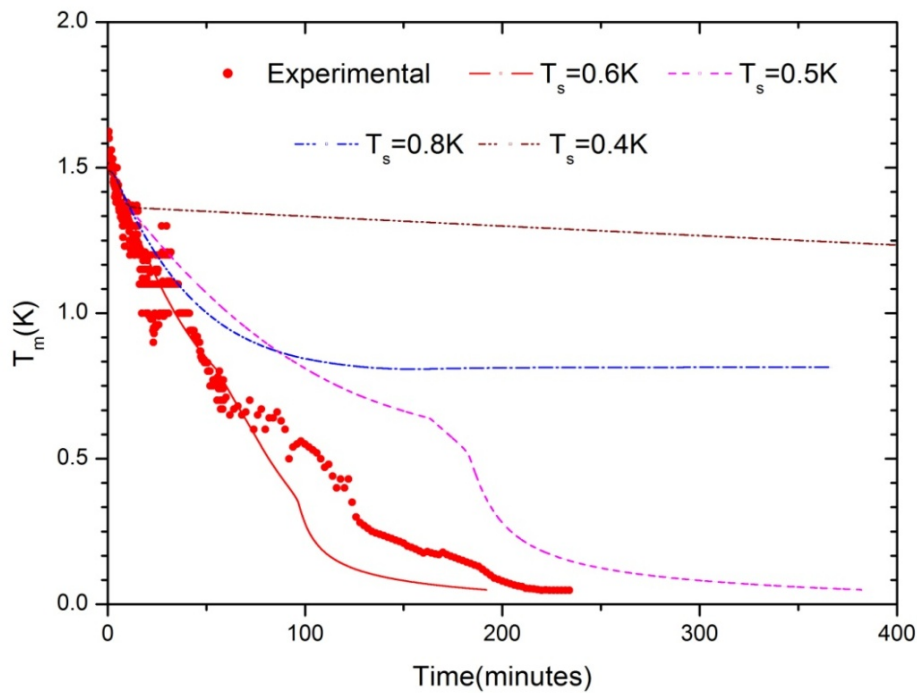


Figure 4.2 Cool-down of MC under four different still temperatures along with experimental cool-down curve

Determination of the appropriate heater power which is needed to achieve the operating temperature is also estimated using extended SIDFO and plotted in figure 4.3 for three different still temperatures. Lower still temperatures lead to longer cool-down times, and temperature above 0.6K cooling time remains almost unchanged. In practice, instabilities sets in towards higher still temperature [48]. For a given still temperature, heater power gradually increases and subsequently reduces as the phase separation reaches the MC. The optimum still power during operation of the machine is obtained by observing carefully its

behaviour. Extended SIDFO analysis reveals that a still temperature of 0.6-0.7K is sufficient to yield the necessary osmotic pressure for maintaining a continuous flow of  $^3\text{He}$  across the dilute side and phase separation to occur inside the MC for a mixture containing 30% of  $^3\text{He}$ . It also shows that a circulation for about two hours is required to get the pressure of 0.05 mbar inside the still with a corresponding flow rate of 15-20  $\mu\text{mol/s}$ .

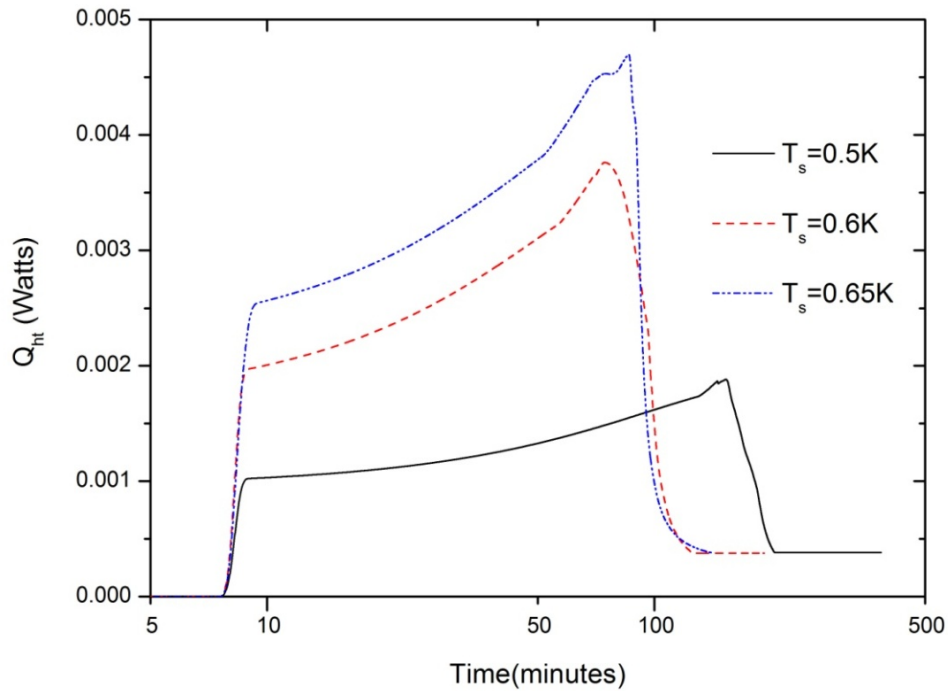


Figure 4.3 Variation of still heater powers with time to maintain a given still temperature.

The results given in table 4.1 are obtained from an auxiliary module by solving the Eq. (4.5), (4.6), (4.7) & (4.8) and show that for higher  $^3\text{He}$  concentration phase separation occurs at a relatively higher temperature.

For a system having excess  $\text{He}^3$ , the most probable consequence is that the system will seriously degrade and eventually stop functioning as the phase separation is likely to occur in the dilute side of the system. Simulation suggests that as the pumping continues the still attains phase separation temperature in about 10-15 minutes and  $^3\text{He}$  rich mixture

with  $x_3 > 90\%$  fills the concentrated side of the DR while  $^4\text{He}$  rich mixture occupies the rest of the dilute side.

Table 4.1

Phase separation temperatures under different $^3\text{He}$ concentration in the $^3\text{He}/^4\text{He}$ mixture	
$^3\text{He}$ concentration in mixture (molar fraction)	Phase separation temperature (K)
0.2	0.456
0.25	0.534
0.3	0.602
0.35	0.663
0.4	0.719

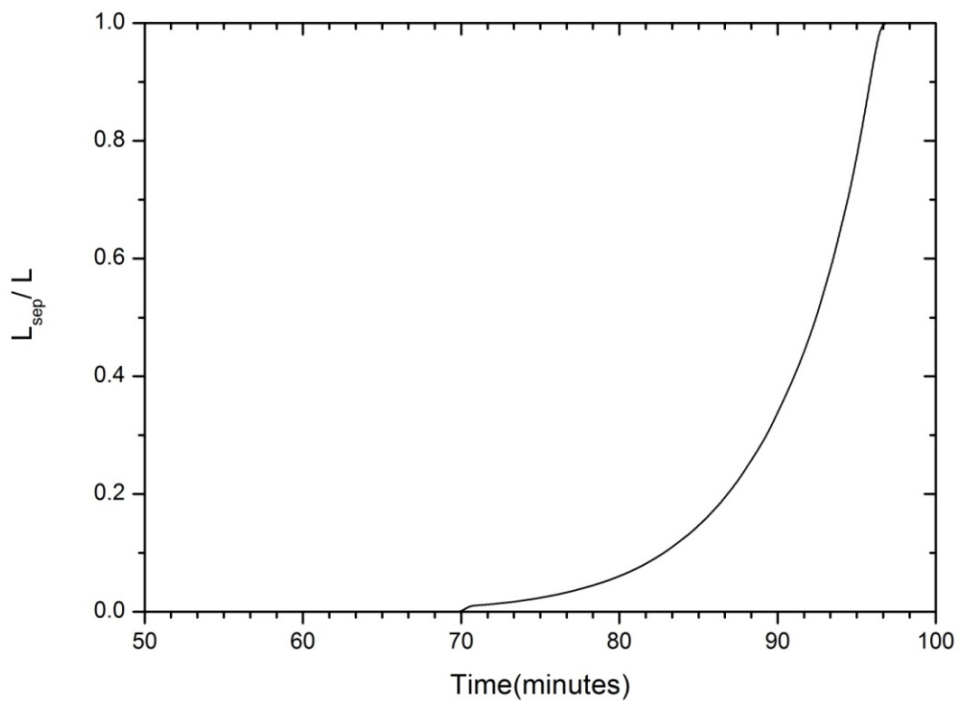


Figure 4.4 Time evolution of phase separation interface along the length of the concentrate channel of HeX

Figure 4.4 reveals that as the temperature decreases phase separation in the concentrated line of HeX moves towards the MC in an estimated time of ~100 mins from the beginning of circulation. As the phase boundary approaches the MC, the efficiency of the HeX increases and fills the HeX rapidly with concentrated mixture in the downstream as seen from figure 4.5. The simulation is performed for an initial concentration of  $^3\text{He}$  ( $x_i=0.3$ ) and with two values of  $rr$  ( $=V_s/V_{mc}$ ) which measures the initial volume of liquid within the still while  $V_{mc}$  is filled up with the liquid. As the phase separation interface enters the MC, and the system approaches steady state condition, the  $^3\text{He}$  concentration in the dilute solution of the MC and still settles at 6% and 1% respectively as shown in figure 4.6.

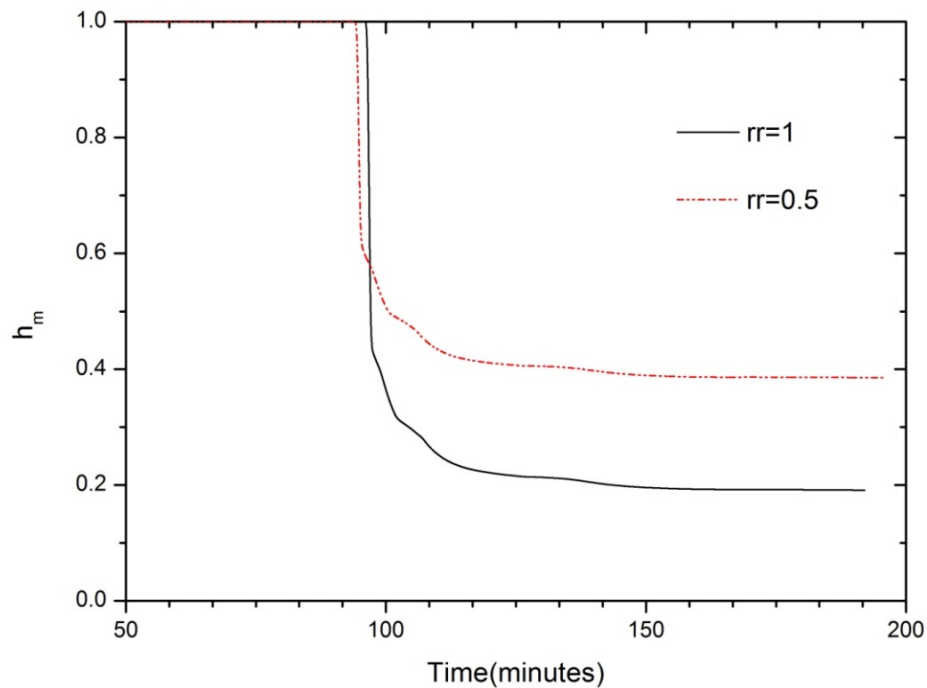


Figure 4.5 Time evolution of accumulated fraction of dilute solution  $h_m$ , and within the MC under two different  $rr$  values

It is always desirable to ensure that the phase separation sits in the MC at all operational temperatures. This is accomplished by choosing the appropriate ratio of isotopic composition and initial volume of the mixture. If  $h_m < 0$  the mixer is flooded with

concentrated  ${}^3\text{He}$  and the interface will move towards the still or possibly towards the HeX. In this case the refrigerator would fail to operate. On the other hands,  $h_m > 1$  implies

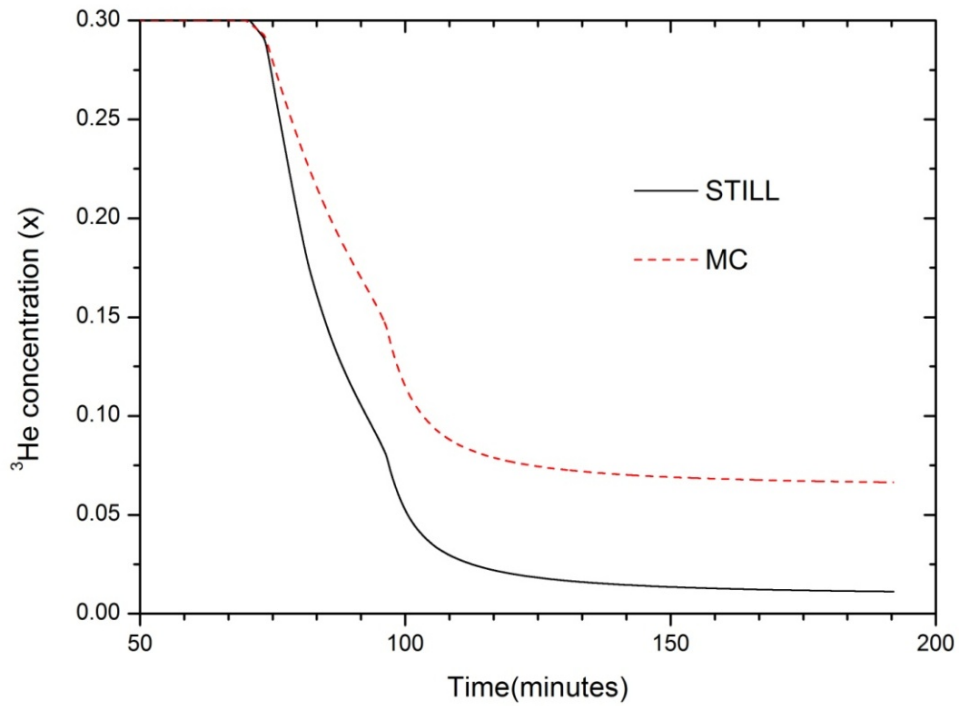


Figure 4.6 Time evolution of  ${}^3\text{He}$  concentration within the MC and still

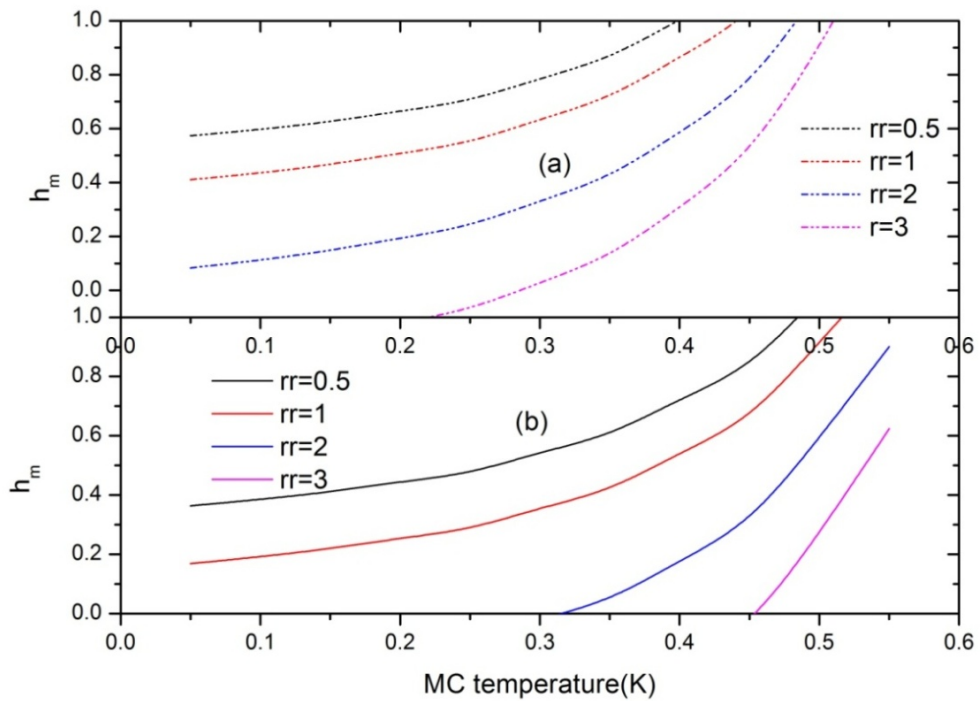


Figure 4.7 Fraction of accumulated dilute solution inside MC,  $h_m$  under different MC temperatures considering an initial  ${}^3\text{He}$  concentration of 0.25 and 0.3 respectively.

that dilute solution completely fills the MC and is further diluted from its equilibrium value. The dilution inside the concentrated side of HeX will cause the mixer to cool, but at the cost of reducing the effective length of the HeX resulting in performance degradation. We have estimated the optimum values of these quantities using extended SIDFO, so that the phase separation occurs inside the MC. The results are plotted in figure 4.7(a) and figure 4.7(b) which correspond to initial  $^3\text{He}$  concentrations of 0.25 and 0.3 respectively. We have considered the liquid volume of the condenser and HeX separately besides MC and still during calculation unlike the one given in reference [28], where the liquid volume inside the HeX has been negotiated with the volumes of still and mixing chamber and assumed a linear concentration gradient along the dilute channel. It is also noted that the value of  $h_s$  increases with decreasing MC temperature though the value is rather small.

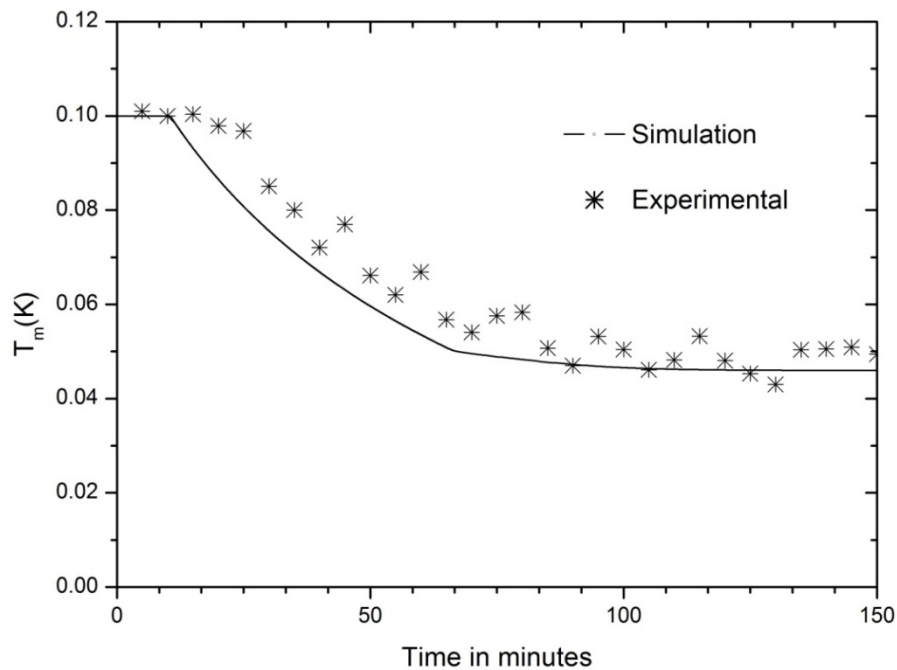


Figure 4.8 Comparisons between simulation results and experimental data for transient response of MC temperature by reducing heater power attached to MC.

The transient behaviour of dilution refrigerator by turning on and off the heater power of the MC to reach the thermal equilibrium is calculated and compared with the experimental

measurement as shown in figure 4.8. During the experiment, the MC is initially at 100mK temperature with its heater power at about  $60 \mu\text{W}$ . The heater power is then turned off and temperature is monitored continuously and reach to  $\sim 50 \text{ mK}$  in approximately two hours. In the figure 4.8, this simulation is represented by a solid line which is in good agreement with the measured values.

# Chapter 5

## Conclusions and Future Outlook

### 5.1 Summary

This thesis work is set out to develop a reliable and complete thermodynamic simulation of dilution refrigerator for a given design. A thermal model is formulated using a numerical simulation program SIDFO, based on control-volume approach which is precise, efficient and flexible. It can simulate varying process parameters and can be used for calculations prior to any process modifications. Further more, with this approach new process equipments can be easily added.

While many analyses and models of the thermodynamical process related to dilution refrigerator already exist, the present work describes the congregation of all components of the dilution refrigerator making up a complete closed cycle simulation. The simulation is further upgraded to accommodate the stages of development preceding the steady state condition by introducing time dependent variations. To our knowledge, no comprehensive study to investigate the time dependent manifestation of transitory phases in DR has been done earlier. This simulation has enabled us to study the progression of the phase interface along the concentrated channel of HeX and its arrival at the mixing chamber for a given physical situation. The transient study endows various process parameters responsible for the optimal cool-down and operation of the machine. The simulation also takes care of the intricate relationships among the subsystems/components and provides a better understanding for trouble shooting during operation of the refrigerator. Moreover, simulation has produced several unique results of the underlying phenomena occurring at

various stages of the very low temperature process. The presence of  $^4\text{He}$  in the circulating gas and its consequences to the generalized cooling power is thoroughly examined and revisited. In addition, the simulation also takes into account the effect of arbitrary flow rates in the circulating  $^3\text{He}$  gas on the resulting performance. The interplay between the still power and the flow rate and their effect on the cooling power and the mixing chamber temperature is also investigated in details. The composition of isotopic mixture for successful operation of the dilution refrigerator is thoroughly analysed. The thermodynamic property of helium isotopic mixture has been compiled for different temperature range down to sub-kelvin temperature from several literatures for the purpose of simulation.

The results derived from this model are compared to the experimental data obtained from different measurements carried out at various laboratories. While estimating cooling power with traces of  $^4\text{He}$  in the circulating gas under different flow conditions, the cooling power obtained from simulation provides a better result as compared to others models. Significant effort was put for developing the analysis and fabrication of dilution refrigeration system as set forth in this thesis. The primary objective was to develop a complete simulation tool to design and optimize a dilution refrigerator and gather valuable data for practical operation.

In conclusion, thermo dynamical analysis of steady state and transient processes through SIDFO has helped us to conceptualize and design a complete dilution refrigeration system. The dilution refrigerator was successfully built and temperature down to below 50mK have been achieved and maintained for hours. The results of simulation were compared with experimental data derived from measurements during operation of the machine and found to be satisfactory. The project is aimed at developing

technologies relevant to dilution refrigerator. It is valuable low temperature equipment and a convenient tool for low temperature experiments.

## 5.2 Scope of Future Works

The measurement of  $^4\text{He}$  flow rate present in the circulating gas which does not contribute to the cooling process can provide valuable information on the performance of DR, this is a direction for future experiments. One of the possible reasons for which we could not reach below 40 mK in the experiment carried out is due to high residual heat load in the mixing chamber. The most obvious suggestion for future improvement is to eliminate the possible sources of residual heat in-leak and make effort to achieve lower temperature. However, measuring cooling power at different temperatures and obtaining better results happens to be tedious and somewhat uncertain. The efficiency of HeX needs to be improved to fit the simulated data with experimental observation which we plan to address in future. At the same time effort can be made to achieve still lower temperature by using adiabatic nuclear demagnetisation of selected paramagnetic materials or alloys. Such a scheme with a magnetic field would be an excellent experimental facility for condensed matter physics as well as basic physics research at ultra low temperatures.

As the dry system for DR, based on cryo-cooler is getting more popularity owing to its simple operation without using liquid helium so a computer program may be tailored to include cryo-cooler as a part of its equipment. The present work may further be extended to obtain continuous temperature distribution along the dilution insert under variable loading condition at different temperatures, to simulate a more realistic performance of the machine. Different factors as mentioned in section 3.1 that can degrade the performance of the dilution refrigerator requires thorough studies and extensive analysis for numerical implementations. In addition, computer simulation requires fine

tuning to avoid numerical oscillation and augment the speed of computation. Suggestions for future work may involve the development of complete software package that includes user friendly interface (GUI) for general use.

# Bibliography

- [1] O.V. Lounasmaa: Experimental Principles and Methods Below 1K (1974)
- [2] H. London, G.R. Clarke, E. Mendoza, Phys. Rev. 128, 1992 (1962)
- [3] G.K. Walters and W.M. Fairbank, Phys. Rev.103, 262 (1956)
- [4] V.P. Peshkov and K.N. Zinov'eva, Soviet Phys.- JETP 5, 1024(1957)
- [5] J. G. Daunt, R. E. Probst and H. L. Johnston, Phys. Rev. 73, 638(1948)
- [6] Bruyn Ouboter, R. De, K. W. Taconis, C. Le and J. J. M. Beenakker, Physica 26, 853(1960)
- [7] H. London, G. R. Clarke and E. Mendoza, Phys. Rev. 128, 1982(1962)
- [8] H. E. Hall, P. J. Ford and K. Thompson, Cryogenics 6, 80(1966)
- [9] P. Das, R. De Bruyn Ouboter and K. W. Taconis, Proceedings Ninth International Conference on Low Temperature Physics, Coloumbus, Ohio, 1964, part B, p 1253.
- [10] Edwards, D. O, D. F. Brewer, P. Seligman, M. Skertic, and Yaqub, Phys. Rev. Lett. 15, 773(1965)
- [11] B.Neganov, N. Borisov and M. Liburg, Soviet Phys. JETP 23, 959(1966)
- [12] O. E. Vilches and J. C. Wheatley, Phys. Rev. 148, 509 (1966)
- [13] J. C. Wheatley, Am. J. Phys. 36, 181(1968).
- [14] J. C. Wheatley, O. E. Vilches and W. R. Abel, Physics 4, 1(1968)
- [15] O. E. Vilches and J. C. Wheatley, Phys. Letters 24A, 440(1967)
- [16] T. O. Niinikoski, Proc. 6<sup>th</sup> Int. Cryo. Engin. Conf. (IPC Science and Technology Press, Guilford, 1976), p.102
- [17] D.D. Osheroff, R. C. Richardson and D. M. Lee, Phys. Rev. Lett. 28,885(1972)
- [18] Landau L. D and I. Pomeranchuk, Dokl. Akad. Nauk SSSR 59, 669(1948)
- [19] J. C. Wheatley, R. E. Rapp and R. T. Johnson, J. Low Temp. Phys. 4 (1), 1971

- [20] G. M. Coops, A.T.A.M. de Waele and H. M. Gijsman, Phys. Rev. B25, 4879 (1982)
- [21] C.A.M. Castelijns, J. G. M. Kuerten, A.T.A.M. de Waele and H. M. Gijsman, Phys. Rev. B32, 2870 (1985)
- [22] J. G. M. Kuerten, C.A.M. Castelijns, A.T.A.M. de Waele and H. M. Gijsman Cryogenics 24, pp. 419-443 (1985)
- [23] J. Zeegers, J. G. M. Kuerten, A.T.A.M. de Waele and H. M. Gijsman, Jpn. J. Appl. Phys. 26, 63(1987)
- [24] G. L. Pollack, Rev. Mod. Phys. 41, 48 (1969)
- [25] N. S. Snyder, Cryogenics 10, 89 (1970)
- [26] N. S. Snyder NBS Technical note 385 (1969)
- [27] A.C. Anderson, W.R. Roach, R. E. Sarwinski, J. C. Wheatley, Phys. Rev. Lett. 16,263(1966)
- [28] R. Radebaugh NBS Technical Note, p 362 (1967).
- [29] G. Frossati, H. Godfrin, B.Hebral, G. Schumacher, D. Thoulouze, Proc. U.L.T. Hakone Symp. (Phys. Soc. Japan, Tokyo, 1977), p.205
- [30] G Frossati, J. Phys. (Paris) 39, C6-1578(1978)
- [31] G. Frossati, J. Low Temp. Phys. 87,595(1992)
- [32] Y. Takano, Rev. Sci. Instrum. 65(5),1667(1994)
- [33] P. Wikus, T. O. Niinikoski, J. Low Temp. Phys. 158 , p 901-921(2010)
- [34] P. Wikus, Dilution refrigeration of multi-ton cold masses. PhD Thesis, Vienna University of Technology, Austria (2007).
- [35] F. Pobell (1995) Matter and Methods at Low Temperatures, Springer, Berlin, Heidelberg, New York.

- [36] J. Wilks *The Properties of Liquid and Solid Helium* Oxford: Clarendon Press, 1967 p 245.
- [37] D.S. Greywall, *Phys. Rev. B* 27,2747 (1983).
- [38] Jedidiah Pradhan, Nisith K. Das and Alok Chakrabarti, *Cryogenics* 57, 158-165(2013).
- [39] Jedidiah Pradhan, Nisith K. Das and Alok Chakrabarti, *Cryogenics* 63, 69-76(2014).
- [40] N.K. Das, J. Pradhan, Md. Z.A. Naser, A. Roy, B.Ch. Mandal, C. Mallik and R.K. Bhandari, *Cryogenics* 52,679-684(2012).
- [41] V.P.Peshkov in *Proceedings of the Eleventh International Conference on Low Temperature Physics*, St. Andrews, 1968 edited by J.F. Allen, D.M.Finlayson and D.M. McCall (University of St. Andrews, Scotland, 1968), Vol.1, p. 653.
- [42] P.A. Warkentin, H.J. Haueke, H.J. Lucas and J.C. Wheatley in *Proc. National Academy of Science, USA*, Vol.77, No. 12,p 6983-6987, 1980, *Physics*.
- [43] J.R.G. Keyston and J.P.Laheurte, *Phys. Letters* 24A, 132(1967).
- [44] J.C.Wheatley in *Progress in Low Temperature Physics* Vol. VI, ed. C.J. Gorter (North Holland Publishing Company Amsterdam, 1970), P 77.
- [45] G.A. Vermeulen, G. Frossati, *Cryogenics* 27,139(1987).
- [46] D.S. Easton, D.M. Kroeger and A. Moazed (1976) *Appl. Phys. Lett.*29, 382.
- [47] F.K.Miller and J.G. Brisson, *Cryogenics* 41 (2001) p 311-318.
- [48] Donald Otis Pederson, PhD Thesis (RICE University), 1971.
- [49] J.D. Siegwarth and Ray Radebaugh, *Rev. Sci. Instrum.* 42(8), 1111 (1971).
- [50] R L Fagaly and DN Paulson, *Cryogenics*, Vol 32, N0.8 (1992)
- [51] H Postma *NIM* 88, 45-50(1970)
- [52] K N Chaffin, M Sc Thesis (Texas Tech University), 1978.

## Appendix A: Flow Impedance Analysis

The flow of liquid helium inside the capillary impedance driven by the pressure gradient is highly inhomogeneous. In general, the capillary characterization and sizing is determined experimentally. The liquid helium undergoes phase transition to superfluid with a drop of pressure along the length of the impedance resulting in two phase fluid. At the exit, more liquid is evaporated creating larger fraction of gas. Detailed analysis of the flow inside the capillary is performed numerically considering continuous variation of properties with temperature and pressure.

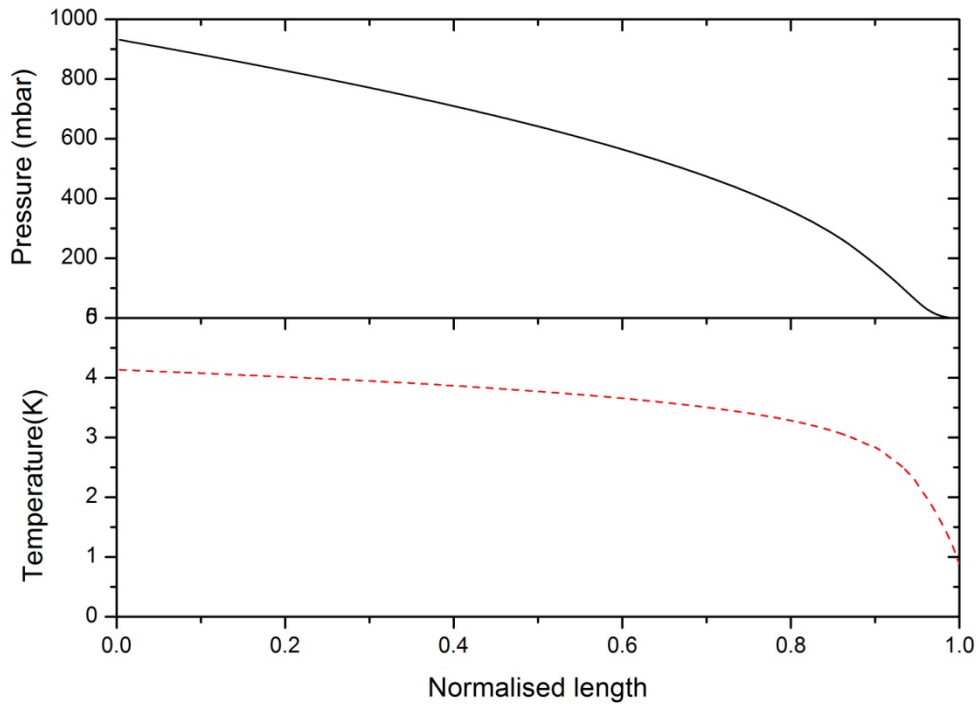


Figure A. Temperature and pressure variation along the length of impedance

$$(Z_p = 2 \times 10^{12} \text{ cm}^{-3})$$

In the analysis the capillary impedance is divided into small differential impedances connected in series. The pressure drop across each differential impedance is calculated as  $dZ_p \times \eta \times \dot{V}$ , where  $dZ_p$  is the incremental value of impedance,  $\eta$  is the viscosity at the given temperature and  $\dot{V}$  stands for volume flow rate. The volume flow is calculated based

on local temperature and the quality of two phase mixture. The subsequent temperature is obtained assuming saturated liquid and using its vapour pressure curve. The energy balance across each section is used to get the mass which is converted to gaseous phase. It is assumed that there is no heat transfer with the surroundings and liquid flows through capillary is saturated throughout. Ideally, the partial vapour phase takes away a part of the heat from the liquid thereby lowers its temperature. However, in reality the system is not adiabatic cold from the evaporator conducted through the capillary re-condenses the vapour inside the capillary.

## Appendix B: Flow Chart for Steady State Simulation

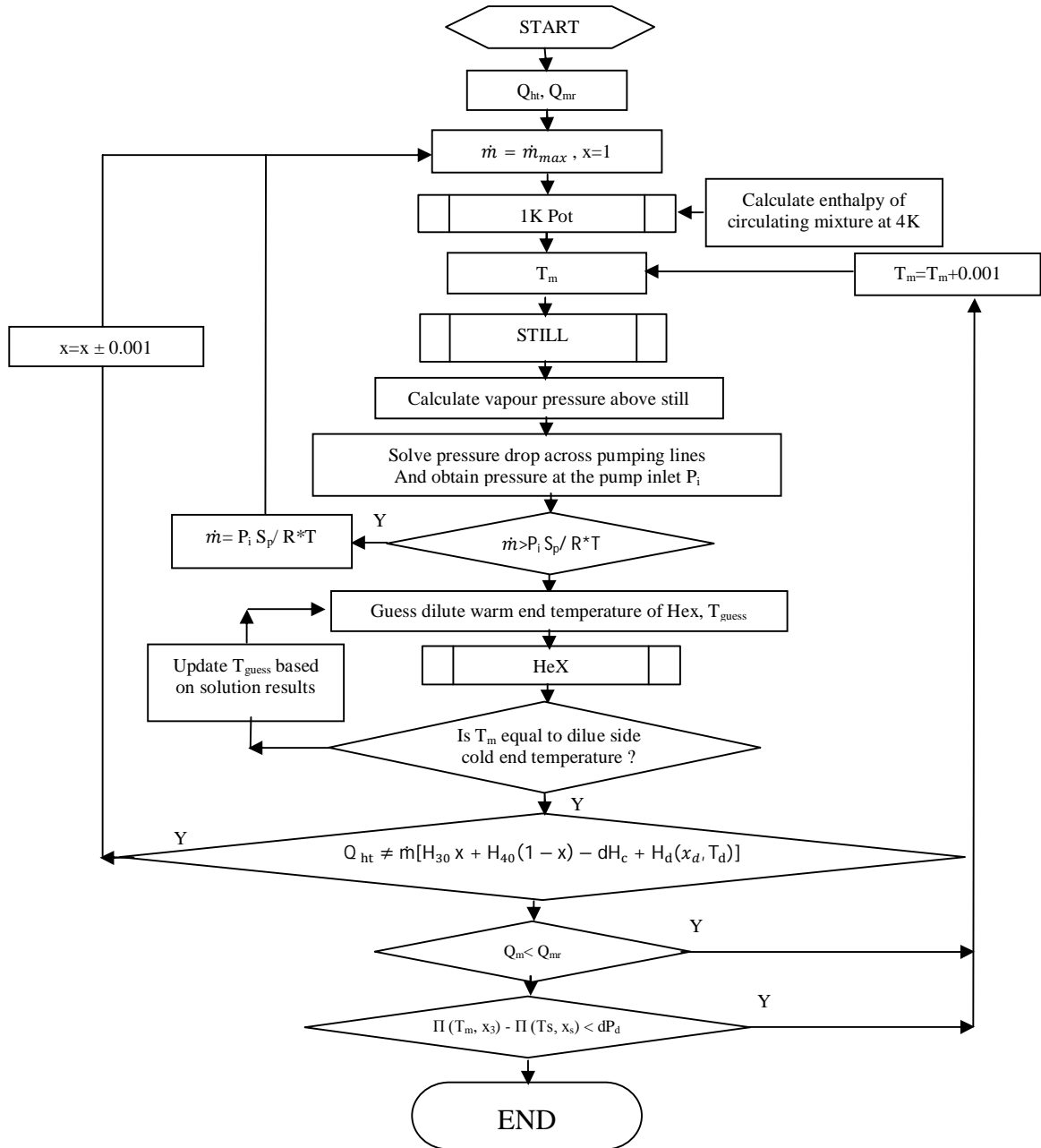


Figure B. Algorithm for simulating steady state